NTNU
Norwegian University of
Science and Technology

Magnon Excitations of a Dzyaloshinskii-Moriya Coupled Insulating 2D Antiferromagnetic Skyrmion

Sondre Bergem Sørheim

Master of Science in Physics and Mathematics
Submission date: June 2018
Supervisor: Arne Brataas, IFY
Co-supervisor: Roberto Troncoso, IFY

Norwegian University of Science and Technology
Department of Physics

Abstract

Motivated by recent experimental progress in realizing novel antiferromagnetic phases with state-of-the-art characteristics for memory storage and information processing, we study the magnon excitation spectra and eigenmodes around the antiferromagnetic skyrmion. In the micromagnetic limit of an insulating nearest-neighbour spin coupled two-sublattice antiferromagnet, we derive from Hamilton's principle a new set of coupled Schrödinger-like equations for perpendicularly excited magnons with respect to an inhomogeneous chiral texture.

In the limit of a homogeneous antiferromagnetic ground state, the impact of various interaction mechanisms on the dispersion relation is discussed. A nonzero external magnetic field lifts the degeneracy of right-circularly and left-circularly polarized modes, while the asymmetric Dzyaloshinskii-Moriya interaction shifts the continuous spectra in momentum space along particular directions dictated by the polarization degree of freedom.

For the chiral antiferromagnetic skyrmion, the Hamiltonian matrix subject to various pinning strengths of the texture-induced potential is numerically diagonalized for azimuthally symmetric modes. We find that the out-of- and in-plane, with respect to the skyrmion basal plane, excitation modes decouple. The presence of the Dzyaloshinskii-Moriya coupling and the localized feature of the skyrmion make Goldstone, bound and unbound modes emerge for both in-plane and out-of-plane magnons. The Goldstone modes can be interpreted as a collective excitation of the entire skyrmion, or as equally likely exponentially damped evanescent or growing resonant modes for which further consideration by for instance kinetic theory and Landau damping is necessary to collapse the modes onto either solution. We find that the relative strength of the intrinsic coupling mechanisms is decisive for the magnon states that appear.

Sammendrag

Med bakgrunn i nye eksperimentelle fremskritt i å fremstille antiferromagnetiske faser med enestående egenskaper for minnehåndtering og informasjonsprosessering, studerer vi eksitasjonsspektret og eigentilstandene til magnoner rundt et antiferromagnetisk skyrmion. I den mikromagnetiske grensen for en isolerende dobbelt-gitter antiferromagnet med spinnkoblinger mellom nabo-gitterpunkt, utleder vi med utgangspunkt i Hamiltons prinsipp et sett med nye Schrödinger-lignende likninger for magnonske ortogonale eksitasjoner av en inhomogen kiral tekstur.

I grensen for en homogen antiferromagnetisk grunntilstand, diskuterer vi hvordan ulike vekselvirkningsmekanismer påvirker dispersjonsrelasjonen. Et eksternt magnetfelt løfter degenerasjonen av høyre- og venstrepolariserte tilstander. Den asymmetriske Dzyaloshinskii-Moriya-interaksjonen forskyver det kontinuerlige spekteret langs enkelte retninger i impulsrommet, hvilket avhenger av polarisasjonen.

For kirale antiferromagnetiske skymioner, diagonaliserer vi Hamilton-matrisen numerisk for ulike styrker av den tekstur-induserte potensialbrønnen for rotasjonssymmetriske tilstander. Vi observerer at tilstander som befinner seg i og normalt på baseplanet til skyrmionet ikke lenger er koblet sammen. Tilstedeværelsen av Dzyaloshinskii-Moriya-koblingen og den endelige utstrekningen av skyrmionet gjør at både Goldstone-, bundne og ubundne tilstander eksisterer for magnonene både i og ut av baseplanet. Goldstone-tilstandene kan forstås som en enhetlig eksitasjon av skyrmionet, eller som en kombinasjon av like sannsynlige eksponentielt dempede flyktige og ustabile resonante tilstander hvor bruk av kinetisk teori og Landau-demping kan være nødvendig for å få en selvkonsistent løsning. Den relative styrken mellom de intrinsike koblingsmekanismene er avgjørende for hvilke tilstander magnonene kan befinne seg i.

Preface

This is the final thesis accomplished during the last semester of the five-year master's degree programme in Applied Physics and Mathematics at the Norwegian University of Science and Technology.

I would like to thank my supervisors Postdoc. Roberto Troncoso, researcher Alireza Qaiumzadeh and Prof. Arne Brataas for invaluable guidance during the semester. I am also grateful to all my friends that have made the last five years more than just books and lectures. Last but foremost, special thanks to my father, mother, brother and girlfriend for infinite support and for will have been letting me pursue my passions without hesitation.

Sondre Bergem Sørheim
Trondheim, Norway
June 2018

Nomenclature

Symbols

N_{sk}	Topological quantum number of skyrmions
D	The inhomogeneous Dzyaloshinskii-Moriya interaction strength
M_s	Saturation magnetization
d	The homogeneous Dzyloshinskii-Moriya interaction strength
γ	Helicity of skyrmion
m	Vorticity of skyrmion
$\mathcal{A}$	The Euclidian action
$\mathcal{F}$	Free energy
$\mathcal{K}$	Kinetic energy
α_G	The Gilbert damping constant
c	Lattice constant of a squared 2D lattice

Conventions

- **Bold text** implies vectors
- Repeated indices implies the Einstein summation convention
- $\nabla_\rho^2 = \frac{1}{\rho}\partial_\rho(\rho\partial_\rho)$ is the radial derivative of the cylindrical Laplacian

Contents

Abstract **i**

Sammendrag **iii**

Preface **v**

Nomenclature **vii**

1 Introduction **1**

1.1 Motivation 1

1.2 Structure of the thesis 4

2 Antiferromagnetic micromagnetics **7**

2.1 The antiferromagnetic system 7

2.2 The symmetric Heisenberg exchange 8

2.3 The Dzyaloshinskii-Moriya interaction 9

2.4 Magnetocrystalline anisotropy 11

2.5 Demagnetization 13

2.6 Zeeman coupling 14

2.7 The antiferromagnetic free energy 14

3 Chiral antiferromagnetic textures **17**

3.1 The homogeneous antiferromagnetic ground state 17

3.2 Domain walls 18

3.3 Skyrmions 22

4 Antiferromagnetic spin wave dynamics **29**

4.1 The equations of motion for the order parameter and the magnetization 29

4.2 Spin waves 33

4.3 Spin wave excitations of the homogeneous ground state 36

4.4 Spin wave excitations of inhomogeneous chiral textures 38

5 Eigenspectra and eigenmodes for magnons around the antiferromagnetic skyrmion **43**
5.1 Dimensionless equations and magnon ansatz 43
5.2 Azimuthally symmetric modes 45
5.2.1 Anisotropy parameter $k_z = 0.1$ 47
5.2.2 Anisotropy parameter $k_z = 1.0$ 58
5.2.3 Anisotropy parameter $k_z = 10$ 63
5.3 Analogy to the easy-plane antiferromagnetic vortex 69
5.4 Highly excited magnon regime 73

6 Conclusion **77**
6.1 Summary and concluding remarks 77
6.2 Outlook 78

Appendices **81**

A Antiferromagnetic spin interactions **83**
A.1 Symmetric Heisenberg exchange 83
A.2 Inhomogeneous Dzyaloshinskii-Moriya interaction 86
A.3 Homogeneous Dzyaloshinskii-Moriya interaction 88

B Derivation of the equations of motion for antiferromagnetic spin waves **91**

Bibliography **101**

1 Introduction

In this chapter we will firstly motivate for the study of antiferromagnetic magnonics by establishing the historical and theoretical development of the field and discuss some of the present research activities and prospects. Secondly, we will describe the structure of the thesis.

1.1 Motivation

The electron is a fundamental particle that can be attached different labels such as mass and charge to define its properties. The extensive use of the charge property of electrons in applications can be traced back to the first patent of the telegraph in 1837 [1], long before the detection of the electron itself by Thomson [2] or its charge property by Millikan [3]. Since then, via the birth of mobile phones and computers, the number of electronic devices has skyrocketed, with an ever-increasing demand to computational power. To accommodate this issue, the use of the spin property of electrons has been explored in the field of spintronics [4], allowing for more subtle treatment of memory storage and information processing in devices. For now, the industry primarily uses ferromagnetic materials [5], where the spins tend to align parallel, setting up a spontaneous magnetization in the ground state of the system. To meet the needs of tomorrow, new technology with more versatile and robust design is needed. Such a candidate could be antiferromagnetic materials, where adjacent spins tend to align antiparallel in the ground state. They are by far more common in nature [6] and are operating in a frequency range much higher than ferromagnets, allowing for shorter response time [7, 8]. Also, they do not generate any stray fields perturbing components in the vicinity as the net magnetic moment is zero [9]. Information storage in such constructions is favourable as antiferromagnetic materials

are insensitive to magnetic reading and field perturbations from other components, allowing fore more densely packed devices increasing the memory storage capacity [6].

The theoretical framework for applications based on ferromagnetic and antiferromagnetic materials started with Heisenberg in 1926. Heisenberg proposed that the spontaneous magnetization observed in some materials below the Curie temperature was the result of an exchange coupling between neighbouring spins resulting in a ferromagnetic ground state [10]. In the 1930s, Néel found interest in materials containing magnetic elements such as Fe and Cu, which did not show any bulk magnetization far below the Curie temperature. Bloch had in 1930 introduced the concept of quantized spin waves (magnons) - thermal excitations of the spins around some equilibrium - to describe the drop in spontaneous magnetization when approaching a critical temperature from below [11]. At this temperature, the system undergoes a phase transition and the spontaneous magnetization perish. But these magnons could not account for the absent magnetization far below the critical temperature. Instead, Néel addressed the lack of a net magnetic moment to a local molecular field [12], changing rapidly on interatomic distances and pointed out that the exchange interaction favouring antiparallel alignment of neighbouring spins was the responsible mechanism. The theory for such systems was extended the succeeding decades, covering new interaction mechanisms between spins [13, 14] and the dispersion relation of systems comprising large magnonic occupation numbers and magnon-magnon interactions [15].

These materials first found their route to applications by the independent discovery of the giant magnetoresistance in 1988 by the groups of Fert [16] and Grünberg [17]. Less than 10 years later, the work of Berger [18] and Slonczewski [19] on spin transfer torque (STT) between currents and ferromagnetic domains in thin film sandwich structures paved the way for the use of ferromagnetic spin valves in magnetoresistive random access memory (MRAM) and hard drive read heads [20]. Since then, it has been a research area of vast interest, and new types of STT-MRAM with improved properties are being produced [21]. Most of these devices are based on ferromagnetic materials, while antiferromagnets as for today have only been used for pinning ferromagnetic layers by the exchange bias [22]. Yet, perturbation of the magnetic moments in antiferromagnets by electrical currents was theoretically proposed in 2006 [23], and in 2011 it was reported magnetoresistance phenomena in spin-valve

configurations of antiferromagnets [5], similar to those for ferromagnets. Switching phenomena of two stable states in the antiferromagnet CuMnAs for current densities $j \sim 10^6 \mathrm{A/cm}^2$ have been experimentally realized close to room temperature [24], allowing for antiferromagnets to enter the branch of applied spintronics.

One area of potential applications is embedded in the area of soliton-magnon interactions. A soliton is a topologically protected, nonlinear excitation of the order parameter (the spin magnetization for ferromagnets and the staggered magnetization for antiferromagnets). They appear spontaneously in materials to reduce the total free energy of the system, and are a result of the subtle interplay between interaction mechanisms of spins. One type of soliton with particle-like properties that has attained a lot of interest recently are skyrmions [25–30]. Similarly to electrons having an electric charge, skyrmions have a *topological* charge [9], taking both negative and positive integer values. This suggest skyrmions could act as information bits in memory devices. Quantized spin wave excitations are compatible with such equilibrium textures; the skyrmion texture could play the role of memory storage while the magnons take care of information processing. Magnons are preferable to domain walls for information transport, as the bottle-neck for magnon propagation is the velocity of the spin wave excitations [31], which is order of magnitude larger than the limiting Walker breakdown of domain walls [32]. It has been showed that a spin current carried by transient conduction electrons perish over a very short distance due to the damping of the electron movement [33]. However, a spin current carried by a spin wave is much more persistent as it is a collective excitation of the magnetic moments mounted on the strong exchange coupling between adjacent lattice sites [34]. Hence, there is no need for the material to be conducting, meaning thermal heating is avoided compared to electronic transport, theoretically supporting lossless information processing.

Antiferromagnetic order can be viewed as two ferromagnetic sublattices with opposite magnetization put together to form a single lattice where every spin is oppositely oriented to its nearest neighbours. Materials supporting ferromagnetic order only contain one such lattice, which again only allows for right-circularly polarized magnon modes [35, 36]. In antiferromagnetic materials the two sublattices allows for left- and right-circular polarization of the spin waves and hence a polarization degree of freedom, with all types of linear or elliptical modes also being possible [36]. With this additional degree of freedom, one have another way of reading in-

formation processed by the quantized spin waves. One of the main tasks in going from electronics to spintronics/magnonics lies in constructing magnetic logic circuits replacing today's electronic ones. For instance, MRAM can only be used to store information, not process or manipulate [37]. Amplitude magnoninc transistors [38], amplitude magnonic multiplexers [39] and amplitude magnonic nanocircuits for spin wave detection [40] have all been realized, and work on magnonic phase difference logic gates and circuits is also showing promising results [41–43].

Despite the vast assortment for applications being established, and the magnonic circuitry business keeping pace, there is still a theoretical gap yet to be explored regarding soliton-magnon interactions from a fundamental physics point of view. We will therefore look into the unreported formalism of magnon excitations around antiferromagnetic skyrmions, which have been experimentally observed recently [44], taking on a semi-classical quest to discover the spin wave excitation spectra and eigenmodes.

1.2 Structure of the thesis

In our endeavour on understanding the complexity of magnon dynamics in insulating antiferromagnets, we will start by introducing some general coupling mechanisms between spins before considering magnetic textures and spin wave excitations. In Chapter 5 we consider the eigenspectra of such excitations around an antiferromagnetic skyrmion.

More detailed, we will in Chapter 2 discuss the interaction mechanisms of symmetric Heisenberg exchange coupling and antisymmetric Dzyaloshinskii-Moriya interaction (DMI), the Zeeman coupling between electron spins and an external magnetic field, magnetic anisotropy and the demagnetizing field. The resulting antiferromagnetic free energy functional is the concluding remark in this chapter.

In Chapter 3, we consider antiferromagnetic textures for the staggered magnetization. The visual appearance and some physical properties will be discussed. We look at both homogeneous and chiral inhomogeneous textures.

In Chapter 4 we discuss spin wave excitations around the static antiferromagnetic textures considered in the previous chapter. The dispersion relation of the homogeneous ground state is derived, and a new set of equations for spin waves around antiferromagnetic Dzyaloshinskii-Moriya coupled chiral solitons are established.

In Chapter 5, we consider the wave function solutions to the new equations

of motions and their belonging eigenspectra. We will investigate the lowest-lying angular modes and solve the equations by a numerical diagonalization scheme. We also consider the asymptotic behaviour far from and near the skyrmion core. We end the chapter by comparing the results to antiferromagnetic easy-plane vortices and look at the highly excited regime.

Finally, we will summarize the work and discuss the outlook in Chapter 6.

2

Antiferromagnetic micromagnetics

We begin our endeavour by considering the interaction mechanisms present in antiferromagnetic spin systems. The different coupling mechanisms can give rise to a large variety of static spin textures and dynamics and establish the foundation of the expected physical behaviour of the system at hand. Our starting point will be of the semi-classical type, starting with spins represented by vectors in 3D, localized at lattice sites. From the discrete semi-classical starting point, we will move to the micromagnetic limit where the localized spin landscape is transformed into a smoothly varying spin texture, described by a set of continuous vector fields.

2.1 The antiferromagnetic system

Materials can be subdivided into different classes by their magnetic properties. Antiferromagnetic materials are substances where the arrangement of the magnetic moments takes on a checkerboard pattern; each magnetic moment favours to align antiparallel to their neighbouring moments. We can assign each magnetic moment to one of two sublattices, where the magnetization of one sublattice is equal and opposite to the other in the absence of an external magnetic field. The sublattices are fully compensated by the intrinsic couplings, and the bulk magnetization is zero below the critical Néel temperature T_{N}. Above this temperature, the antiferromagnetic arrangement becomes disordered by the thermal agitation inducing fluctuations of the moments. One example of such a material could be manganese.

There also exist other materials with different magnetic properties than antiferromagnets. We call it a ferromagnetic material if adjacent magnetic moments tend

to align parallel. This will typically lead to a nonzero spontaneous magnetization below the Curie temperature T_C of the material, even in the absence of an external magnetic field. By decreasing the temperature, the magnetization will at some point reach saturation. Above the Curie temperature, the thermal fluctuations of the moments break the ferromagnetic order and the magnetization disintegrates. Examples of such substances would be iron, cobalt and nickel, but the crystallographic structure will influence the temperature and pressure requirements to have ferromagnetic order [45]. Other magnetic classes are ferrimagnetic substances which are similar to antiferromagnets but where the two sublattices are not fully compensated, diamagnetic ones where the atoms are non-magnetic and paramagnetic materials where the intrinsic moments are very weakly coupled.

In this thesis we will mainly focus on the antiferromagnetic type. An antiferromagnetic system with spins localized at lattice sites described by unit vectors $\{\mathbf{S_x}\}$, is typically divided into two sublattices $k = \{\alpha, \beta\}$ [46–49], where neighbouring spins belong to different sublattices. We define c as the nearest neighbour lattice constant. Below the Néel temperature, the modulus of the magnetization of each sublattice $\mathbf{M}_k(\mathbf{x})$ is fixed, and only contains orientational degree of freedom. Hence, we can write $\mathbf{M}_k = M_s\mathbf{m}_k(\mathbf{x})$, where M_s is the saturation magnetization. $\mathbf{m}_k$ is a vector pointing along the local magnetization direction of sublattice k. As we limit our study to 2D antiferromagnetic systems, we can label each site by a set of two indices i, j for both sublattices. We define the magnetization $\mathbf{m}_{i,j}$ and the staggered magnetization $\mathbf{l}_{i,j}$ at lattice site (i, j) according to

$$\mathbf{m}_{i,j} = (\mathbf{S}^{\alpha}_{i,j} + \mathbf{S}^{\beta}_{i,j})/2, \qquad \mathbf{l}_{i,j} = (\mathbf{S}^{\alpha}_{i,j} - \mathbf{S}^{\beta}_{i,j})/2. \tag{1}$$

$\mathbf{S}^{\alpha(\beta)}_{i,j}$ is the spin at lattice site (i, j) in sublattice $\alpha(\beta)$. The staggered field and the magnetization are so far just a discrete set of vectors. We will use the above relations to derive the energy contributions to the free energy of an antiferromagnet in terms of the magnetization and the staggered field only. We start with the symmetric Heisenberg exchange.

2.2 The symmetric Heisenberg exchange

The exchange interaction originates from the Pauli exclusion principle and the Coulomb interactions. By symmetry, fermions cannot occupy the same quantum state simul-

taneously within a system. For a system which favours neighbouring electron spins to be aligned antiparallel, the exchange constant is positive. For a system which favours adjacent spins to be aligned parallel, the exchange constant is negative. In the classical Heisenberg model, treating the spins of the electrons as vectors, the Hamiltonian is then given by

$$\mathcal{H}_{\mathrm{H}} = \sum_{\langle \mathbf{x},\mathbf{x}' \rangle} J_s \, \mathbf{S}_{\mathbf{x}} \cdot \mathbf{S}_{\mathbf{x}'}, \tag{2}$$

where $\langle \mathbf{x}, \mathbf{x}' \rangle$ denotes sum over nearest neighbours, revealing the short-ranged nature of the interaction. For an isotropic material, we can suppress the spatial/directional dependence of the exchange tensor J_s, and treat it as a coupling constant between spins at neighbouring sites. The exchange coupling will typically be the dominating term in the free magnetic energy of a system with respect to other sources of magnetic energies. We refer to this as the exchange approximation, where $\mathbf{S}^{\alpha}_{i,j} \simeq -\mathbf{S}^{\beta}_{i,j}$, with the constraints $\mathbf{m}_{i,j} \cdot \mathbf{l}_{i,j} = 0$ and $\mathbf{m}^2_{i,j} + \mathbf{l}^2_{i,j} = 1$. Within this approximation, we define the Néel vector (order parameter) $\mathbf{n} = \mathbf{l}/|\mathbf{l}|$. $|\mathbf{l}| \simeq 1$, so we can replace $\mathbf{l} \to \mathbf{n}$ everywhere.

For the centred squared 2D lattice, the symmetric exchange contribution to the free energy is in the micromagnetic limit to leading order (see Appendix A.1 for the derivation)

$$\mathcal{H}_{\mathrm{H}} = \int \frac{d\mathbf{x}}{V} \left(\frac{a}{2}\mathbf{m}^2 + A\Big(\sum_{i=x,y} (\partial_i \mathbf{n})^2 + \frac{1}{2} \sum_{i \neq j} \partial_i \mathbf{n} \cdot \partial_j \mathbf{n} \Big) + L \sum_{i=x,j} (\mathbf{m} \cdot \partial_i \mathbf{n}) \right), \tag{3}$$

with $V = 2c^2, a = 8J_s, A = 2J_s c^2, L = 2\sqrt{2} J_s c$. There are two apparent parity-breaking terms, ($\propto \mathbf{m} \cdot \partial_i \mathbf{n}$) and ($\propto \partial_i \mathbf{n} \cdot \partial_j \mathbf{n}$). These terms can be neglected when the net magnetization of the system is zero, even for materials with a noncollinear staggered magnetization texture [50].

2.3 The Dzyaloshinskii-Moriya interaction

The DMI is a coupling mechanism that favours a noncollinear orientation of neighbouring spins. It was proposed by Dzyaloshinskii in 1958 [13], emerging as a result of the underlying crystal symmetry in $\alpha - \mathrm{Fe_2O_3}$, giving rise to a nonzero spontaneous magnetic moment in certain magnetic states. However, the true origin of the effect

was not proposed for another two years; in 1960 Moriya [14] showed how spin-orbit coupling in systems with low magnetic order gives rise to an antisymmetric interaction mechanism between neighbouring spins $\mathbf{S_x}$ and $\mathbf{S_{x'}}$ forming the Hamiltonian

$$\mathcal{H}_{\mathrm{DM}} = \sum_{\langle \mathbf{x},\mathbf{x'} \rangle} \mathbf{D}_{\mathbf{x},\mathbf{x'}} \cdot (\mathbf{S_x} \times \mathbf{S_{x'}}), \tag{4}$$

where $\mathbf{D}_{\mathbf{x},\mathbf{x'}}$ is the DMI vector. The DMI strength D is generally weaker than the exchange coupling [14]. Interchanging the two spins $\mathbf{x} \leftrightarrow \mathbf{x'}$ flips the sign of the Hamiltonian $\mathcal{H}_{\mathrm{DM}} \rightarrow -\mathcal{H}_{\mathrm{DM}}$, reflecting the asymmetry of the DMI. Both for noncentrosymmetric crystals without a centre of inversion and asymmetric thin films, noncollinear magnetic structures are stabilized by the DMI [51, 52]. Derrick was the first to propose that the exchange interaction and magnetic anisotropies are not adequate to stabilize a noncollinear magnetic configuration [53]. Rather, systems with such exotic features, like 2- and 3D localized magnetic vortices, are stabilized by the DMI [54]. Some phases, such as the skyrmion lattice in MnSi [55], cannot exist with only symmetric exchange and anisotropies present as it will not be thermodynamically stable. That DM interactions are more commonly encountered in antiferromagnets than ferromagnets [13, 14] is another argument for studying antiferromagnetic DMI stabilized phases which provides a richer and more fine-tuning assortment for applications.

There are typically two types of DMI to consider; bulk and interfacial DMI. The bulk DMI is experimentally shown to stabilize noncollinear magnetic textures in bulk magnets where the DMI vector is parallel to the position vector between neighbouring spins [55–57]. The other commonly encountered DMI, interfacial DMI, has the DMI vector perpendicular to the position vector joining adjacent spins. The latter is found in ultrathin films with sandwich structure comprising metallic layers with strong spin-orbit coupling and at surfaces with broken inversion symmetry [28, 58–62]. We refer to these in-plane types of DMI as the inhomogeneous DMI. If the DMI vector has a nonzero out-of-plane component, we call it the homogeneous DMI contribution. The names originate from the micromagnetic form of the DMI free energy arising from the different components, which we will come back to. Recently, is has been discovered that skyrmions in IrMn/CoFeB, a multilayer antiferromagnetic/ferromagnetic heterostructure, exist in the antiferromagnetic material at room temperature for a negative DMI constant and a left-handed chirality [44]. There

are no geometric constraints for the existence of the skyrmion phase, but there are constraints on the geometry for the heavy metal/ferromagnetic multilayers. As interfacial skyrmions are smaller than bulk type ones, and are experimentally observed, we henceforth restrict our study to systems with interfacial type DMI.

As for the symmetric exchange coupling, we consider a centred cubical two-dimensional lattice (x-y plane) in the exchange approximation of a slowly varying spin texture. The centred site belongs to sublattice α, while the four nearest neighbours belong to sublattice β. The in-plane interfacial DMI vector is orthogonal to the position vector joining two adjacent spins:

$$\begin{aligned} \mathbf{D}_{\mathbf{x},\mathbf{x}'=\mathbf{x}+\hat{y}} &= D\hat{x}, \\ \mathbf{D}_{\mathbf{x},\mathbf{x}'=\mathbf{x}+\hat{x}} &= -D\hat{y}, \end{aligned} \tag{5}$$

and zero otherwise. We sum only over the unit cells for one sublattice to avoid double-counting, and arrive at the inhomogeneous interfacial Hamiltonian

$$\mathcal{H}_{\mathrm{DM,inhom}} = \int \frac{d\mathbf{x}}{V} D\left((\hat{z}\cdot\mathbf{n})(\nabla\cdot\mathbf{n}) - (\mathbf{n}\cdot\nabla)(\hat{z}\cdot\mathbf{n})\right). \tag{6}$$

in the micromagnetic limit. The broken spatial inversion symmetry manifests from Eq. (6) as first order gradients of the order parameter are present. Its contribution to the free energy is spatially inhomogeneous, thereby the name. The DMI constant, which have been calculated for a wide range of surfaces, will depend upon the underlying symmetry of the system, as opposed to its symmetric counterpart [52]. The homogeneous DMI, with DMI vector $\mathbf{d}||\hat{z}$ and perpendicular to the basal plane, gives the interfacial DMI Hamiltonian

$$\mathcal{H}_{\mathrm{DM,hom}} = \int \frac{d\mathbf{x}}{V} \left(\mathbf{d}\cdot(\mathbf{m}\times\mathbf{n})\right). \tag{7}$$

This DMI does not hold any derivatives of neither the magnetization nor the Néel field, and its contribution is spatially homogeneous, so the name. For a full derivation of the homogeneous and inhomogeneous DMI, see Appendix A.2.

2.4 Magnetocrystalline anisotropy

Magnetocrystalline anisotropy favours the magnetization of a system to orient along certain crystallographic directions. For instance, cobalt, with hexagonal crystallographic structure, obtains stronger magnetization along the hexagonal axis under the

influence of a collinear external magnetic field, compared to other directions. For iron, which is cubical, the cube edges are the directions of which the magnetization reaches its maximum value, while for nickel it is the cube diagonals [63]. When a certain crystallographic direction is energetically favourable, it is called an easy-axis. Similarly, a direction of which is energetically unfavourable, is called a hard-axis.

We will only consider a phenomenological treatment here, as a full quantum mechanical approach is beyond the scope of the thesis. Also, we will only treat the anisotropy interactions through coupling constants and suppress any temperature dependence. The anisotropy Hamiltonian for localized spins $\mathbf{S}_\mathbf{x}$ at lattice site $\mathbf{x}$ is to lowest order

$$\mathcal{H}_{\text{aniso}} = \sum_{\mathbf{x}} K_{\text{aniso}} (\mathbf{S}_\mathbf{x} \cdot \hat{n})^2 \tag{8}$$

where a negative (positive) anisotropy parameter K_{aniso} yields an easy- (hard-)axis along $\hat{n}$. In general, the anisotropy parameter will not be constant, but vary as a function of temperature [64]. Easy (hard) planes are planes which tend to align (not align) the spins within them, where the direction in the plane is arbitrary. A combination of several planes and axes, both easy and hard, is also possible. $\hat{n}$ is the (local) direction dictated by the lattice structure which is energetically favourable for the spins to align with, which in principle could be position-dependent.

The magnetocrystalline anisotropy arises due to the coupling between the electric field induced by the ions and the magnetic moments of the electrons. From a microscopic point of view, the electric field experienced by the electrons introduces an anisotropy in the occupation of the orbitals and thereby an anisotropy in the orbital angular momentum of the electrons. By the spin-orbit coupling, the magnetic moment of the electrons will experience the same anisotropy, which is the magnetocrystalline anisotropy. The electron spins will align according to the direction being most energetically favourable, dictated by the crystal lattice [45, 65]. With the z-axis as the easy axis, allowing for biaxial anisotropy, the contribution to the micromagnetic free energy to leading order is

$$\mathcal{H}_{\text{aniso}} = -K_z \int \frac{d\mathbf{x}}{V} (\hat{z} \cdot \mathbf{n})^2. \tag{9}$$

with $K_z > 0$. We have assumed we are in the exchange approximation where $|\mathbf{m}| \ll |\mathbf{n}|$ and $J_s \gg K_z$.

2.5 Demagnetization

For spins $\mathbf{S}_\mathbf{x}$ located at lattice sites $\mathbf{x}$, the magnetostatic dipole-dipole interaction is incorporated similarly as for magnetic dipoles. The energy contribution is

$$\mathcal{H}_{\text{dipole}} = J_d \sum_{\mathbf{x}\neq\mathbf{x}'} \frac{\mathbf{S}_\mathbf{x}\cdot\mathbf{S}_{\mathbf{x}'}\, r_{\mathbf{x}\mathbf{x}'}^2 - 3(\mathbf{S}_\mathbf{x}\cdot\mathbf{r}_{\mathbf{x}\mathbf{x}'})(\mathbf{S}_{\mathbf{x}'}\cdot\mathbf{r}_{\mathbf{x}\mathbf{x}'})}{r_{\mathbf{x}\mathbf{x}'}^5}, \tag{10}$$

where $J_d > 0$ is the dipole coupling constant and $r_{\mathbf{x}\mathbf{x}'} = |\mathbf{x}-\mathbf{x}'|$ is the distance between spins at lattice sites $\mathbf{x}$ and $\mathbf{x}'$. The interaction between two dipoles scales as $\sim 1/r_{\mathbf{x}\mathbf{x}'}^3$, suggesting that the coupling should be rather short ranged. But, as the number of neighbours scales as distance cubed (or squared for 2D systems), the effect is cancelled, and the interaction is in fact long-ranged. For a large system, the above sum is quite hard to compute. Rather, in the micromagnetic limit of large occupation numbers, we would like to replace the sum over spins at discretely localized lattice sites by an integral where we instead consider the magnetization $\mathbf{m}$: $\sum_\mathbf{x}\big((...)\cdot\mathbf{S}_\mathbf{x}\big) \to \int d\mathbf{x}(...\cdot\mathbf{m})$. The total effective field due to the long-ranged dipole-dipole interactions at position $\mathbf{x}$ is the self-interacting demagnetization field $\mathbf{h}_d(\mathbf{x})$, which gives the energy contribution

$$\mathcal{H}_{\text{demag}} = -\int \frac{d\mathbf{x}}{V}\,(\mathbf{h}_\text{d}\cdot\mathbf{m}), \tag{11}$$

where we have incorporated the relevant prefactors in the field. The demagnetizing field will only for ellipsoidal geometries take a uniform value [66]. In a magnetic material, the demagnetizing field will try to encapsulate the magnetic field lines within the material. As a result, the field counteracts a spontaneous magnetization of the system and will be aligned (at least to a certain extent) antiparallel to the magnetization of the material.

For antiferromagnets, the dipole-dipole interactions are small because the net magnetization is close to zero. The magnetic moments in checkerboard pattern are already compensated by their neighbours because of the dominating exchange coupling. The demagnetization energy can thus be considered as a higher order correction to the free energy, similarly to quadratic terms in the magnetization arising from the Heisenberg exchange or the magnetocrystalline anisotropy [67].

2.6 Zeeman coupling

The Zeeman coupling is the interaction between a magnetic field and a body carrying a magnetic moment, which can be of both intrinsic (spin) and orbital nature. For an electron with intrinsic spin $\mathbf{S}$ in the presence of a magnetic field $\mathbf{H}$, the single spin Hamiltonian reads

$$\mathcal{H}_{\text{ZE}} = -\mathbf{S} \cdot \mathbf{H}, \tag{12}$$

where the prefactors related to the magnetic moment of the electron is absorbed into the external field which now has units of energy. For an ensemble of electrons, the total Hamiltonian is

$$\mathcal{H}_{\text{ZE}} = -\sum_{\mathbf{x}} \mathbf{S}_{\mathbf{x}} \cdot \mathbf{H}, \tag{13}$$

In the micromagnetic limit of a bulk magnetization, the spin of the electron is replaced with the local magnetization $\mathbf{m}(\mathbf{x}, t)$, and $\sum_i \to \int d\mathbf{x}/V$. The energy then reads

$$\mathcal{H}_{\text{ZE}} = -\int \frac{d\mathbf{x}}{V} (\mathbf{m} \cdot \mathbf{H}). \tag{14}$$

The Zeeman coupling tries to align the spin of the electron with the magnetic field by exerting a torque on it. This phenomena is utilized in several memory storage and reading devices through the giant magnetoresistance effect (GMR) [68], where the resistance is observed to substantially increase when applying a current through an antiparallel alignment of ferromagnetic layers [16, 17].

2.7 The antiferromagnetic free energy

The above-mentioned coupling mechanisms will be the main constituents in the antiferromagnetic free energy we will consider for the thesis. The free energy is to be invariant under sub-lattice exchange and respect rotational invariance of the spin vectors [48, 69]. With these requirements, the total antiferromagnetic free energy takes the form

$$\begin{aligned} \mathcal{F} = \int \frac{d\mathbf{x}}{V} \Big(& A(\partial_i \mathbf{n})^2 + a\mathbf{m}^2 - K_z(\mathbf{n} \cdot \hat{z})^2 - 2\mathbf{m} \cdot \mathbf{H} + 2\mathbf{d} \cdot (\mathbf{m} \times \mathbf{n}) \\ & + D\big((\hat{z} \cdot \mathbf{n})(\nabla \cdot \mathbf{n}) - (\mathbf{n} \cdot \nabla)(\hat{z} \cdot \mathbf{n})\big)\Big). \end{aligned} \tag{15}$$

We have re-scaled some of the interaction constants to smooth the notation for the remaining part of the thesis. The apparent parity-breaking exchange terms from the symmetric Heisenberg coupling are disregarded, and the free energy respects $C_{n\nu}$ symmetry.

3

Chiral antiferromagnetic textures

In the previous chapter we discussed some of the most fundamental interaction mechanisms and the resulting free energy functional of an antiferromagnetic system. The interaction parameters span a multidimensional parameter space. In different regions in the space of parameters, different antiferromagnetic phases exist. In this chapter we start with the trivial antiferromagnetic ground state, and quickly increase the level of complexity by considering chiral structures.

3.1 The homogeneous antiferromagnetic ground state

For both ferromagnetic and antiferromagnetic materials, a uniform order parameter (the Néel field for antiferromagnets and the magnetization for ferromagnets) corresponds to an exchange dominated free energy minima. The antiferromagnetic ground state takes a homogeneous distribution $\mathbf{n} = \hat{z}$, while the magnetization is identically zero: $\mathbf{m} = 0$. The arrangement of the magnetic moments in the ground state for both ferromagnetic and antiferromagnetic materials is shown in Figure 1. The antiferromagnetic ground state is shown as a linear chain with neighbouring spins being antiparallel. The staggered magnetization in the antiferromagnetic ground state takes the same distribution as the magnetic moments in the ferromagnetic ground state. The antiferromagnetic ground state ordering in a higher dimensional lattice can be degenerate, depending on the lattice symmetry. After Louis Néel first addressed the antiferromagnetic nature of substances consisting of ferromagnetic elements to the local molecular field and the exchange interaction, the antiferromagnetic ground state energies and wave functions became hot topics of theoretical interest [70, 71].

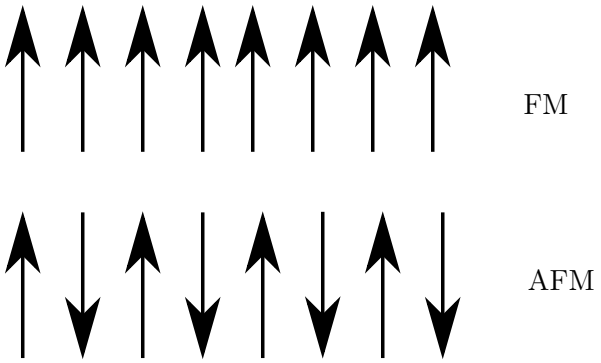

Figure 1: The homogeneous ferromagnetic, abbreviated FM, and antiferromagnetic, abbreviated AFM, ground states. The arrows indicate the orientation of nearest neighbour magnetic moments. The antiferromagnetic order parameter, the staggered magnetization, will take on an identical distribution as the magnetization in a ferromagnetic system in the ground state (top picture).

Despite the gloomy future predicted by Néel in his Nobel lecture in 1970 for the feasibility of using antiferromagnets in applications [72], detecting antiferromagnetic ground states in materials is now a popular area of research [73, 74].

If we start perturbing the antiferromagnetic ground state by an external magnetic field, or there are several intrinsic interaction mechanisms present, we move from the region in phase space where the antiferromagnetic order is the stable configuration into regions with less trivial stable arrangements. One of those phases are the chiral domain walls and skyrmions, which we will have a closer look at.

3.2 Domain walls

The subtle interplay of different energy contributions in Eq. (15) makes it energetically favourable for the order parameter to take on a non-uniform distribution. The exchange coupling is by far the strongest, and favours a uniform alignment of the spins in both sub-lattices, with the magnetization in each sublattice opposite to the other, $\mathbf{M}_\alpha = -\mathbf{M}_\beta$. For spins far apart, the exchange interaction is negligible

as it drops off quickly when increasing the distance and is only present as a weak chain effect. In a ferromagnetic material where the order parameter is the magnetization, an energy penalty emerges for domain-free spin structures. The demagnetizing, long-ranged dipole-dipole interactions tries to reduce the overall magnetization. As a result, the conflicting interests prevents a uniform magnetization of the material. Instead, a compromise consisting of domains with noncollinear magnetic moments to reduce the total magnetization and at the same time preserve the local collinearity of the spins without too much frustration are established [75, 76]. For an antiferromagnetic material, however, the sub-lattice magnetizations are already compensated, so ideally there should be no need to introduce energy penalties by splitting up into domains with noncollinear orientation of the staggered magnetization. The dipole-dipole interactions reducing the overall magnetization is irrelevant. Domain walls are thermodynamically stable, but the entropy gain cannot compensate the energy cost for splitting up into domains. One of the mechanisms that can be (partially) responsible for the domain formation are magnetoelastic forces [77], induced by material imperfections as dislocations and grain boundaries [78].

The region where the order parameter spatially reorient is called the domain wall, with a characteristic width λ_{DW}. These are planar defects [48], meaning the reorientation takes place along one spatial direction only. The width of this region is determined by the relative strength of the anisotropy and the exchange interaction. For the sake of argument, consider a 180° rotation between two domains with an easy-axis along $\hat{z}$. A slowly varying texture will reduce the exchange energy cost of the domain wall. On the contrary, the easy-axis anisotropy favours a reduced spatial extension of the wall such that the area of a noncollinear order parameter with the preferred crystallographic direction is reduced. If the order parameter rotates helically around the axis connecting the two domains, it is called a Bloch wall, and if it rotates around the out-of-plane axis, it is called a Néel wall, pictured in Figures 2 and 3, respectively. The type of rotation is dictated by the symmetry group of the system considered [48].

If the material considered instead was ferromagnetic, and the arrows were indicating the rotation of the magnetization, we observe that domain walls induce magnetic surface charges σ_m on the edges. The Néel configuration will have surface charges on the planes with unit normal $\pm\hat{x}$ and the Bloch type will have surface charges on the planes with unit normal $\pm\hat{y}$. The net stray field generated by sur-

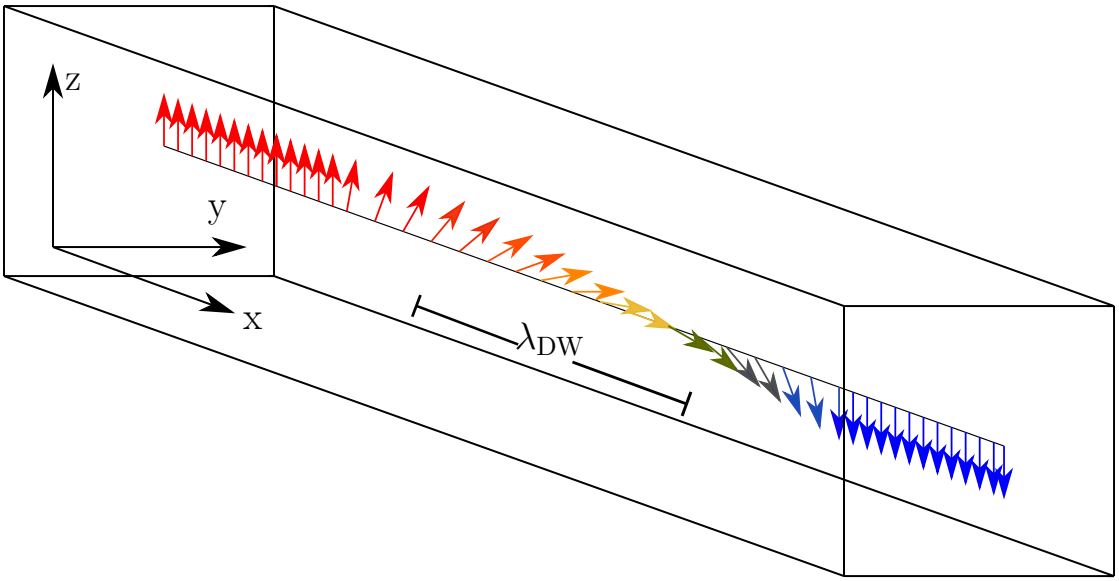

Figure 2: An antiferromagnetic Néel wall configuration. The colour of the arrows reflects the orientation of the staggered magnetization with respect to the z-axis. Red arrows are parallel to the z-axis, blue arrows are antiparallel. The order parameter rotates cycloidally when moving from one domain with staggered magnetization $+\hat{z}$ to the other domain with staggered magnetization $-\hat{z}$. λ_{DW} is a typical length scale for the width of the domain wall.

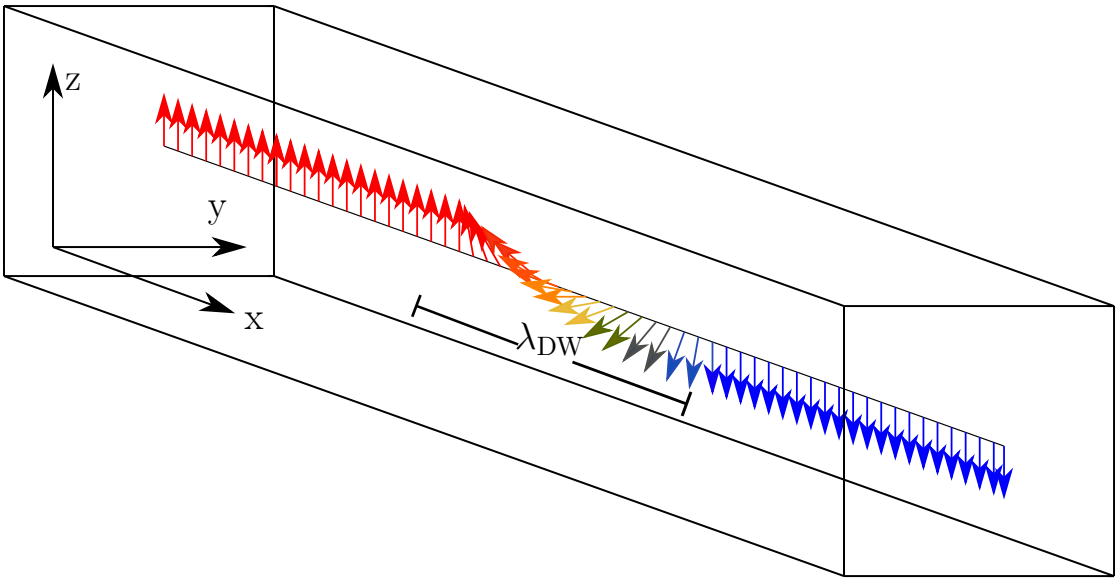

Figure 3: An antiferromagnetic Bloch wall configuration. The colour of the arrows reflects the orientation of the order parameter with respect to the z-axis; blue arrows indicate when the order parameter $\mathbf{n}$ is antiparallel to $\hat{z}$, while the red arrows show $\mathbf{n}$ parallel to $\hat{z}$. The order parameter rotates helically when moving from one domain with $\mathbf{n} = +\hat{z}$ to the other domain with $\mathbf{n} = -\hat{z}$. λ_{DW} is a typical length scale for the width of the domain wall.

face charges put up an energy penalty which is not present in an antiferromagnetic material as it is the compensated staggered magnetization that reorients [32].

3.3 Skyrmions

For a magnetic field parallel to $\hat{z}$, the original Hamiltonian leading to the free energy in Eq. (15) is invariant under rotations about this axis of symmetry [48]. Excitations of the staggered magnetization answering this basal plane symmetry inherit vortex structure. Such 2D, both delocalized and, more recently, localized structures have been experimentally observed [44, 79]. The delocalization of the vortices reflects the ambiguous orientation of the staggered magnetization far from the vortex core. For a vortex, the staggered magnetization is parallel to the axis of symmetry at the core and lies in the basal plane far from the centre orthogonal to the local azimuthal direction. Localized vortices, or skyrmions, are excitations where the staggered magnetization undergoes a rotation of 180° from the centre to the rim of the skyrmion. An illustration of a staggered magnetization configuration for a cylindrically symmetric skyrmion is provided in Figure 4.

Skyrmions, or the skyrmion lattice phase, is a topological stable magnetic excitation of a material. The presence of skyrmions in spintronics and condensed matter physics is a derivation from the original introduction to theoretical physics proposed by Skyrme in 1962 [81]. He found that topologically protected irregularities in field theory respect particle-like behaviour and properties such as (topological) charges and phase transitions. The concept of skyrmions has been adapted widespreadly in a vast amount of fields in physics, like quantum Hall phenomena [82], Bose-Einstein condensates [83] and chiral vortex-like magnetization excitations [55]. After attaining more theoretical and numerical attention in magnetic materials through the 1990s [84, 85], the first experimental evidence of the existence of such a phase was reported in 2009 [55]. The skyrmion phase was detected in a ferromagnetic antisymmetric bulk magnet without a centre of inversion. More recently, it has been identified in thin magnetic nanostructures too [25], and finally in antiferromagnetic thin film structures [44]. Typical for these types of materials is the presence of the asymmetric DMI, either bulk type or interfacial in the case of thin multilayers, inducing vortex-like spin textures. In the limit of zero DMI, the Hamiltonian resemble the non-linear sigma model [86], where such structures are thermodynamically unstable and collapses when subject to magnetocrystalline anisotropies or magnetic fields [54,

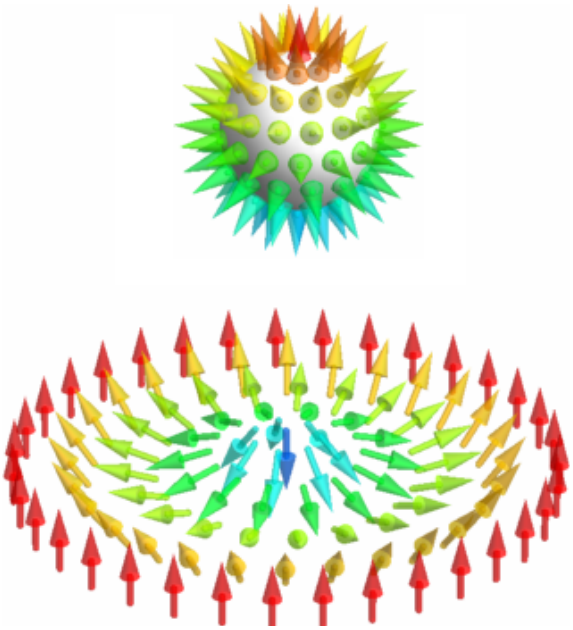

Figure 4: The Néel-type skyrmion stabilized by the interfacial DMI. The lower figure shows the spatial orientation of the staggered magnetization. It is cylindrically symmetric, with the order parameter pointing down in the core and up at the edge. The upper inset shows how the staggered magnetization maps onto the unit sphere taking a hedgehog-like configuration. The figure is reproduced with permission from Ref. [80].

84, 87]. Hence, the DMI is necessary to stabilize the skyrmions.

The stability of skyrmions is encoded in their topology. The order parameter (the magnetization for ferromagnetic systems and the staggered magnetization for antiferromagnetic systems) cannot be smoothly deformed into other stable configurations due to its topological features. We assign to this a topological number (or charge), known as the skyrmion number, which is the number of times the order parameter maps the unit sphere. In the micromagnetic limit for a skyrmion in the $x-y$ plane, it is defined similarly for both ferromagnetic and antiferromagnetic systems in terms of the appropriate order parameter [32, 88]:

$$N_{sk} = -\frac{1}{4\pi}\int d\mathbf{x}\left(\mathbf{n}\cdot(\partial_x\mathbf{n}\times\partial_y\mathbf{n})\right) \tag{16}$$

Also, we can assign a topological charge to each sublattice, where the staggered magnetization in Eq. (16) is replaced by the sublattice magnetization [88]. Then, $N_{sk,\alpha} = -N_{sk,\beta} = 1$, establishing the topological protection.

We will consider skyrmions localized in the $x-y$ plane. The cylindrical symmetry of the skyrmions suggests that the polar angle Θ of the staggered magnetization only contains a radial dependence and no azimuthal dependence: $\Theta = \Theta(r)$. The next assumption to make is that the azimuthal angle Φ of the spins is solely dependent on the azimuthal angle ϕ of their in-plane position vector: $\Phi = \Phi(\phi)$. The latter allows for different vorticity of the skyrmions. By this ansatz, the staggered magnetization $\mathbf{n}(\mathbf{x})$ is parameterized as

$$\mathbf{n}(\mathbf{x}) = (\sin\Theta(r)\cos\Phi(\phi), \sin\Theta(r)\sin\Phi(\phi), \cos\Theta(r)). \tag{17}$$

.

In addition to the skyrmion number, two other characteristics of the skyrmions are necessary to fully describe them: the above-mentioned vorticity and the helicity. While the vorticity is directly related to the skyrmion number, the helicity is determined by the type of DMI. The vorticity m is defined as

$$m = \frac{\Big[\Phi(\phi)\Big]_0^{2\pi}}{2\pi}, \tag{18}$$

and is the integer number of rotations the staggered magnetization projected onto the $x-y$ plane, i.e. the in-plane component, circumvents the out of-plane axis when

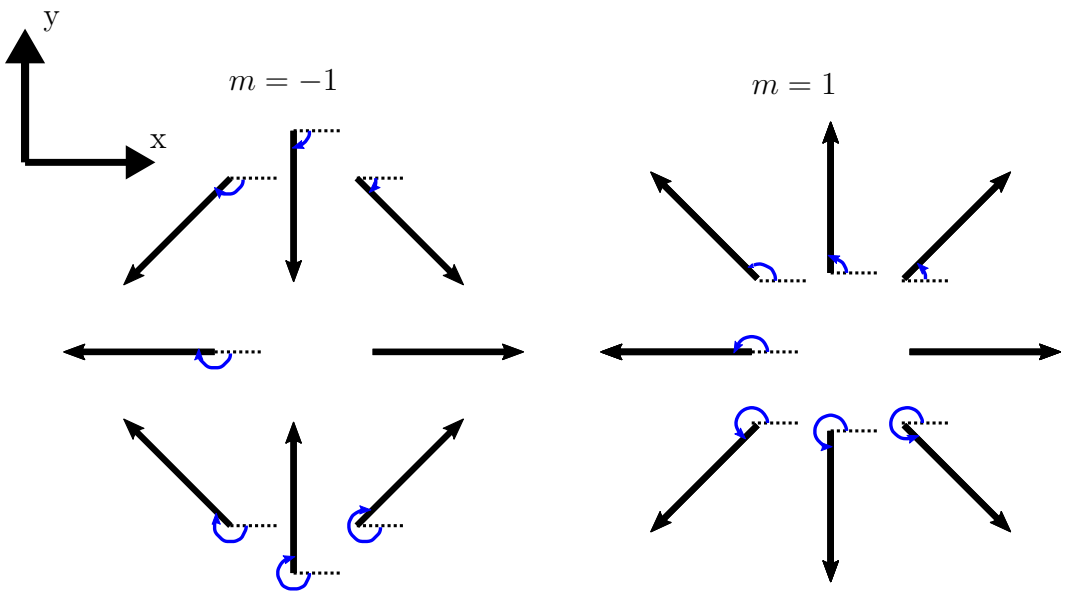

Figure 5: The in-plane component of the staggered magnetization for two skyrmions of vorticity $m = -1$ to the left, and vorticity $m = 1$ to the right. When moving clockwise around $\hat{z}$, the in-plane component rotates clockwise for $m = -1$ and counter-clockwise for $m = 1$.

rotating in the $\hat{\phi}$-direction. A clockwise rotation of the component yields $m < 0$ and a counter-clockwise rotation of the component yields $m > 0$. This is illustrated in Figure 5.

The helicity γ is defined by

$$\Phi(\phi) = m\phi + \gamma, \tag{19}$$

and its value will be determined by minimizing the DMI energy of the skyrmion. Using this ansatz, following Nagaosa and Tokura [9], we will compute the skyrmion number and the DMI energy to see which configurations of m and γ are possible.

Carrying out the cross-product according to Eq. (16) and dotting the resultant vector with $\mathbf{n}$ gives

$$\mathbf{n} \cdot (\partial_x \mathbf{n} \times \partial_y \mathbf{n}) = \frac{1}{r} \frac{\mathrm{d}\Theta}{\mathrm{d}r} \frac{\mathrm{d}\Phi}{\mathrm{d}\phi} \sin\Theta. \tag{20}$$

Integrating the above result over the area of the skyrmion in the limit $r \to \infty$ and using the definition of the vorticity we get

$$N_{sk} = \frac{m}{2}\left[\cos\Theta(r)\right]_{r=0}^{r=\infty}. \tag{21}$$

Now the close relation between the skyrmion number and the vorticity is clear. If we take the skyrmion to have spin down at its centre, $\theta(0) = \pi$ and spin up at its boundary, $\theta(r \to \infty) = 0$, we find $N_{sk} = m$. Oppositely, with spin up in the centre and spin down at the boundary, we get $N_{sk} = -m$.

If we compute the DMI energy density, we find for the interfacial case using Eq. (6)

$$h_{\text{int}} = D\cos\left((m-1)\phi + \gamma\right)\Big(\frac{\mathrm{d}\Theta}{\mathrm{d}r} + \frac{m}{2r}\sin\left(2\Theta\right)\Big). \tag{22}$$

If $m \neq 1$, both terms in Eq. (22) give zero contribution to the energy after integration over ϕ due to the orthogonality of the trigonometric system. Therefore, $m = 1$ is necessary to obtain a minima in this case. Minimization of the energy is then obtained for $\gamma = 0, \pi$. Under the assumption of $D > 0$, the only remaining factor influencing the energy density is the profile of Θ, and whether its derivative positive or negative. Explicitly, for the interfacial case we can have the two stable configurations $\gamma = 0$ and spin down at core and spin up at boundary ($d\Theta/dr < 0$) or $\gamma = \pi$ with spin up at the core and spin down at the boundary ($d\Theta/dr > 0$). In Figure 6, we show the in-plane orientation of the staggered magnetization for different helicites. We have included $\gamma = \pm\pi/2$, which correspond to unstable configurations for this type of DMI.

The remaining part to determine is the radial profile of the skyrmion: $\Theta(r)$. It can be done by seeking the minima of the free energy of the antiferromagnetic system in Eq. (15). The minima is obtained with claiming zero variation of the free energy. The resulting Euler-Lagrange equation for Θ yields

$$\frac{\mathrm{d}^2\Theta}{\mathrm{d}\rho^2} + \frac{1}{\rho}\frac{\mathrm{d}\Theta}{\mathrm{d}\rho} - \frac{\sin\Theta\cos\Theta}{\rho^2} + \frac{4D}{\pi D_0}\frac{\sin\Theta^2}{\rho} - \Big(1 - \frac{H^2}{H_0^2}\Big)\sin\Theta\cos\Theta = 0, \tag{23}$$

with $\rho = r/x_0$, $x_0 = \sqrt{A/K_z}$, $H_0 = \sqrt{aK_z}$ and $D_0 = 4\sqrt{AK_z}/\pi$. D_0 is the critical value of the inhomogeneous DMI which stabilizes the skyrmion, H_0 is the spin-flop field and x_0 is a typical length scale of the skyrmion [69]. We solve the equation with boundary conditions $\Theta(0) = \pi, \Theta(\infty) = 0$, using a shooting method with a 5^{th} order explicit Runge-Kutta integration routine and the secant method. The profile for

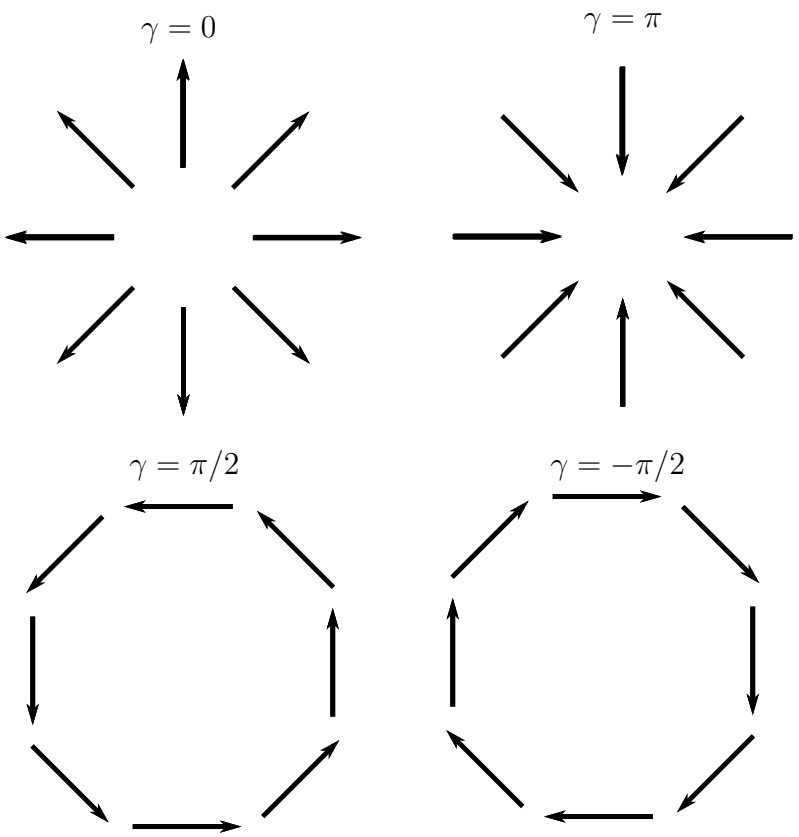

Figure 6: The in-plane staggered magnetization component for skyrmions of different helicity. The two upper are thermodynamically stable configurations showing hedgehog-like structure, while the two lower ones are unstable with vortex-like structure. They will be stable phases for a different system symmetry.

$D/D_0 = 0.9, H/H_0 = 0.3$ is shown in Figure 7. If we increase the external magnetic field to exceed the spin-flop field, the antiferromagnetic order is destroyed and the spins start to flip to align with the strong external magnetic field. In this region of parameter space, the sublattice magnetization is no longer compensated yielding a nonzero total magnetization.

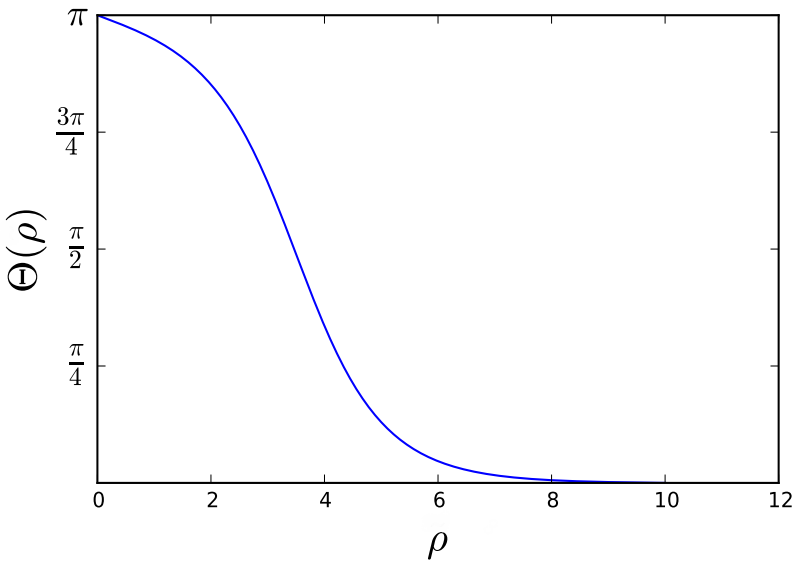

Figure 7: The radial profile of the staggered magnetization for an antiferromagnetic skyrmion. The profile is dictated by the differential equation Eq. (23), corresponding to a minima of the antiferromagnetic free energy functional comprised by symmetric exchange coupling, inhomogeneous DMI, easy-axis anisotropy and an external magnetic field. Θ is the angle between the staggered magnetization and $\hat{z}$, subject to boundary condition $\Theta(0) = \pi, \Theta(\infty) = 0$, where the latter condition is implemented by a shooting routine. The parameter choice is $D/D_0 = 0.9, H/H_0 = 0.3$.

4

Antiferromagnetic spin wave dynamics

So far, we have treated time-independent antiferromagnetics in terms of interaction mechanisms, material properties, phases and textures. In this chapter, we will explore the dynamical properties of antiferromagnets. The dynamics play a crucial part in a wide spectra of novel application prospects [24, 49, 57, 89]. We mainly focus on the collective excitation of the spins resembling a spin wave in the large occupation number limit. To motivate for dynamical excitations, we start with a quantum mechanical introduction, before considering the micromagnetic limit of spin waves and look at the dispersion relation around the homogeneous antiferromagnetic ground state. Finally, we derive a new set of equations describing spin wave excitations around an inhomogeneous chiral soliton.

4.1 The equations of motion for the order parameter and the magnetization

From a quantum mechanical point of view, the time evolution of the expectation value of an observable F, $\langle F \rangle$, is governed by the equation

$$i\hbar \frac{d\langle F \rangle}{dt} = \Big\langle [F, \mathcal{H}] \Big\rangle + i\hbar \frac{\partial \langle F \rangle}{\partial t}, \tag{24}$$

where $[F, \mathcal{H}]$ is the commutator of F and the Hamiltonian $\mathcal{H}$. For the time-independent spin operator $\mathcal{S}$ in the presence of a magnetic field $\mathbf{H}$ (with units of energy), we find for the z-component according to Eqs. (12) and (24)

$$i\hbar \frac{d\langle S_z \rangle}{dt} = \big\langle -[S_z, S_i H_i] \big\rangle, \tag{25}$$

Now, using the commutation relations for the spin operators (taken to be dimensionless) $[S_x, S_y] = iS_z$ with cyclic permutation, the time evolution of S_z reads

$$\frac{d\langle S_z\rangle}{dt} = \left\langle -\frac{1}{\hbar i}(iH_xS_y - iH_yS_x)\right\rangle = \frac{1}{\hbar}(\langle \mathbf{S}\rangle \times \mathbf{H})_z, \tag{26}$$

The magnetization $\mathbf{m}_\alpha$ of a (sub)lattice α can be defined as the expectation value of the spins. Thus, Eq. (26) describes precessional motion of the magnetization around some magnetic field. Denote that Eq. (26) upon treating the magnetization as the expectation value of the spins, conserves the magnitude of the magnetization. This is obtained by noting that for the magnitude to be conserved ($\mathbf{m}_\alpha^2 = 1$), we need $\dot{\mathbf{m}}_\alpha = \mathbf{\Omega} \times \mathbf{m}_\alpha$. Then, $\frac{d(\mathbf{m}_\alpha^2)}{dt} \propto \mathbf{m}_\alpha \cdot (\mathbf{\Omega} \times \mathbf{m}_\alpha) = 0$, as required. $\mathbf{\Omega}$ is the angular velocity of the magnetization. A slow dynamics approximation is captured by excluding possible higher order time-derivatives [15].

Phenomenologically, magnetic moments are known to align with the present effective field (like a compass needle does with the Earth's magnetic field) [90]. The torque Eq. (26) above cannot induce such motion. This was the motivation for Landau and Lifschitz to introduce a damping term in the equation of motion for the magnetization to obtain a more realistic equation:

$$\frac{d\mathbf{m}_\alpha}{dt} = -\frac{1}{\hbar}\mathbf{m}_\alpha \times \mathbf{H} - \frac{\alpha}{\hbar}\mathbf{m}_\alpha \times (\mathbf{m}_\alpha \times \mathbf{H}). \tag{27}$$

The Landau-Lifschitz (LL) equation above gives damped precessional motion around the effective magnetic field $\mathbf{H}$, as shown in Figure 8 for the magnetization $\mathbf{m}_\alpha$. Later, Gilbert conducted experiments on ferromagnetic sheets where he observed that the precessional damping will be material dependent. Thus, a modification of the LL equation is the Landau-Lifschitz-Gilbert equation

$$\frac{d\mathbf{m}_\alpha}{dt} = -\frac{1}{\hbar}\mathbf{m}_\alpha \times \mathbf{H} + \alpha_G \mathbf{m}_\alpha \times \frac{d\mathbf{m}_\alpha}{dt}. \tag{28}$$

The LLG equation follows directly from the LL equation under the substitution $\hbar \to \hbar(1+\alpha_G^2)$ and $\alpha/\hbar \to \alpha_G/(\hbar(1+\alpha_G^2))$ in the original LL equation. α_G is the Gilbert damping factor, which is a material dependent parameter [91]. The form of the damping term resembles that obtained from a generic Rayleigh dissipation function used to introduce friction in the Lagrange formalism. Originally, it was the gyromagnetic ratio and not the inverse of the Planck constant that was used as prefactor in front of the vector products. With our definition of the magnetic field, we use $\hbar$ to retain consistency of units.

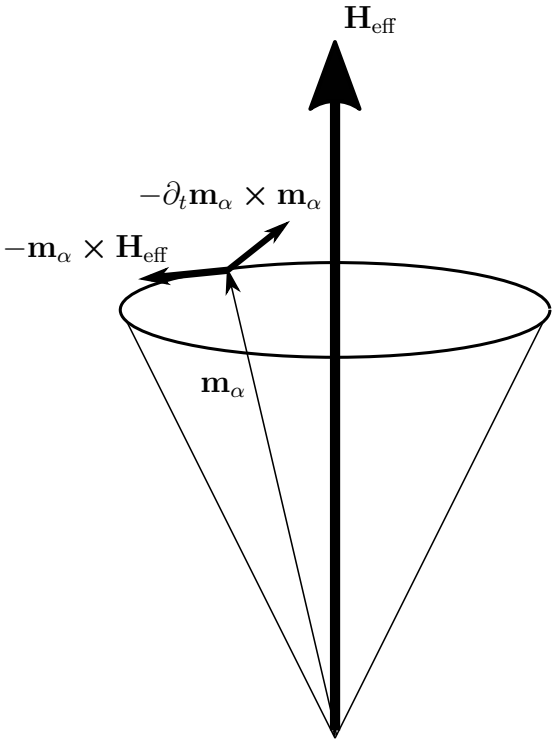

Figure 8: Precession of the magnetization $\mathbf{m}_\alpha$ around some effective field $\mathbf{H}_{\text{eff}}$. The term $-\mathbf{m}_\alpha \times \mathbf{H}_{\text{eff}}$ shows the change in magnetization without damping. $-\partial_t \mathbf{m}_\alpha \times \mathbf{m}_\alpha$ is the Gilbert damping term, which acts as a torque on $\mathbf{m}_\alpha$ trying to align it with the effective field. This causes a damped precession, where the magnetization spirals towards the orientation of the effective field. The illustration is based on figure 2, chapter 1 in Ref. [90].

A more general starting point when deriving the LLG equation is to adapt a full Lagrangian formalism and derive it from an action principle. This was first done by Döring for ferromagnets [92]. However, in multi-sublattice substances such as antiferromagnets the story is different. When we have two sublattices α, β, the dynamics of each sublattice is described by the LLG Eq. (28), and the effective field is $\mathbf{H}_{\alpha(\beta)} = \frac{\partial \mathcal{F}}{\partial \mathbf{m}_{\alpha(\beta)}}$, respectively. The damping parameter α_G is assumed to be identical for the two sublattices, despite the complex relaxation mechanisms and the inter-sublattice couplings present in magnetic materials [93].

In spite of the opportunity of evaluating the dynamics of two sublattices in an antiferromagnet, it is more convenient to look at the staggered magnetization $\mathbf{n}$ and the magnetization $\mathbf{m}$, and their respective dynamics. We obtain these new equations of motion from a variational principle using the free energy functional in Eq. (15) which we already have written in the generalized coordinates $\mathbf{q} = (\mathbf{n}, \mathbf{m})$. We apply Hamilton's principle on the Euclidian action $\mathcal{A} = \int dt\, L(\{\mathbf{q}_i, \dot{\mathbf{q}}_i\}, t)$ where $L(\{\mathbf{q}_i, \dot{\mathbf{q}}_i\}, t) = \mathcal{K} - \mathcal{F}$ is the Lagrangian described by the set of general coordinates $\{\mathbf{q}_i, \dot{\mathbf{q}}_i\}$, $\mathcal{K}$ is the kinetic energy and $\mathcal{F}$ is the free energy. Henceforth we will disregard dissipational terms and spin torque terms under the assumption of the material being insulating.

The kinetic term arising quantum mechanically from the Berry phase is deeply rooted to the vector potential of a magnetic monopole. As a full treatment of this is beyond the scope of the thesis, we will not elucidate the topic any further, and refer to Refs. [94–96] for a rigorous treatment. In the micromagnetic limit, the kinetic term reads [50]

$$\mathcal{K} = 2\hbar \int d\mathbf{x} \big(\mathbf{m} \cdot (\dot{\mathbf{n}} \times \mathbf{n}) \big). \tag{29}$$

The equations of motion for the magnetization and the Néel vector are obtained by variation of the action $\delta_{\mathbf{q}} \mathcal{A} = 0$ with respect to $\mathbf{q} = (\mathbf{n}, \mathbf{m})$. We obtain a coupled set of equations of motion for the magnetization and the order parameter:

$$\dot{\mathbf{n}} = \frac{1}{2\hbar} \mathbf{n} \times \frac{\delta \mathcal{F}}{\delta \mathbf{m}}, \tag{30}$$

$$\dot{\mathbf{m}} = \frac{1}{2\hbar} \mathbf{n} \times \frac{\delta \mathcal{F}}{\delta \mathbf{n}} + \frac{1}{2\hbar} \mathbf{m} \times \frac{\delta \mathcal{F}}{\delta \mathbf{m}}, \tag{31}$$

where we have made use of the orthogonality properties of $\mathbf{n}$ and $\mathbf{m}$. Eqs. (30) and (31) are the antiferromagnetic counterparts to the single-lattice LLG equation, and are the main tools we need to study antiferromagnetic spin waves.

When carrying out the functional derivative of the free energy and the cross products, we find from Eq. (30)

$$\mathbf{m} = \frac{\hbar}{a}\dot{\mathbf{n}} \times \mathbf{n} - \frac{1}{a}\mathbf{n} \times (\mathbf{n} \times \mathbf{H}) - \frac{1}{a}\mathbf{n} \times \mathbf{d}. \tag{32}$$

We denote that the magnetization is in fact a slave variable of the order parameter, and both its static and dynamic behaviour is fully dictated by $\mathbf{n}$. The static equilibrium solution to the equation above, $\mathbf{m}_0$, is given by

$$\mathbf{m}_0 = -\frac{1}{a}\mathbf{n} \times (\mathbf{n} \times \mathbf{H}) - \frac{1}{a}\mathbf{n} \times \mathbf{d} \tag{33}$$

which yields a nonzero magnetization even in the absence of external perturbations canting the sublattices with respect to each other [69]. In the absence of an external magnetic field and the homogeneous DMI, the magnetization is identically zero. Still, a noncollinear staggered magnetization is possible. As the magnetization is fully dictated by the order parameter as it slowly tracks the variations of the Néel vector captured by the temporal first order derivative, we can construct an equation with only the order parameter being the unknown variable.

4.2 Spin waves

We can separate the magnetization dynamics into two regimes in what concerns how the amplitude of the order parameter varies. For instance, in ferromagnetic materials with large amplitude oscillations, we observe phenomena such as coherent magnetization reversal in single-domain magnets [97] and ultrafast precessional magnetization reversal in soft nanomagnets [98]. In antiferromagnetic multiorbital systems excited by lasers, we also find large amplitude oscillations of the order parameter, originating from the Coulomb interaction [99].

The other limit, which we will consider, is the small amplitude oscillation limit. Such oscillations can manifest by various perturbation mechanisms. A perpendicularly injected spin current can for instance excite an anisotropic easy-plane antiferromagnetic bi-layer of Pt and NiO to the THz-regime by the spin-transfer torque,

which effect (surprisingly) does not cancel by the compensation of the two sublattices [100]. Other excitation techniques demonstrated are oscillating magnetic fields in Dzyaloshinskii-Moriya coupled easy-axis antiferromagnetic field effect transistors [101] and temperature gradients in synthetic multilayered sandwich structures in antiferromagnetic thin films [102].

Formally, we treat this by splitting the order parameter $\mathbf{n}(\mathbf{x}, t)$ into time-dependent small excitations $\delta\mathbf{n}_\perp(\mathbf{x}, t)$ around some static equilibrium texture $\mathbf{n}_0(\mathbf{x})$:

$$\mathbf{n}(\mathbf{x}, t) = \mathbf{n}_0(\mathbf{x}) + \delta\mathbf{n}_\perp(\mathbf{x}, t). \tag{34}$$

The equilibrium part is determined by the minimization of the system free energy, and can be both homogeneous and position-dependent, as discussed in Chapter 3. Small amplitude deviations means that the magnitude of the excitation field is much smaller than the background texture: $|\delta\mathbf{n}_\perp| \ll |\mathbf{n}_0|$. Also, to first order, the deviations are orthogonal with respect to the equilibrium configuration: $\mathbf{n}_0(\mathbf{x}) \perp \delta\mathbf{n}_\perp(\mathbf{x}, t)$. In the micromagnetic limit of a large occupation number they resemble a spin wave [15], illustrated in Figure 9. The arrows symbolizing the staggered magnetization precess with a fixed phase around $\hat{z}$ with a wavelength λ_{sw}. These spin waves, or magnons, are particle-like excitations of the spin configuration, just like phonons are quantized thermal vibrations of the lattice, with a quantized linear and angular momentum. The angular momentum of the magnons are $\hbar$, meaning they are spin-1 particles subject to Bose statistics [64].

Spin waves incident on a soliton texture transfers linear and angular momentum inducing soliton dynamics unless the pinning potential is strong enough to suppress the motion. The soliton dynamics, typically governed by a variation of the Thiele equation, has been an on-going topic of research for a while, including both skyrmions, domain walls and vortices [36, 49, 69, 103, 104]. We are mainly interested in the reactive part of the soliton-magnon interactions, namely the influence of the soliton on the magnons. When entering a region of a noncollinear texture, the effective potential felt by the magnons is altered, and scattering phenomena and magnon trapping can take place.

To obtain the equation of motion for the spin waves, we substitute in our ansatz Eq. 34 into the equations of motion Eqs. (30) and (31) after deriving the effective forces $\frac{\delta\mathcal{F}}{\delta\mathbf{n}}, \frac{\delta\mathcal{F}}{\delta\mathbf{m}}$. After some tedious manipulations we find

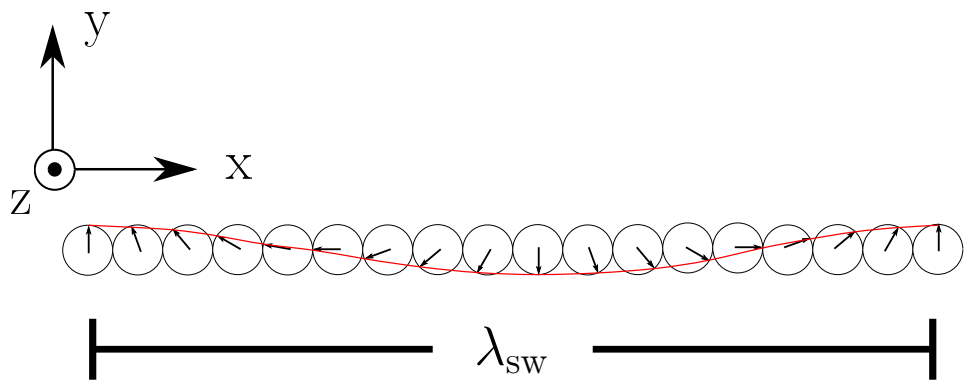

Figure 9: A visual representation of a spin wave comprised by strongly coupled spins. The red line shows the wave behaviour of the precessional motion of the order parameter, which we have taken to be aligned with $\hat{z}$, while the black arrows show the small deviations $\delta\mathbf{n}_\perp(\mathbf{x},t)$, which are orthogonal to the static equilibrium. The precession is counter-clockwise with a given wavelength λ_{sw}. The figure is inspired by figure 11.5 in Ref. [64].

$$\begin{aligned}\frac{\hbar}{a}\delta\ddot{\mathbf{n}}_\perp = &\frac{1}{\hbar}A\nabla^2\delta\mathbf{n}_\perp - \frac{1}{\hbar}A\delta\mathbf{n}_\perp(\nabla^2\mathbf{n}_0\cdot\mathbf{n}_0) - \frac{1}{\hbar}K_z(\mathbf{n}_0\cdot\hat{z})^2\delta\mathbf{n}_\perp + \frac{1}{\hbar}K_z(\delta\mathbf{n}_\perp\cdot\hat{z})\hat{z}\\ &+\frac{1}{\hbar}D(\nabla\cdot\mathbf{n}_0)(\mathbf{n}_0\cdot\hat{z})\delta\mathbf{n}_\perp - \frac{1}{\hbar}D(\nabla\cdot\delta\mathbf{n}_\perp)\hat{z} - \frac{1}{\hbar}D((\nabla(\hat{z}\cdot\mathbf{n}_0)\cdot\mathbf{n}_0)\delta\mathbf{n}_\perp\\ &+\frac{1}{\hbar}D\nabla(\hat{z}\cdot\delta\mathbf{n}_\perp) + \frac{2}{a}\mathbf{n}_0\times\delta\dot{\mathbf{n}}_\perp(\mathbf{H}\cdot\mathbf{n}_0) + \frac{1}{a}\mathbf{n}_0\times\delta\mathbf{n}_\perp(\dot{\mathbf{H}}\cdot\mathbf{n}_0) + \frac{1}{\hbar a}(\mathbf{H}\cdot\mathbf{n}_0)^2\delta\mathbf{n}_\perp.\end{aligned} \tag{35}$$

We have disregarded all terms that are higher order in the excitation fields as we are only interested in the equation of motion to first order in the deviations. Furthermore, we have disregarded all terms that are of zeroth order in the excitation field. The reason is that the solution $\delta\mathbf{n}_\perp(\mathbf{x},t) = 0$ is a perfectly allowed solution, both physically and mathematically, which means that in the limit of zero spin wave excitations, the zeroth order terms combine to zero to lowest order. We have made use of the orthogonality property of $\delta\mathbf{n}_\perp(\mathbf{x},t)$ and $\mathbf{n}_0$. For the derivation, see Appendix B. This is the full equation of motion for spin wave excitations to first order around a static texture stabilized by an interfacial-like DMI in the presence of an external, time-dependent magnetic field with the crystallographic easy-axis being $\hat{z}$.

4.3 Spin wave excitations of the homogeneous ground state

The most fundamental scenario are spin wave excitations around some static uniform background texture which is not position-dependent: $\mathbf{n}_0 = \hat{z}$. We seek plane wave excitation solutions around this equilibrium, meaning we have the spin wave ansatz

$$\delta\mathbf{n}_\perp(\mathbf{x}, t) = (\delta n_x \hat{x} + \delta n_y \hat{z}) e^{i(\mathbf{k}\cdot\mathbf{x} - \omega t)}, \tag{36}$$

with $\mathbf{k} = k_x\hat{x} + k_y\hat{y}$ being the wave vector. Here, the wave vector is limited to the $x - y$ plane by the first order orthogonal relation, ω is the spin wave frequency and $\delta n_y, \delta n_x$ are the amplitudes of the transverse excitations. We will find the dispersion relation and discuss the impact of different coupling mechanisms on the spin wave dynamics. First, in the absence of DMI, we observe that all the spatial and temporal derivatives in Eq. (35) rule out the time- and position-independent ground state, leaving us with the following equation of motion:

$$\hbar^2 \delta\ddot{\mathbf{n}}_\perp = aA\nabla^2\delta\mathbf{n}_\perp - aK(\mathbf{n}_0 \cdot \hat{z})^2 \delta\mathbf{n}_\perp + 2\hbar H \mathbf{n}_0 \times \delta\dot{\mathbf{n}}_\perp + \delta\mathbf{n}_\perp H^2 \tag{37}$$

where we have redefined $H = \mathbf{H} \cdot \mathbf{n}_0$ and taken the magnetic field to be constant in time. By substituting in the ansatz for the spin wave excitations Eq. (36) and the staggered magnetization ground state $\hat{z}$, we find the dispersion relation

$$\omega^* = \sqrt{(k^*)^2 + \tilde{K}} \pm 1. \tag{38}$$

We have introduced the dimensionless frequency $\omega^* = \omega/\omega_0$ with $\omega_0 = H/\hbar$, the dimensionless wavevector $k^* = |\mathbf{k}|/k_0$, with $k_0 = H/\sqrt{aA}$ and the dimensionless anisotropy $\tilde{K} = aK/H^2$. Back-substituting the expression for the eigenfrequency into the equation of motion yields a phase shift of $\pi/2$ between the two excitation directions: $\delta n_x = \delta n_y e^{\mp i\pi/2}$. The highest-lying branch, with the plus sign in the dispersion relation Eq. (38), correspond to plane wave excitations where the y-component is $-\pi/2$ out of phase with the x-component. Hence, the wave is right-circularly polarized. For the lower-lying branch, with the minus sign in the dispersion relation, the y-component leads the x-component with $\pi/2$, resembling a left-circularly polarized wave. We plot the dispersion relation for the left and right polarized waves in Figure 10. The presence of the magnetic field lifts the degeneracy of the right-circularly and left-circularly polarized waves. In the absence of

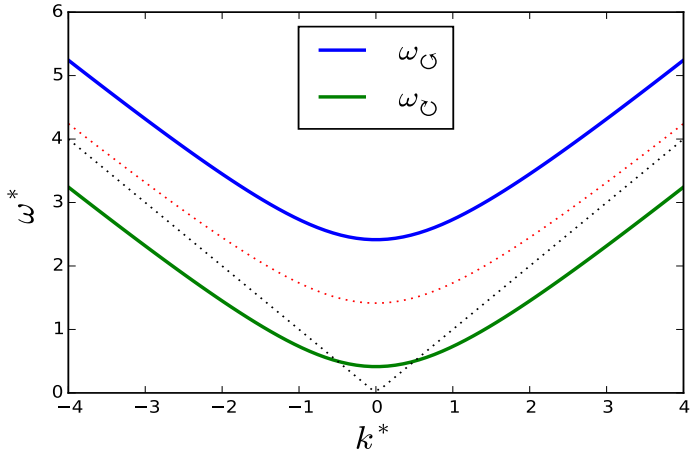

Figure 10: Dispersion relation for ω^* as a function of k^*, which is the dimensionless frequency ω in units of $\omega_0 = H/\hbar$ and the dimensionless wavevector k in units of $k_0 = H/\sqrt{aA}$. The dashed black line is the dispersion relation in presence of only symmetric exchange coupling. The red line is the dispersion relation if we turn on the easy-axis anisotropy. The right-circularly and left-circularly modes are degenerate. When turning on the magnetic field, the degeneracy is lifted and the blue line shows the right-circularly polarized waves, while the lower green line shows the left-circularly polarized waves. We have set $\tilde{K} = 2$.

an external magnetic field, the modes are degenerate, indicated by the red dotted line. In the limit of zero anisotropy, the dispersion relation is linear in $|\mathbf{k}|$, shown by the dashed black line. The linear, relativistic behaviour is a characteristic feature of antiferromagnetic spin waves. For ferromagnetic systems, the dispersion relation is quadratic, and such systems cannot have both linearly and circularly polarized spin waves.

Now, we will consider systems having a nonzero DMI in the free energy. When the ground state $\mathbf{n}_0 = \hat{z}$ and the spin wave excitations are in the $x - y$ plane, the presence of the DMI is in fact insignificant to the dispersion relation, as can be seen from Eq. (35). The reason is that the lowest order, nonzero DMI contributions to the equation of motion scales as $\mathcal{O}(\delta n_i^2)$, $i = (x, y)$, and are thus negligible. For the DMI to alter the dispersion relation, we need another form than the interfacial DMI considered above, *or* another ground state than $\mathbf{n}_0 = \hat{z}$. Consider now instead $\mathbf{n}_0 = \hat{y}$ as the ground state. Now, the order parameter lies within the plane, still with orthogonal spin wave excitations and the form of the interfacial DMI as in Eq.

(35). After substituting in the spin wave ansatz (now with excitations along $\hat{x}, \hat{z}$) and the ground state $\hat{y}$, and rewriting it into an equation for ω, yields

$$\left(\omega \mp \frac{H}{\hbar}\right)^2 = \frac{1}{\hbar^2}\left(aAk^2 + aK \pm Dk_x\right) \tag{39}$$

Back-substituting the expression for ω in the equation of motion gives $\delta n_x = e^{\mp i\pi/2}\delta n_z$. Hence, for the highest-lying branch (most energetic), the z-component is $-\pi/2$ out of phase with the x-component, meaning we have a right-circularly polarized wave. For the lower-lying branch, the z-component leads the x-component by $\pi/2$, representing a left-circularly polarized wave. This is the same as we get when considering the ground state to be $\hat{z}$ and rotating the inhomogeneous DMI vector to lie in $x - z$ plane. The dispersion relations for these two branches, together with the DMI-free, zero field degenerate branch, are shown in Figure 11. We plot ω^* as a function of the dimensionless wave vector along x, using $\tilde{K} = 2$ and the ratio $D/A = 1$ to enhance the effect of having a nonzero DMI. Typically, A will dominate D. The presence of the DMI now shifts the dispersion relation along one of the wave vector directions (here along k_x). They are still linear for large values of $k(k_x)$, but no longer degenerate when turning off the magnetic field. Along the other wave vector direction, the dispersion relation is not altered, so the symmetry is broken. This has been experimentally observed for antiferromagnetic magnons recently [105].

4.4 Spin wave excitations of inhomogeneous chiral textures

We have seen that a non-trivial position-dependent texture is thermodynamically stable and experimentally realizable. In Chapter 4.3 we looked at plane wave solutions to the small-amplitude excitations of the staggered magnetization in a (global) plane orthogonal to the texture. Now, we increase the complexity by considering spin wave excitations around an inhomogeneous chiral staggered magnetization in the presence of both Heisenberg exchange, DMI, anisotropy and an external time-dependent magnetic field.

When the order parameter spatially reorients, we need the plane containing the perpendicular excitations to spatially reorient accordingly to remain orthogonal to the texture to lowest order in the excitation fields. Our ansatz for the order parameter will be that of Eq. (34) with the equilibrium texture $\mathbf{n}_0$ given by Eq. (17). We define the local spherical coordinate frame with unit vectors $\hat{r}, \hat{\theta}, \hat{\rho}$ according to

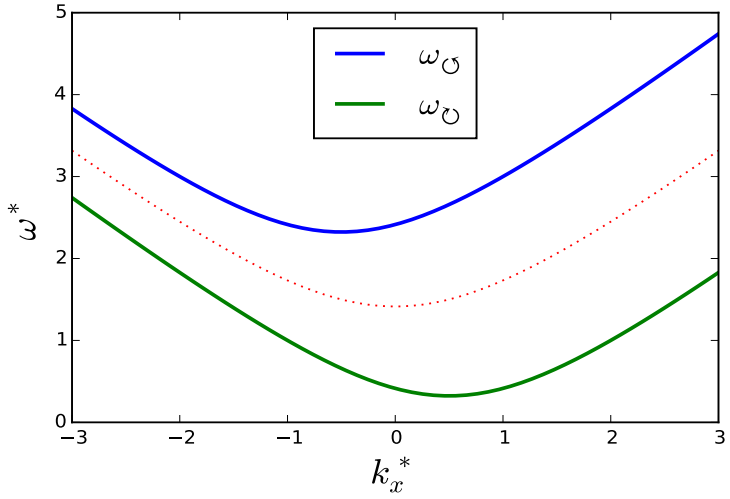

Figure 11: Dispersion relation ω^*, with $\omega^* = \omega/\omega_0$ and $\omega_0 = H/\hbar$, for right-circularly polarized (blue line) and left-circularly polarized (green) spin waves as a function of $k_x^* = k_x/k_0$ with inhomogeneous DMI in the presence of anisotropy and an external magnetic field along $\hat{z}$. We have put the ratio $D/A = 1$, and $\tilde{K} = 2$. Compared to the k_y-direction, the dispersion relation is shifted along k_x. The red dotted line is for illustration and shows the degenerate dispersion relation for the spin waves in the absence of DMI and external fields.

$$\begin{aligned}
\hat{r} &= (\sin\Theta\cos\phi, \sin\Theta\sin\phi, \cos\Theta), \\
\hat{\theta} &= (\cos\Theta\cos\phi, \cos\Theta\sin\phi, -\sin\Theta), \\
\hat{\phi} &= (-\sin\phi, \cos\phi, 0),
\end{aligned} \tag{40}$$

where the components are in the (x, y, z)-direction. Clearly, $\mathbf{n}_0 = \hat{r}$ now, meaning the linear deviations are confined to the plane spanned by $\hat{\theta}, \hat{\phi}$. Hence, we can expand the staggered magnetization according to

$$\mathbf{n}(\mathbf{x}, t) = \left(1 - \frac{h^2}{2}(n_\theta^2(\mathbf{x}, t) + n_\phi^2)\right)\hat{r} + h(n_\theta(\mathbf{x}, t)\hat{\theta} + n_\phi(\mathbf{x}, t)\hat{\phi}) \tag{41}$$

where h is some small expansion parameter, as in Ref. [49]. We are only interested in first order deviations, meaning the deviations to lowest order in h are

$$\delta\mathbf{n}_\perp(\mathbf{x}, t) = hn_\theta(\mathbf{x}, t)\hat{\theta} + hn_\phi(\mathbf{x}, t)\hat{\phi} \tag{42}$$

We call n_ϕ the in-plane field because these excitations only live in the basal plane of the skyrmion by the definition of $\hat{\phi}$. Similarly, we call n_θ the out-of-plane field as it is the excitation direction which holds the only component orthogonal to the basal plane. A visual representation of how these fields relate to some static equilibrium $\mathbf{n}_0$ is provided in Figure 12.

As a side note, this is in fact similar to what done in Ref. [106] for domain walls, where a global basis which span the plane of the orthogonal excitations (at every point in space) is introduced. They are $\hat{e}_1(\mathbf{x}) = \frac{\partial \mathbf{n}_0}{\partial \Theta}, \hat{e}_2(\mathbf{x}) = \frac{1}{\sin\Theta}\frac{\partial \mathbf{n}_0}{\partial \phi}, \hat{e}_3 = \hat{e}_1 \times \hat{e}_2 = \mathbf{n}_0$. By our definition of $\mathbf{n}_0$, we have $\hat{e}_1 = \hat{\theta}$, $\hat{e}_2 = \hat{\phi}$, $\hat{e}_3 = \hat{r} = \mathbf{n}_0$, i.e. the two usual ways of constructing the local coordinate frame is equivalent.

A main obstacle with the local redefinition of the coordinate frame, is that the unit vectors $\hat{\Theta}, \hat{r}, \hat{\phi}$ are position-dependent, too. When carrying out the spatial derivatives arising from the DMI and the symmetric exchange coupling, this needs to be accounted for, which makes the computation of the equations of motion for the fields somewhat more complicated. When carrying out the derivatives, the cross products and the scalar products using the ansatz

$$n_\theta(\mathbf{x}, t) = n_\theta(\mathbf{x}) e^{-i\omega_\theta t}, \qquad n_\phi(\mathbf{x}, t) = n_\phi(\mathbf{x}) e^{-i\omega_\phi t}, \tag{43}$$

we find, using trigonometric identities and combinations of the component-wise equations from Eq. (35), a coupled set of Schrödinger-like equations. For the in-plane field n_ϕ we get

$$\begin{aligned}\frac{\omega_\phi^2 \hbar^2}{a} n_\phi = &\left(A\Big(-\nabla^2 - (\partial_r \Theta)^2 + \frac{\cos^2\Theta}{r^2}\Big) + K_z \cos^2\Theta - D\Big(\frac{\sin 2\Theta}{2r} + \partial_r \Theta\Big) - \frac{H^2}{a}\cos^2\Theta \right) n_\phi \\ &- \left(\Big(\frac{2A\cos\Theta}{r^2} - \frac{D\sin\Theta}{r}\Big)\partial_\phi - \frac{i2\hbar H\omega\cos\Theta}{a} + \frac{\hbar \dot{H}\cos\Theta}{a} \right) n_\theta,\end{aligned} \tag{44}$$

while we for the out-of-plane field we obtain the Schrödinger-like equation

$$\begin{aligned}\frac{\omega_\theta^2 \hbar^2}{a} n_\theta = &\left(A\Big(-\nabla^2 + \frac{\cos 2\Theta}{r^2}\Big) + K_z \cos 2\Theta - \frac{D\sin 2\Theta}{r} - \frac{H^2}{a}\cos^2\Theta \right) n_\theta \\ &+ \left(\Big(\frac{2A\cos\Theta}{r^2} - \frac{D\sin\Theta}{r}\Big)\partial_\phi - \frac{i2\hbar H\omega\cos\Theta}{a} + \frac{\hbar \dot{H}\cos\Theta}{a} \right) n_\phi.\end{aligned} \tag{45}$$

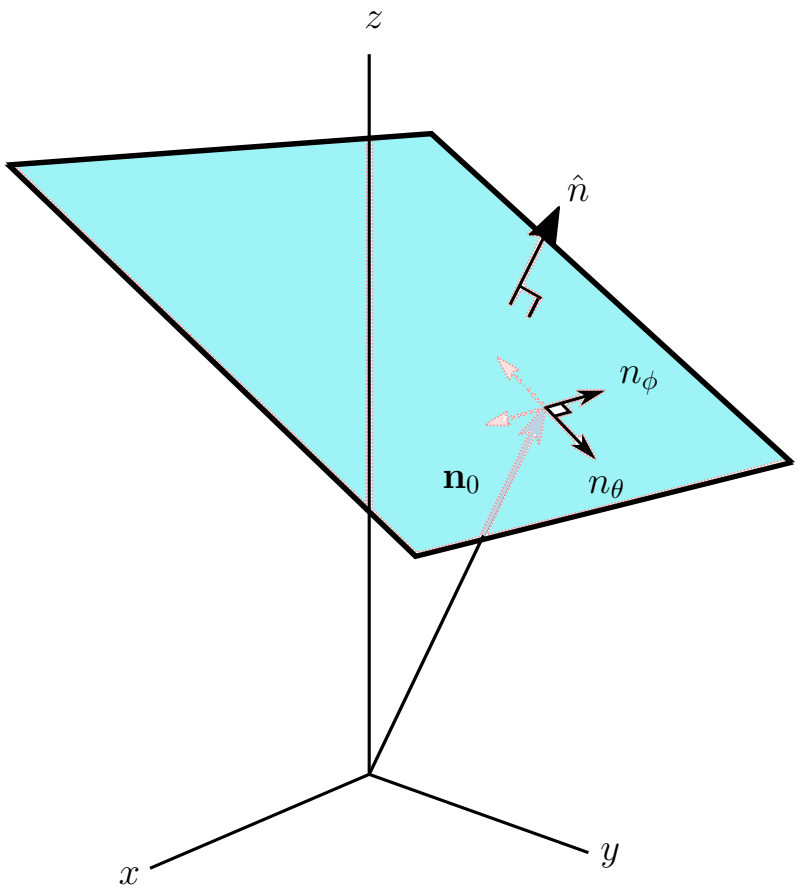

Figure 12: The orthogonal spin wave excitations n_ϕ, n_θ shown as black arrows around the static order parameter $\mathbf{n}_0$ pictured as the black/blue arrow. $\hat{n}$ is the unit normal of the blue plane of which the spin wave excitations are confined to. The light red arrows show the oscillating behaviour of the fields. $\mathbf{n}_0$ is taken along an arbitrary direction, and as the staggered magnetization changes, so does the plane and the excitation directions. Both n_ϕ and n_θ lives in the plane.

There is no trivial route to for instance decouple the two equations to simplify the system when looking for analytic solutions. In the ferromagnetic case of magnon excitations around a skyrmion [107] and for antiferromagnetic domain walls with magnon excitations [49, 106], one can construct the field $\psi_\pm = n_\phi \pm i n_\theta$ ($n \to m$ for ferromagnets) and find a single Schrödinger-like equation $E\psi_\pm = \hat{H}\psi_\pm$. If we rewrite our system into a matrix equation, we observe that the off-diagonal elements in the potential matrix are similar to each other. However, the diagonal potential elements are substantially different, not allowing us to rewrite the system into a more compact form without making some assumptions. Instead of looking for a full general solution to the Schrödinger-like equations, we will look for particular solutions, sub-scenarios and some limiting behaviour, both for the system size and the spin waves. This will be treated carefully in the next chapter.

5

Eigenspectra and eigenmodes for magnons around the antiferromagnetic skyrmion

In this chapter we will examine the new set of Schrödinger-like equations derived in the previous chapter. As the radial-dependence of the antiferromagnetic skyrmion requires a numerical solution, and the symmetry of the equations are reduced compared to antiferromagnetic domain wall or ferromagnetic skyrmion excitations, an exact analytic result is not possible. We could, as done for the insulating ferromagnetic skyrmion excitations [107], substitute an analytic ansatz mimicking the profile of Θ, but the reduced symmetry do not allow us to construct single field equations. Instead, we will take on a numerical diagonalization procedure and consider some limiting behaviour.

5.1 Dimensionless equations and magnon ansatz

As we have discussed earlier, the Hamiltonian at hand is invariant under rotation about the z-axis. The azimuthal variation of the in-plane and out-of-plane field has to preserve this invariance. That is, 2π-periodic boundary conditions in ϕ: $n_{\theta(\phi)}(\phi) = n_{\theta(\phi)}(\phi + 2\pi m)$, where m is an integer. Following papers on antiferromagnetic delocalized azimuthally symmetric vortices which encounter a somewhat similar structure for the Schrödinger-like equations [108–110], we make the generic ansatz

$$n_\phi(\rho,\phi) = \sum_{m=-\infty}^{\infty} n_{\phi,m}(\rho) F_m(\phi), \qquad n_\theta(\rho,\phi) = \sum_{l=-\infty}^{\infty} n_{\theta,l}(\rho) G_l(\phi). \tag{46}$$

where we have introduced the azimuthal functions $F_m(\phi) = ae^{im\phi} + be^{-im\phi}$, $G_l(\phi) = i(ae^{il\phi} - be^{-il\phi})$ with a, b arbitrary constants and $l, m \in \mathbb{Z}$. This way of introducing the azimuthal numbers m, l allow for degeneracy of modes $\pm(m, l)$, which is not the case for ferromagnetic skyrmions [107] nor ferromagnetic vortices [87, 111, 112]. Denote that in general the two azimuthal numbers m, l are independent.

Regarding the inhomogeneous chiral texture for which we derived the new set of Schrödinger-like equations, we have not yet assumed any radial profile. The parameterization of the staggered magnetization introduced in Eq. (17) used to describe skyrmions is in fact a fairly general parameterization as we take two generalized angles to describe the unit vector. Our assumption for the antiferromagnetic texture is that it takes on the skyrmion profile considered in Chapter 3. To confirm that the skyrmion profile we have arrived at is in fact the *true* profile of the order parameter, we need to perform a time integration of a randomly oriented set of spins localized at discrete lattice sites in the presence of the coupling mechanisms introduced in Chapter 2, and see if the order parameter takes on such a profile. As this is beyond the scope of the thesis, we (safely) assume that the skyrmion at hand is identical or close to identical to the real antiferromagnetic skyrmion.

While applying an oscillating external magnetic field is a route to excite spin waves in an insulating material for which currents are inappropriate, it is not needed to stabilize the chiral skyrmion texture we consider. Hence, in the interesting region close to the skyrmion, we can disregard the external magnetic field in Schrödinger-like equations Eqs. (44) and (45) for the in-plane and out-of-plane fields. Making the equations dimensionless and substituting in our ansatz Eq. (46) for the magnon wave functions yield

$$\begin{aligned} \frac{\omega_\phi^2}{\omega_0^2} n_\phi = &\left(-\nabla_\rho^2 - (\partial_\rho \Theta)^2 + \frac{\cos^2\Theta}{\rho^2} - \frac{\sin 2\Theta}{2\rho} - \partial_\rho \Theta + k_z \cos^2\Theta \right) n_\phi \\ &+ \frac{1}{\rho^2} \sum_m \left(m^2 F_m \, n_{\phi,m} \right) + \left(\frac{2\cos\Theta}{\rho^2} - \frac{\sin\Theta}{\rho} \right) \sum_l (l F_l \, n_{\theta,l}), \end{aligned} \tag{47}$$

and

$$\frac{\omega_\theta^2}{\omega_0^2} n_\theta = \left(-\nabla_\rho^2 + \frac{\cos 2\Theta}{\rho^2} - \frac{\sin 2\Theta}{\rho} + k_z \cos 2\Theta \right) n_\theta + \frac{1}{\rho^2} \sum_l \left(l^2 G_l \, n_{\theta,l} \right) + \left(\frac{2\cos\Theta}{\rho^2} - \frac{\sin\Theta}{\rho} \right) \sum_m \left(m G_m \, n_{\phi,m} \right). \tag{48}$$

We have introduced a characteristic frequency of the system, $\omega_0 = \sqrt{aD^2/\hbar^2 A}$, the reduced anisotropy $k_z = K_z A/D^2$, a typical length scale $\lambda_{\text{sky}} = A/D$ and the dimensionless radial coordinate $\rho = r/\lambda_{\text{sky}}$.

5.2 Azimuthally symmetric modes

The angular quantum numbers m, l couples the Schrödinger-like equations. Hence, for a system in the angular ground state, that is $m = l = 0$, the equations decouple, and the transverse excitation fields do not feel the presence of each other. These wave functions are azimuthally symmetric, and obey radial equations similar to the radial part of the wave function for an electron in the H-atom: $E_{\theta(\phi)} n_{\theta(\phi)} = \hat{H}_{\theta(\phi)} n_{\theta(\phi)}$. The Hamiltonian is $\hat{H}_{\theta(\phi)} = -\nabla_\rho^2 + V_{\text{out-of-plane(in-plane)}}$, with the out-of-plane potential $V_{\text{out-of-plane}} = \cos 2\Theta/\rho^2 - \sin 2\Theta/(2\rho) + k_z \cos 2\Theta$ and the in-plane potential $V_{\text{in-plane}} = -(\partial_\rho \Theta)^2 + \cos^2\Theta/\rho^2 - \sin 2\Theta/\rho - \partial_\rho \Theta + k_z \cos^2\Theta$. The decoupling of the equations for the lowest angular modes is a distinct feature of antiferromagnets, a feature which is not necessarily present in ferromagnetic systems [110, 112]. The reason is that the coupling of the in-plane and out-of-plane modes are only of azimuthal origin. We have introduced the dimensionless eigenvalues $E_{\theta(\phi)} = \omega_{\theta(\phi)}^2/\omega_0^2$.

Decoupling of the two excitation modes allows for different eigenspectra for the in-plane and out-of-plane polarization directions. As the effective potentials are different, we could have that spin waves incident on the skyrmion will be polarized along either $\hat{\phi}$ or $\hat{\theta}$ after passing through the skyrmion area. Far from the skyrmion, both potentials are constant, and we recover the usual dispersion relation for a uniform staggered magnetization. These effects are similar to that of spin waves excitations of an antiferromagnetic domain wall with nonzero DMI [36].

The effective potentials experienced by the magnon excitations are determined by the numerical solutions of Eq. (23). We have shown the potential alongside some of the wave function solutions in Figures 14, 15, 19, 20, 24 and 25 for different

values of k_z. For now, we only consider some properties of the potentials, and we will come back to and discuss more thoroughly how the wave function solutions and their eigenvalues relate to the potentials. A distinct property of Dzhyaloshinskii-Moriya coupled antiferromagnetic systems emerges when looking at the effective potentials: due to the asymmetry in this coupling mechanism, the potentials for the in-plane and out-of-plane excitations are now fundamentally different in terms of the texture-dependent terms. Yet, both effective potentials approach a constant value far from the skyrmion core and goes to infinity at the core. The reason is that in continuum theory, the core of the skyrmion will be a singularity. The singular behaviour introduces a problem for energy calculations for vortex- or skyrmion-like solitons, which usually have been avoided by introducing some small cut-off distance [113–115].

The in-plane wave functions see a potential well when moving towards the skyrmion from infinity, which is attractive. The depth of the well is dependent on the relative strength of the exchange coupling, DMI and anisotropy, i.e. the value of k_z. The larger the anisotropy or symmetric exchange is compared to the asymmetric DMI, the deeper the well. Irrespective of k_z, the potential reaches a minima at $\rho \approx 3.5$, where $V_{\mathrm{in-plane}}(\rho) < 0$. Furthermore, the global minima of the in-plane potential, V_{min}, appears to be independent of the choice of k_z.

For the out-of-plane excitations, the effective potential diverges close to the skyrmion core for all values of k_z. Similar to the in-plane potential, the potential approaches a constant far from the skyrmion core. This constant value is solely determined by the value of k_z: $V_{\mathrm{out-of-plane}}(\rho \to \infty) = k_z$. Another similar feature for the out-of-plane potential is that they also have global minima cusp. As opposed to the in-plane potentials, the value of k_z seems to strongly influence both the depth of the potential well and the minimum value of the potential. We observe that $V_{\mathrm{min}} \approx -k_z$ for the out-of-plane potential, which is different to the in-plane potential where V_{min} was independent of k_z. The well region of the potential is attractive, allowing for the existence of local modes in this region. The same applies for the in-plane modes, as the potential minima is smaller than the asymptotic value of the potential far from the skyrmion core.

To solve the eigenvalue equations, we will use a numerical diagonalization routine to explicitly find the eigenspectra and the belonging eigenstates in the micromagnetic limit. The skyrmion profile $\Theta(\rho)$ is numerically determined by the 5^{th} order Runge-

Kutta shooting method mentioned in Chapter 3.3. The eigenfrequencies ω and the eigenstates are calculated using the numpy Linear Algebra library in Python. The kinetic part of the Hamiltonian holding spatial derivatives is set-up by a second order local truncation error procedure. We find the eigenfrequencies and eigenstates for three different values of k_z to see how the texture-dependent potential influences the magnon behaviour.

We discover that there is a set of eigenfrequencies with belonging eigenfunctions that solves the decoupled Schrödinger-like equations. To label the ground state, the first excited state and so on, we assign to the radial wave functions the radial quantum number $n_r = 0, 1, 2, ...$, analogous to the radial quantum number in the H-atom. We discuss properties of the spectra and modes being the same for all three values of the reduced anisotropy in Chapter 5.2.1, and address particular differences and features in the succeeding chapters.

5.2.1 Anisotropy parameter $k_z = 0.1$

In Figure 13 the in-plane and out-of-plane eigenfrequencies in units of ω_0 are shown, where we have included frequencies up to $n_r = 9$. The in-plane eigenfrequencies are lower than the out-of-plane frequencies for a given radial number. When increasing n_r, the difference between the in-plane eigenfrequency and the out-of-plane eigenfrequency decreases. The inset in the lower right corner with the 100 lowest-lying frequencies shows that there is a (close-to) linear relationship between the eigenfrequencies and the radial quantum number: $\omega = \omega_0(an_r + b)$. a, b are fitting parameters. The frequency quanta is thus approximately $\omega_0 a$, and the bosonic magnons with energy $\hbar\omega$ shows the same behaviour as the 1D harmonic oscillator. The energy increases in quanta proportional to the excitation number n_r. The line is green because the red crosses and the blue dots merge together as the resolution is reduced. In Figure 13 we have not included the $n_r = 0, 1$ in-plane frequencies. The reason is that the eigenvalues of these states $E_\phi = \omega_\phi^2/\omega_0^2$ is negative as can be seen from Figure 14 and 16, meaning we have a purely imaginary eigenfrequency for these modes.

Figures 14 and 15 show the effective in-plane and out-of-plane potential for $k_z = 0.1$ seen by the magnons, respectively. Alongside the in-plane potential, we have inserted the in-plane states $n_r = 0, 1, 4, 6$, while we have inserted the $n_r = 0, 1, 3, 5$ out-of-plane states in Figure 15. It is the eigenvalue, and not the eigenfrequency,

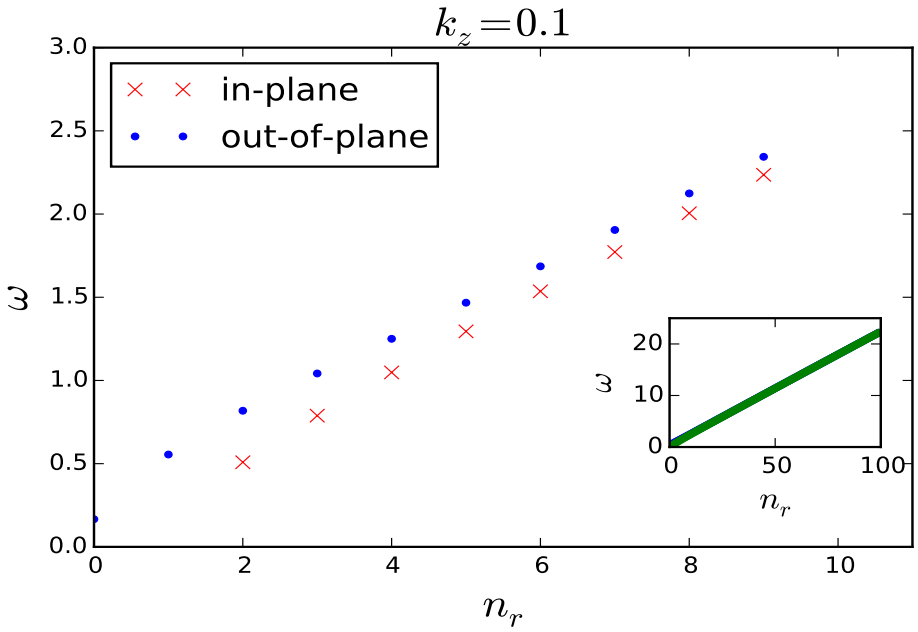

Figure 13: The in-plane and out-of-plane eigenfrequencies ω in units of ω_0 up to $n_r = 9$ for reduced anisotropy $k_z = 0.1$. The $n_r = 0, 1$ in-plane eigenfrequencies are not included as E_ϕ is negative for $n_r = 0, 1$. The in-plane states have lower frequencies than the corresponding out-of-plane states for same level of excitation n_r. The relative difference decreases for increasing n_r. The inset in the right corner shows an extension of the spectra up to $n_r = 100$. The blue dots and red crosses for the out-of-plane and in-plane frequencies merge together into one green line due to limited resolution on the axes. We observe a linear relationship between the frequency and the radial quantum number: $\omega \propto n_r$.

that we can compare to the potential according to Eqs. (47) and (48). Hence, the black dotted lines show the eigenvalue levels E_ϕ and E_θ for increasing values of n_r. We find that the in-plane and out-of-plane states that have eigenvalues larger than the asymptotic value of their respective texture-induced potentials far from the skyrmion core, $V_{\mathrm{in-plane}}(\rho \to \infty) = V_{\mathrm{out-of-plane}}(\rho \to \infty) = k_z$, are linear close to the skyrmion core and undergoes decaying oscillations when moving away from the centre. They have real eigenfrequencies and represent travelling waves. We also discover a bound mode, the $n_r = 0$ out-of-plane state, which is localized close to the skyrmion and trapped by the potential well.

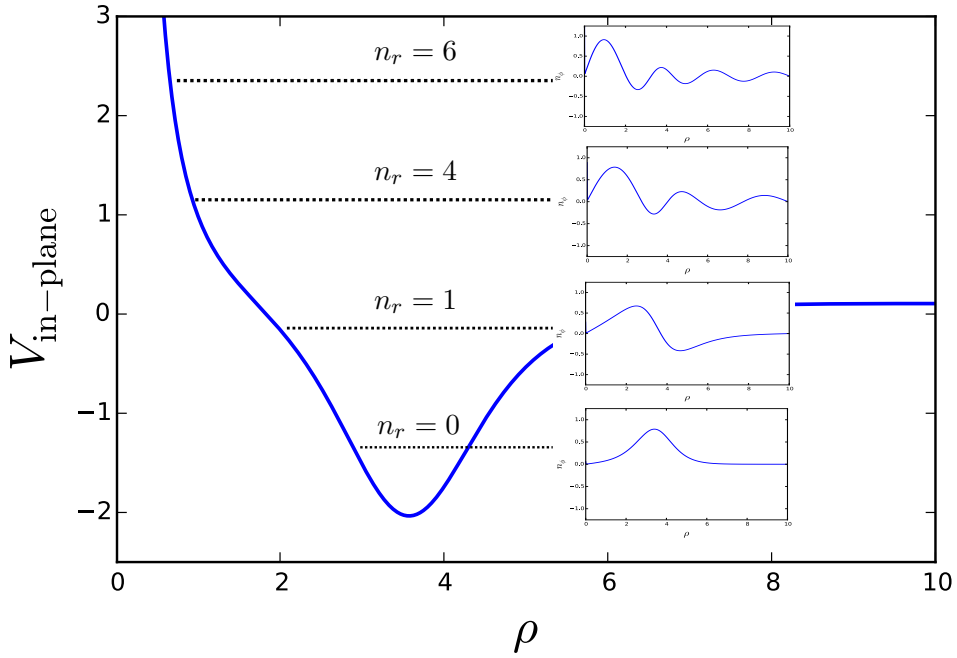

Figure 14: The in-plane potential $V_{\mathrm{in-plane}} = \frac{\cos^2\Theta}{\rho^2} - (\partial_\rho\Theta)^2 - \frac{\sin 2\Theta}{2\rho} - \partial_\rho\Theta + k_z\cos^2\Theta$ for anisotropy parameter $k_z = 0.1$ as a function of ρ. The insets are the in-plane wave functions $n_{\phi,m=0}$ plotted as a function of ρ. The black dotted line shows the corresponding eigenvalue. The lowest inset is the ground state $n_r = 0$ with $E_\phi = -1.27$. The second lowest inset is the 1^{st} excited state with $E_\phi = -0.15$ and $n_r = 1$. The next inset is the 4^{th} excited state with $E_\phi = 1.10$, $n_r = 4$. The uppermost inset is the 6^{th} excited state with $E_\phi = 2.36$ and $n_r = 6$. The two latter show delocalized behaviour compared to the two former modes.

We can make an analogy to the H-atom for the travelling waves and the bound

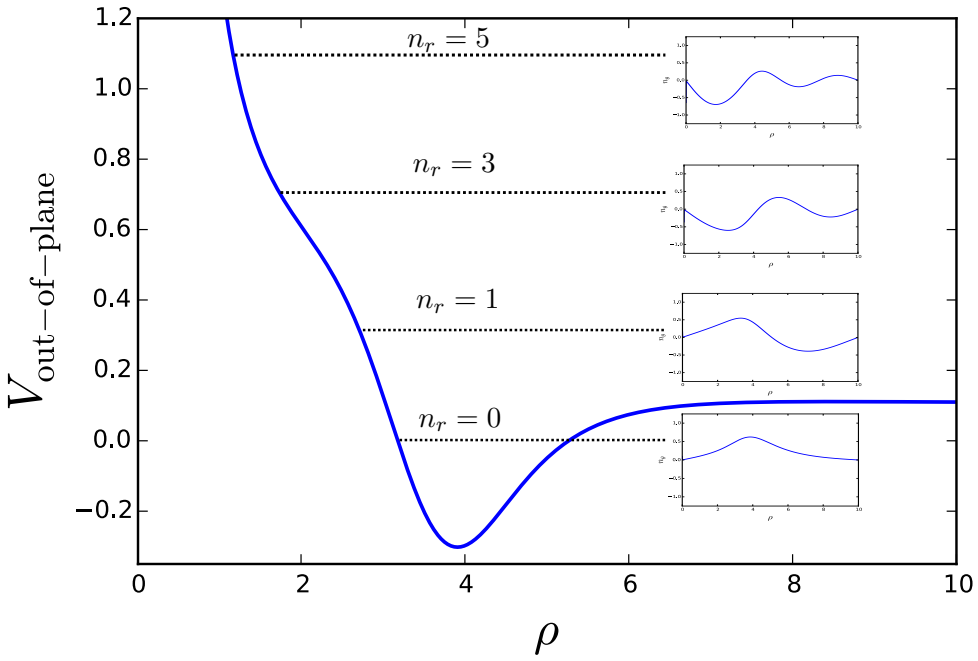

Figure 15: The out-of-plane potential $V_{\text{out}-\text{of}-\text{plane}} = \frac{\cos 2\Theta}{\rho^2} - \frac{\sin 2\Theta}{\rho} + k_z \cos 2\Theta$ for anisotropy parameter $k_z = 0.1$ as a function of ρ. The insets are the out-of-plane wave functions $n_{\theta,l=0}$ plotted as a function of ρ. The black dotted lines show the corresponding eigenvalue. The lowest inset is the ground state with $E_\theta = 0.03$ and radial quantum number $n_r = 0$, having a localized appearance. The second lowest inset is the 1^{st} excited state with $E_\theta = 0.31$. The next inset is the 3^{rd} excited state with $E_\theta = 1.09$. The uppermost inset is the 5^{th} excited state with $E_\theta = 2.15$. The three latter ones are delocalized.

modes discovered here. The bound magnons do not have enough energy to escape the potential trap and are captured by the skyrmion. This is analogous to the bound electron states of the H-atom. When the energy is increased in terms of the eigenfrequency above a certain threshold, which we name the ionization energy, the magnons become unbound to the skyrmion potential, similarly to ionized electrons. The ionization energy for the magnons is $\hbar\omega_0\sqrt{k_z}$. This threshold is the same for both the in-plane and out-of-plane modes.

As mentioned above, the in-plane ground state and the first excited state have negative eigenvalues, yielding purely imaginary eigenfrequencies $\omega_\phi = \pm i\sqrt{E_\phi}\omega_0$. By our ansatz $n_\phi \propto e^{-i\omega_\phi t}$, clearly the sign is of massive importance; the minus

sign results in exponentially damping of the magnon excitations, while the plus sign induces exponentially growth of the amplitude. If there is some initial condition leading to the exponential damping of the magnons, we can simply prepare the system with the same initial conditions but with the magnon velocities reversed, which leads to the instability. In the theory we have adapted, the modes appear to be equally likely, with no indication of whether the unstable (usually explained by being in a region of parameter space where the solution at hand being thermodynamically unstable) or the stable mode is the physical solution. We must address this carefully, and we will look at some physical interpretations of such solutions.

The effective radial 1D Schrödinger-like equations for the in-plane and out-of-plane magnons we have discovered are very similar to magnon excitations around an antiferromagnetic easy-axis domain wall [49]. By analogy, we can interpret imaginary eigenfrequencies in terms of localized "Goldstone modes". Such modes were also introduced for imaginary eigenfrequencies of the zero wavevector mode in the ferromagnetic Bloch wall [116]. For these chiral textures with elementary excitations, bound states and travelling waves were also discovered, similarly to the antiferromagnetic skyrmion studied here. One could project away the Goldstone modes by allowing for a time-dependent position of the solitons, meaning the magnons induce antiferromagnetic and ferromagnetic domain wall motion. Applying the same argument here, the apparent "Goldstone modes" could be understood as a collective excitation of the skyrmion, leading to translational displacement of the skyrmion as a whole.

Another way of interpreting the results is in terms of resonance phenomena and damping. As a motivation, the net effect of having a nonzero Gilbert damping term in the equations of motion for the antiferromagnetic domain wall leads to an explicit term in the dispersion relation being purely imaginary with a minus sign in front [49]. This is equivalent to having $\omega_\phi = -i\sqrt{E_\phi}\omega_0$, which also leads to an exponential damping as time runs by. However, we have disregarded phonon-magnon interactions giving rise to the Gilbert damping term which acts to reduce the magnon density, and we have to address the exponential decay (and growth) as time elapses by some other damping mechanisms.

One explanation could be related to magnon Landau damping and inverse-Landau damping, analogous to electrons in plasma. The beam-plasma modes of an electron beam traversing a region of plasma with an neutralizing ion background

not interacting with the electrons has a dispersion relation with a conjugate pair of complex eignefrequencies, similar to the conjugate pair we found for the magnon excitations around the antiferromagnetic skyrmion, leading to a temporal unstable mode with exponential growth and one mode with exponential decay [117]. We will simply outline the idea for determining which mode is physically plausible. The eigenmodes are explained by kinetic theory where a distribution function $f_e(\mathbf{x}, \mathbf{v}, t)$ of the electron beam is superimposed on a stationary, homogeneous distribution f_0 of the plasma background. By linearizing the Vlasov equation

$$\frac{\partial f}{\partial t} + \mathbf{v} \cdot \nabla_r f + \mathbf{a} \cdot \nabla_v f = 0 \tag{49}$$

where the acceleration $\mathbf{a}$ experienced by the electrons is the effective Lorentz force originating from average quantities of charge and current densities with an electron wave ansatz $f_e = \hat{f}_e e^{i(\mathbf{x}\cdot\mathbf{v}-\omega t)}$, the dielectric function reads $D(k,\omega) = 1 - \frac{\omega_p^2}{k^2} \int \frac{\partial f_0/\partial v}{v-\omega/k} dv$ with ω_p being the plasma frequency [118]. The eigenmodes are zeros in the dielectric function, and the solution requires integration over the complex v-plane with a deformation of the path to account for the complex poles, first solved by Landau with the Landau contour [119]. The residue provides a term $\mathrm{Im}(\omega) \propto \frac{\partial f_0}{\partial v}$ evaluated at the phase velocity, i.e. in the tail of the distribution. For a negative slope like that of a Maxwellian distribution, the mode is exponentially damped and vice versa. It is the contribution of the resonant particles in the tail that leads to Landau damping or bump-on-tail instability for multiply peaked and less trivial velocity distributions.

For further treatment of our system motivated by the analogy to kinetic plasma theory, we could substitute the homogeneous electron distribution by an ideal Bose-gas distribution of magnons and superimpose a small spin wave perturbation. For the effective force term we could use the gradients of the texture-induced in-plane and out-of-plane potentials derived in the thesis. Another route would be to perform a local rotation of the original equation of motion Eq. (35) without any ansatz for neither the texture nor the excitations and derive an effective vector and scalar potential leading to emergent magnetic and electric fields interacting with the magnons, as done in Ref. [107]. A clear analogy to the Lorentz force in the Vlasov equation on the electrons is evident. Instead of considering zeros in the dielectric dispersion, we would rather seek zeros in the apparent susceptibility as that yields the magnon eigenmodes [120]. A remaining question to answer is whether or not this

route collapses the eigenfrequency onto the positive/negative imaginary solution, or if the frequency remains ambiguous, and would be a topic for further research. If the Vlasov equation does not bring a conclusive interpretation, a more rigorous treatment in terms of kinetic theory and the spin-dependent Vlasov-Boltzmann equation could be applied [121].

The Vlasov equation is memory-less as it utilizes average quantities of charge and current density, and disregard the short-ranged correlations and collisions due to particle-particle interactions [117]. Magnon-magnon and four-magnon scattering is therefore to be neglected when taking on this approach. We thus require the magnons to be thermally equilibrated obeying Bose-statistics at a sufficiently low temperature for magnon interference phenomena to be dominated by magnon-soliton interactions [122, 123]. There is not an equally strict constraint on the magnon density as multi-magnon-magnon couplings can be neglected even at very high densities, making the magnons still undergo ideal Bose gas description [124]. To capture the probability distribution in position space by the texture-induced potential, we could include a position-dependent temperature in the distribution [122] or make a separation of variables for the distribution function, spatially modulated by the in-plane and out-of-plane wave functions discovered in the thesis, similarly to what done in Ref. [125] for a magnon gas subject to Bose-Einstein condensation in a box-like potential trap.

The simple picture of resonant particles solely determining whether damping or resonance occurs is not satisfactory for describing beam damping and instabilities in plasma and should probably not be a stand-alone explanation if applicable to magnons either. We will discuss some mechanisms that could account for the damping and/or growth in the following. It has been found that an excess of fast-moving electrons can drive instabilities into turbulence in locally saturated plasma [126]. The unstable eigenmodes grows exponentially in time until saturation is obtained. Saturation of sublattice magnetization will also limit the spin wave amplitude from growing infinitely for magnon excitations of the antiferromagnetic skyrmion, as increasing oscillation amplitudes are compensated by reduction of the static staggered magnetization. Such a feature was also spotted for complex conjugate eigenmodes in the canted antiferromagnet $KMnFe_3$ with magnetocrystalline anisotropy, DMI and exchange coupling. The exponential growth of nonzero wavevector modes superimposed on the uniform collective precession mode $k = 0$ when the driving field exceeded a critical threshold was ultimately limited by the degenerate $-k$ mode

[127]. Below the threshold, the modes are damped and not exponentially growing until saturation. Damping of eigenmodes is also encountered at interfaces, where evanescent modes have been detected in finite sized easy-axis insulating antiferromagnets with magnons at a temperature far below the Néel temperature condensing into a single Bose quantum state [128]. The evanescent modes decay exponentially fast at a normal metal interface, with higher excited travelling wave states similar to those we discovered also present. This could offer the interpretation of the antiferromagnetic skyrmion being an effective interface observed by incoming magnons in a homogeneous texture, with the magnons turning into evanescent modes when entering the region of the skyrmion.

Another piece of the puzzle that can lead to damping phenomena is spin-flip Stoner excitation, where an excitation from an occupied to empty state with a spin flip occurs. Single-electron Stoner excitations can both damp and even make spin waves disappear [129]. Recently it is has been shown that, using time-dependent density functional perturbation theory, Landau damping suppressing magnon excitations occurs when the magnon energy resonates with the Stoner continuum [130]. Also dephasing and back-reaction of scattered magnons with the incidental pumped spin waves can lead to magnon relaxation [131, 132]. Finally yet importantly, we have only considered first order excitations when solving the Schrödinger-like equations. Clearly, if the magnon mode is collapsed onto the resonance state by kinetic theory for instance, we would need to include the higher order corrections of the field excitations as they will no longer be small when they can grow as time elapses. Including higher order corrections might eventually lead to limitation of the exponential growth.

Now, to see how the in-plane and out-of-plane magnon states changes for increasing degree of excitation, we plot the 8 lowest-lying in-plane wave functions in Figure 16 and the 8 lowest-lying out-of-plane states in Figure 17. The ground state and the first excited in-plane state are initially localized around the skyrmion, and dies out rapidly outside the skyrmion region. This applies to the bound out-of-plane ground state too. The first excited out-of-plane state and the second excited in-plane state have a nonzero derivative at $\rho = 10$, illustrating the travelling wave property as these states are delocalized. As we continue to excite our system, the eigenstates accumulate more and more curvature, associated to the increasing kinetic energy. The probability densities become more oscillating, while close to the skyrmion core

the wave functions are linear as a function of ρ.

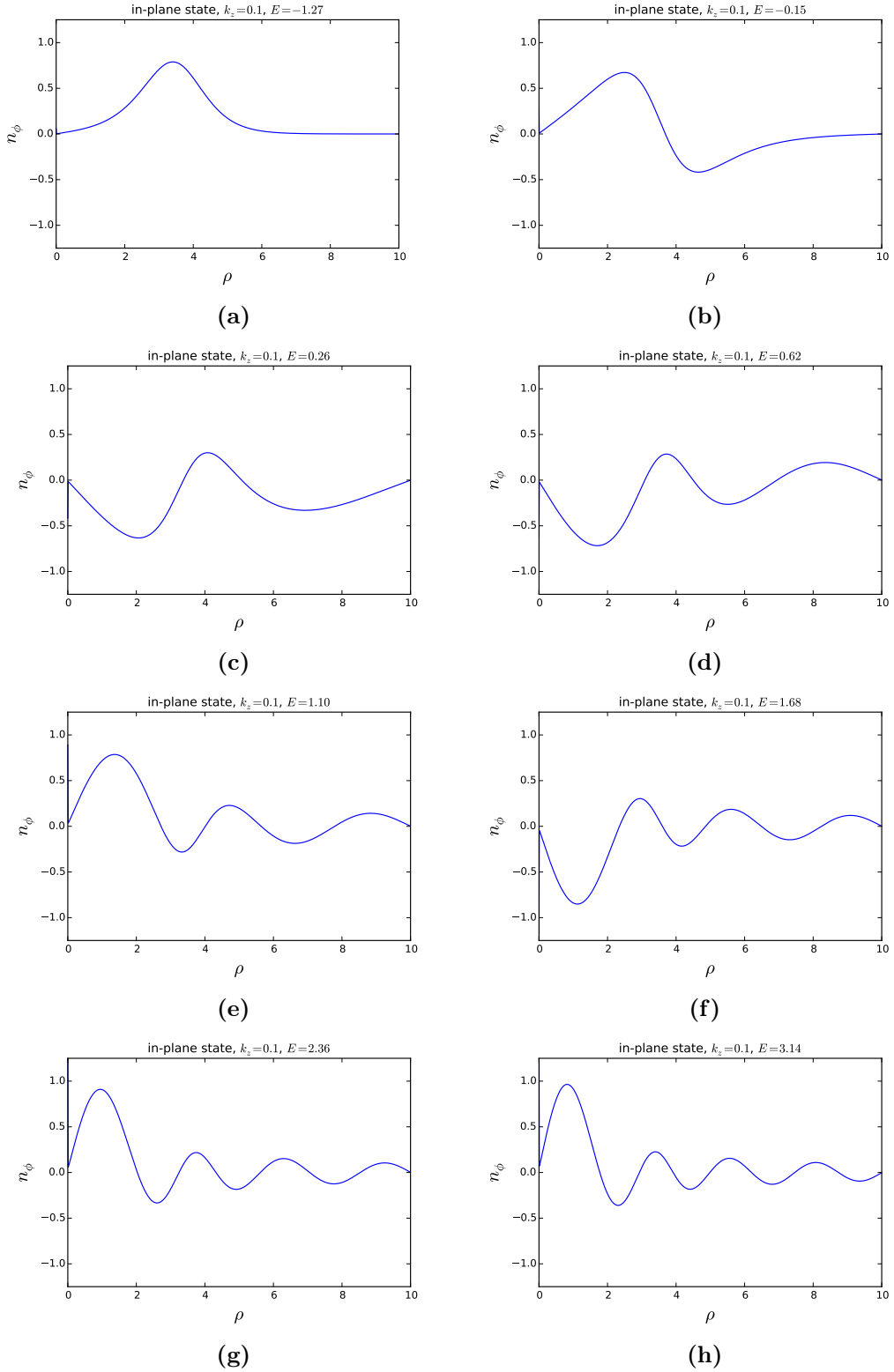

Figure 16: The in-plane wave functions $n_{\phi,m=0}^{56}$ for $k_z = 0.1$. (a): The ground state, with probability density focused around the minima of the potential. (b): The first excited state, being initially localized. (c): The second excited state, which is the first unbound state. It has an asymptotic oscillating behaviour for $\rho \to \infty$. (d)-(h): The $3^{\text{rd}} - 7^{\text{th}}$ excited state, all being unbound, linear at $0 \lesssim \rho$ and oscillating for increasing ρ.

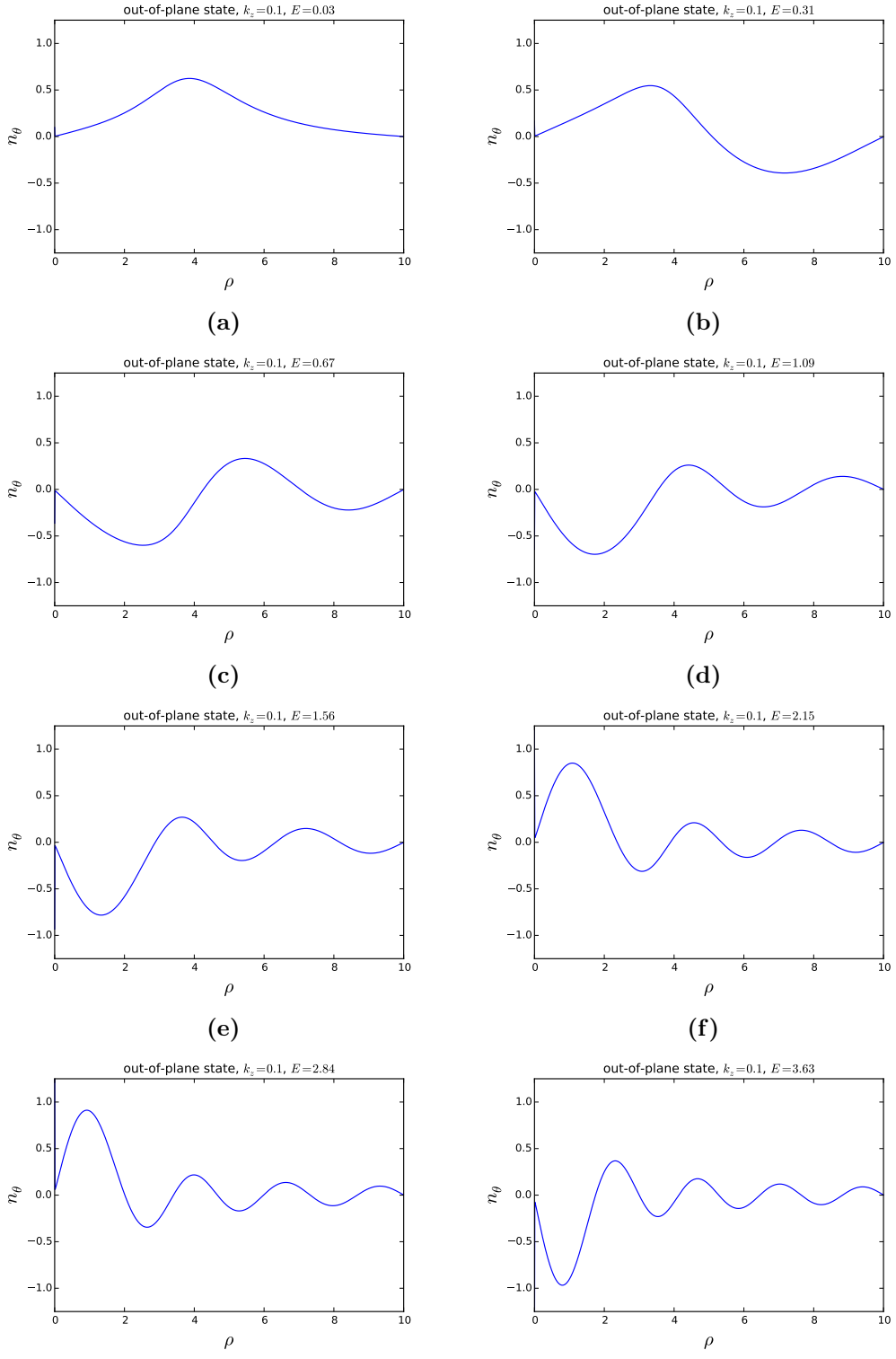

Figure 17: The out-of-plane wave functions $n_{\theta,l=0}$ for $k_z = 0.1$ (a): The localized ground state, with probability density focused around the minima of the potential. (b): The first excited state, which is the first unbound state, being oscillatory far from the skyrmion. (c)-(h): The $2^{\text{nd}} - 7^{\text{th}}$ excited state, all being unbound, linear at $0 \lesssim \rho$ and oscillatory for large ρ.

5.2.2 Anisotropy parameter $k_z = 1.0$

The in-plane and out-of-plane eigenfrequency spectra for reduced anisotropy $k_z = 1.0$ are shown in Figure 18. We include eigenfrequencies up to $n_r = 9$ and deliberately leave out $n_r = 0$ for both in-plane and out-of-plane modes by the same reasoning as for $k_z = 0.1$. Again, the in-plane frequencies are higher for the same level of excitation, with the linear relationship to n_r shown by the inset.

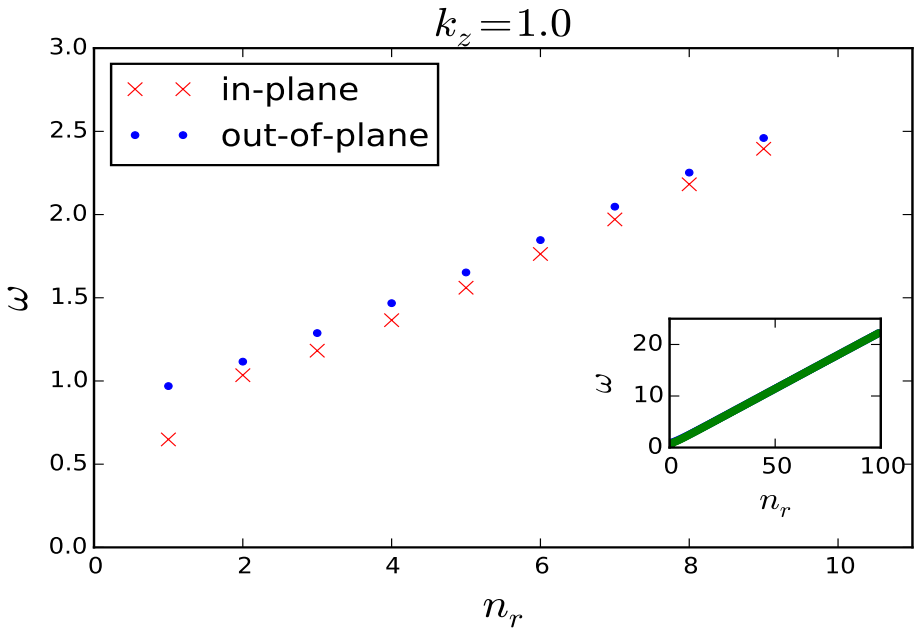

Figure 18: The in-plane and out-of-plane eigenfrequencies ω in units of ω_0 up to $n_r = 9$ for reduced anisotropy $k_z = 1.0$. The $n_r = 0$ ground state for both the in-plane and the out-of-plane eigenfrequency is not included as E_ϕ, E_θ are negative for those values. The in-plane states have lower frequencies than the corresponding out-of-plane states for same level of excitation n_r. The relative difference decreases for increasing n_r. The inset in the right corner shows an extension of the spectra up to $n_r = 100$. The blue dots and red crosses for the out-of-plane and in-plane frequencies melt together into one green line due to limited resolution on the axes. We observe a linear relationship between the frequency and the radial quantum number: $\omega \propto n_r$.

In Figure 19 and 20 the in-plane and out of-plane potential for $k_z = 1.0$ with wave functions $n_r = 0, 1, 3, 5$ included are shown, respectively. The blue line shows the potential as a function of ρ, while the black dotted lines show the eigenvalue

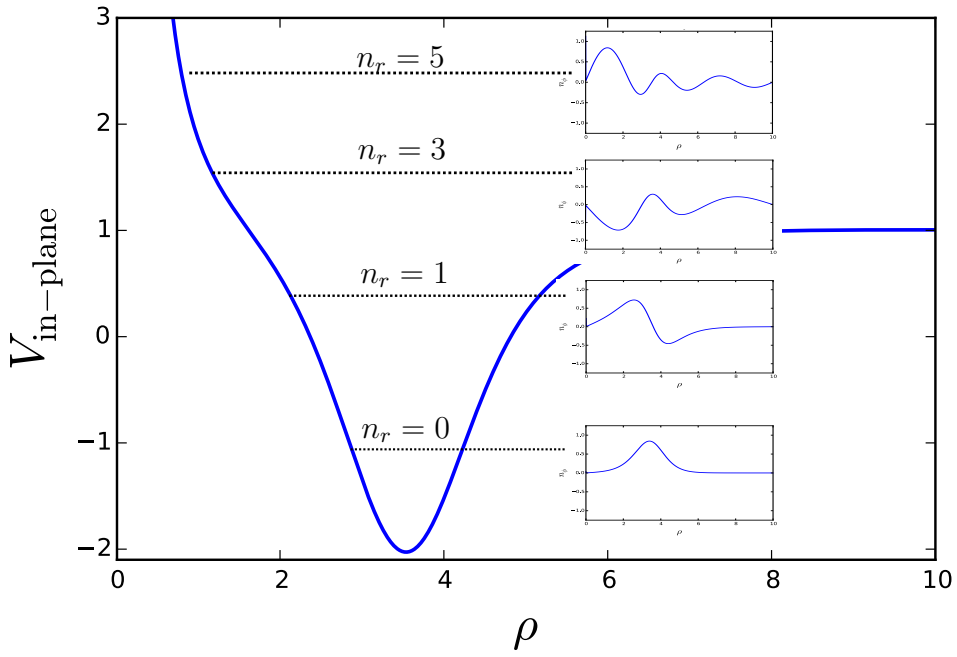

Figure 19: The in-plane potential $V_{\text{in-plane}} = \frac{\cos^2\Theta}{\rho^2} - (\partial_\rho\Theta)^2 - \frac{\sin 2\Theta}{2\rho} - \partial_\rho\Theta + k_z\cos^2\Theta$ for reduced anisotropy $k_z = 1.0$ as a function of ρ. The insets are the in-plane wave functions $n_{\phi,m=0}$ plotted as a function of ρ. The black dotted lines show the corresponding eigenvalues for each wave function. The lowest inset is the ground state with $E_\phi = -1.07$ and $n_r = 0$. The second lowest inset is the 1^{st} excited state with $E_\phi = 0.42$ and $n_r = 1$. The next inset is the 3^{rd} excited state with $E_\phi = 1.40$ and $n_r = 3$. The uppermost inset is the 5^{th} excited state with $E_\phi = 2.43$ and $n_r = 5$. The two latter are unbound states.

for the given radial number. Both ground states have negative eigenvalue, different to the $k_z = 0.1$ scenario where no out-of-plane evanescent or resonant modes manifested. Another difference is the purely bound both in-plane and out-of-plane magnon modes. For $k_z = 0.1$, only out-of-plane modes could be purely bound.

If we consider the higher-lying in-plane and out-of-plane states shown in Figures 21 and 22, respectively, we once again observe the wave functions becoming more oscillatory. The linear dependence on ρ close to the skyrmion core in the classically forbidden region for both the in-plane and out-of-plane modes found for $k_z = 0.1$ is also evident here.

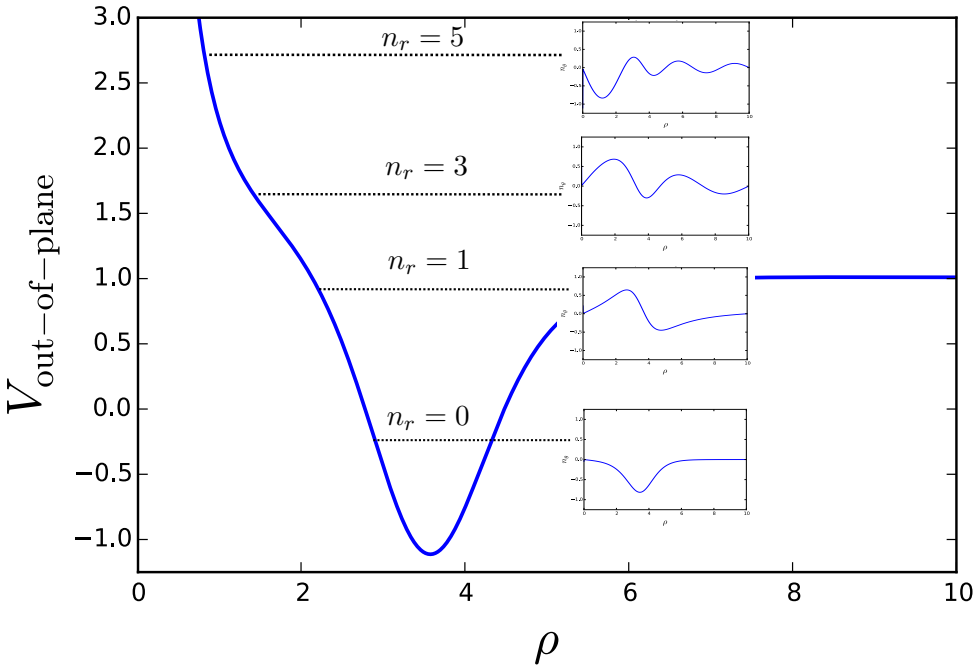

Figure 20: The out-of-plane potential $V_{\mathrm{out-of-plane}} = \frac{\cos 2\Theta}{\rho^2} - \frac{\sin 2\Theta}{\rho} + k_z \cos 2\Theta$ for reduced anisotropy $k_z = 1.0$ as a function of ρ. The insets are the out-of-plane wave functions $n_{\theta,l=0}$ plotted as a function of ρ. The black dotted lines show the corresponding eigenvalues for each wave function. The lowest inset is the evanescent/resonant ground state with $E_\theta = -0.25$ with $n_r = 0$. The second lowest inset is the 1^{st} excited state with $E_\theta = 0.94$ and $n_r = 1$. This state is bound and localized close to the skyrmion. The next inset is the 3^{rd} excited state with $E_\theta = 1.66$ and $n_r = 3$. The uppermost inset is the 5^{th} excited state with $E_\theta = 2.73$ and $n_r = 5$. The two latter insets are both unbound states.

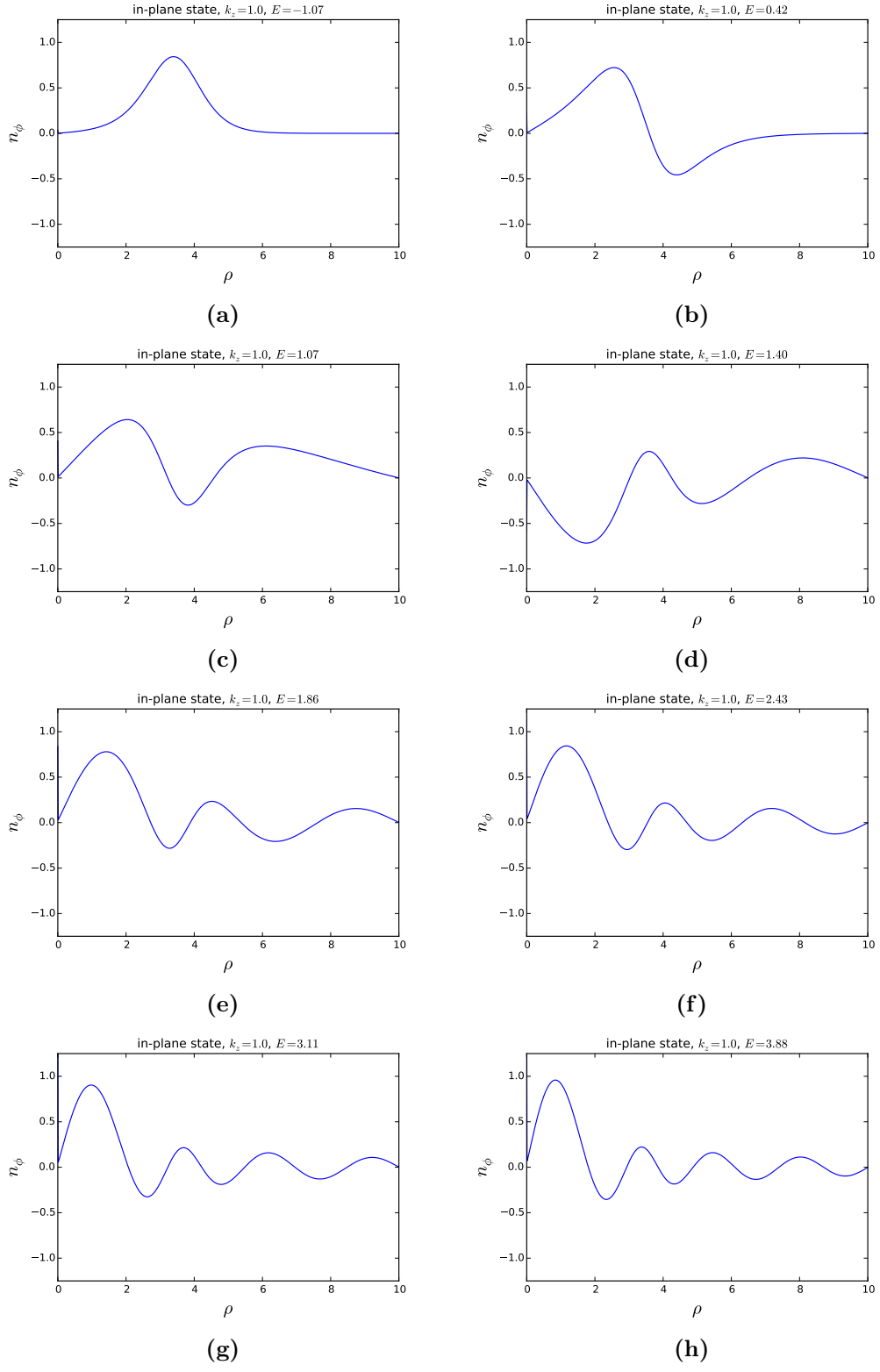

Figure 21: The in-plane wave functions $n_{\phi,m=0}^{61}$ for $k_z = 1.0$ (a): The evanescent/resonant ground state, with probability density focused around the minima of the potential. (b): The first excited state, which is a bound state. (c): The second excited state, which is the first unbound state. It has an asymptotic oscillating behaviour for $\rho \to \infty$. (d)-(h): The $3^{\text{rd}} - 7^{\text{th}}$ excited state, all being unbound, linear at $0 \lesssim \rho$ and oscillating for increasing ρ.

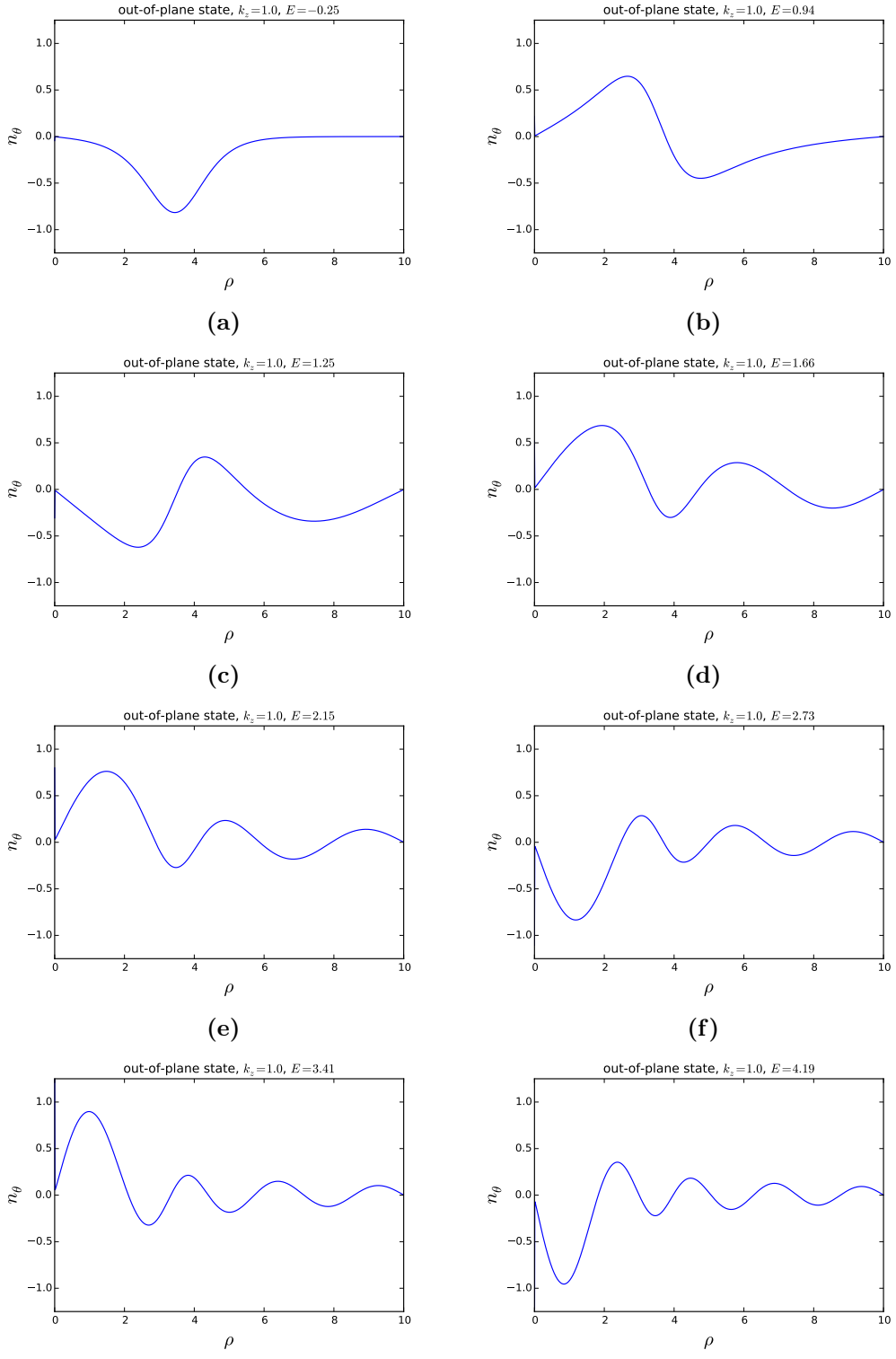

Figure 22: The out-of-plane wave functions $n_{\theta,l=0}$ for $k_z = 1.0$. (a): The evanescent/resonant ground state, with probability density focused around the minima of the potential. (b): The first excited state, which is bound. (c)-(h): The $2^{\text{nd}} - 7^{\text{th}}$ excited state, all being unbound, linear at $0 \lesssim \rho$ and damped oscillatory for increasing ρ.

5.2.3 Anisotropy parameter $k_z = 10$

In Figure 23 we show the in-plane and out-of-plane eigenfrequencies, as usually in units of ω_0 up to $n_r = 9$. We have left out the $n_r = 0, 1$ out-of-plane modes as their eigenvalue is negative. We observe a local accumulation in the density of states around $\omega \sim 3\omega_0$. Such a close-to degeneracy in the energy level is not present for $k_z = 0.1$ nor $k_z = 1.0$ and ensures that a global linear dependency on n_r is not accurate. However, the inset in the lower right corner shows that the asymptotic dependency on n_r is still linear. Another difference to previous k_z-values is that the out-of-plane frequencies are less than the in-plane ones for a given value of n_r.

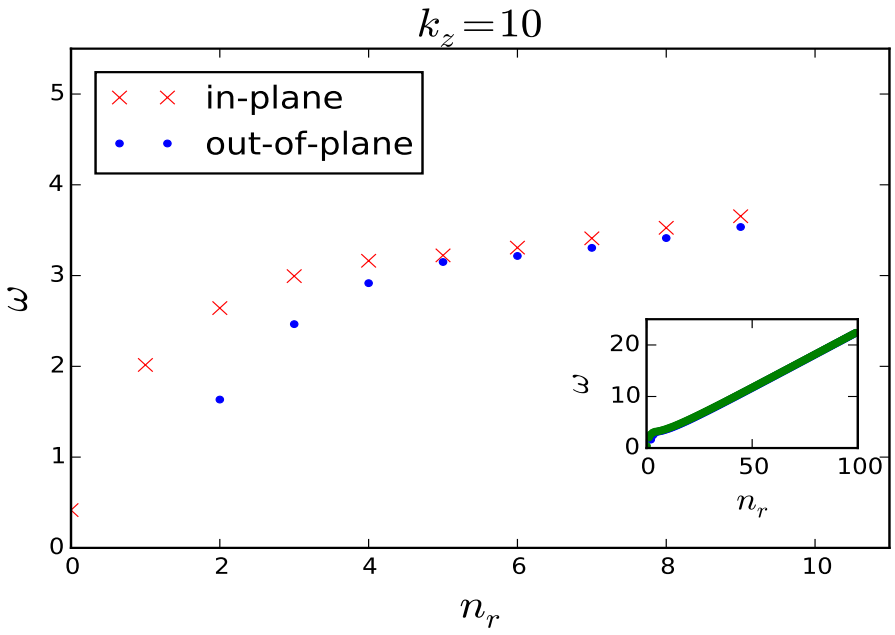

Figure 23: The in-plane and out-of-plane eigenfrequencies ω in units of ω_0 up to $n_r = 9$ for reduced anisotropy $k_z = 10$. The $n_r = 0, 1$ out-of-plane eigenfrequencies are intentionally left out as E_θ is negative for those values. The out-of-plane states have lower frequencies than the corresponding in-plane states for same level of excitation n_r. The relative difference decreases for increasing n_r. There appear to be an accumulation of states around $\omega \approx 3\omega_0$. The inset in the right corner shows an extension of the spectra up to $n_r = 100$. The blue dots and red crosses for the out-of-plane and in-plane frequencies merge together into one green line due to limited resolution on the axes. We observe a linear relationship $\omega \propto n_r$ for $n_r > 10$.

In Figures 24 and 25 we plot the effective in-plane and out-of-plane potential as a function of ρ, respectively. Next to the potentials we have added four wave functions at their corresponding eigenvalue level to illustrate how the eigenstates now changes. The $n_r = 3$ in-plane and $n_r = 5$ out-of-plane wave functions are quite smeared out, reflecting the weakly binding to the skyrmion. Many more bound modes manifest here, as the depth of the potential traps is much larger than previous cases. Particularly, it emerges as a result of the $k_z \cos 2\Theta \in \{-k_z, k_z\}$ vs. $k_z \cos^2\Theta \in \{0, k_z\}$ terms.

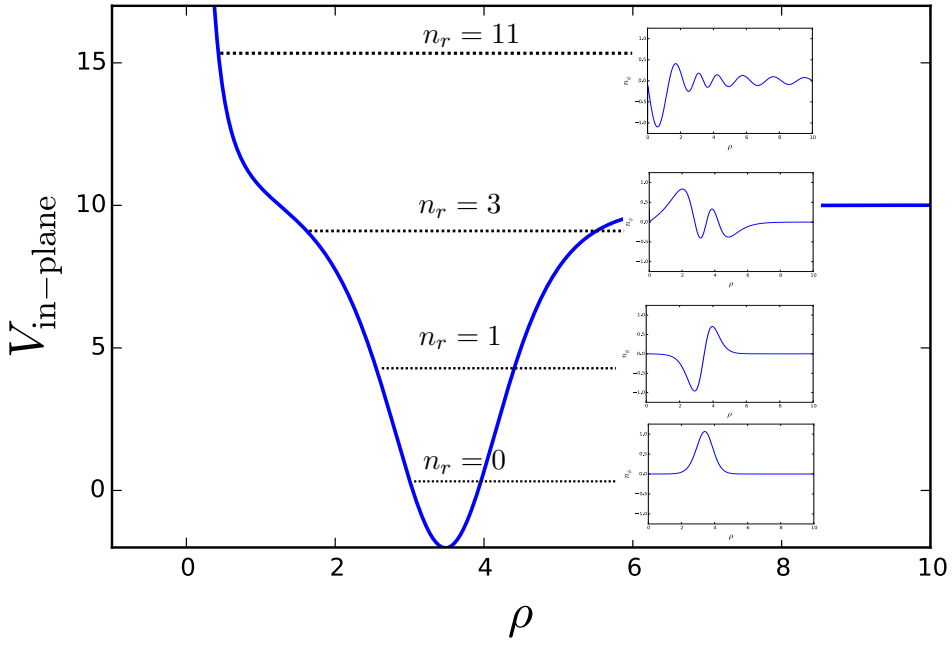

Figure 24: The in-plane potential $V_{\text{in}-\text{plane}} = \frac{\cos^2\Theta}{\rho^2} - (\partial_\rho\Theta)^2 - \frac{\sin 2\Theta}{2\rho} - \partial_\rho\Theta + k_z\cos^2\Theta$ for anisotropy parameter $k_z = 10$ as a function of ρ. The insets are the in-plane wave functions $n_{\phi,m=0}$ plotted as a function of ρ. The black dotted lines show the corresponding eigenvalue for each wave function. The lowest inset is the ground state with $E_\phi = 0.17$ and $n_r = 0$. The second lowest inset is the 1^{st} excited state with $E_\phi = 4.06$ and $n_r = 1$. The next inset is the 3^{rd} excited state with $E_\phi = 8.96$ and $n_r = 3$. These are all bound states. The uppermost inset is the 11^{th} excited state with $E_\phi = 15.51$ and $n_r = 11$, and is an unbound state, linear in ρ close to the core and damped oscillatory far away from the centre.

In Figures 26 and 27 the 8 lowest-lying in-plane and out-of-plane modes are shown, respectively. We observe that the regular damped oscillations and the linear

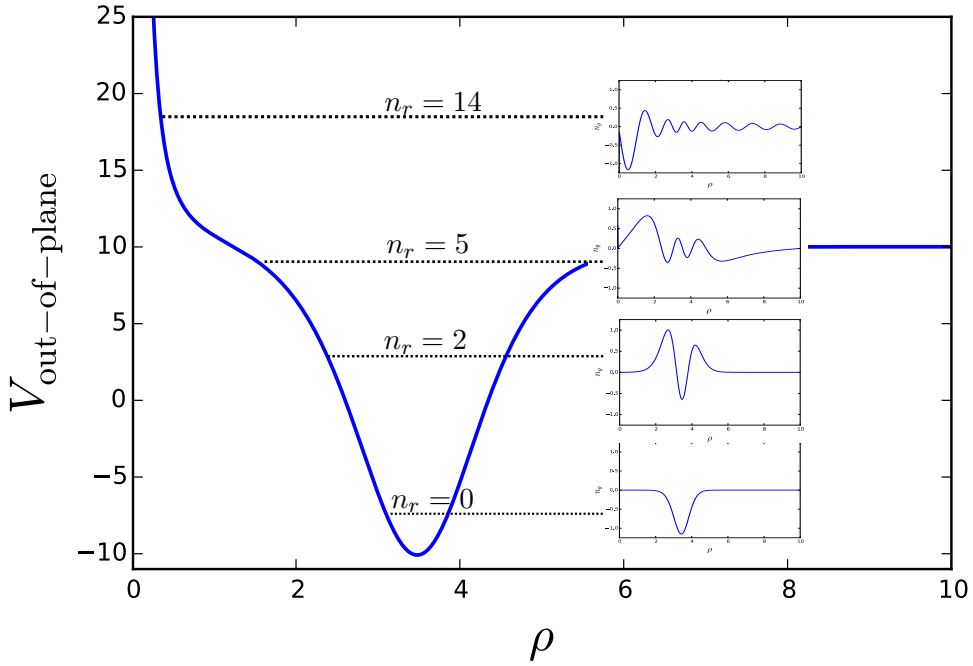

Figure 25: The out-of-plane potential $V_{\text{out}-\text{of}-\text{plane}} = \frac{\cos 2\Theta}{\rho^2} - \frac{\sin 2\Theta}{\rho} + k_z \cos 2\Theta$ for anisotropy parameter $k_z = 10$ as a function of ρ. The insets are the out-of-plane wave functions $n_{\theta,l=0}$ plotted as a function of ρ. The black dotted lines show the corresponding eigenvalue. The lowest inset is the ground state with $E_\theta = -7.13$ and $n_r = 0$, where the probability distribution is centred in the potential well. The second lowest inset is the 2^{nd} excited state with $E_\theta = 2.67$ and $n_r = 2$. The next inset is the 5^{th} excited state with $E_\theta = 9.92$ and $n_r = 5$, which is the last bound state. The uppermost inset is the 14^{th} excited state with $E_\theta = 18.45$ and $n_r = 14$, which is just one of many unbound states.

dependence on ρ close to the skyrmion are not present unless we increase n_r further, as shown by the uppermost insets in Figures 24 and 25. Another effect more prominent here, is that the curvature of the unbound travelling wave magnons increases vastly in the potential well compared to region outside the texture-induced well, see Figures 26(e)-(h) and 27(g)-(h). The wavelength contracts within the well and is extended outside it. Within the trap, the potential energy decreases, and the reduction is picked up by an equal and opposite increment in the kinetic energy to conserve the total energy. Outside the well we observe elongated wavelengths with little curvature, related to less kinetic energy.

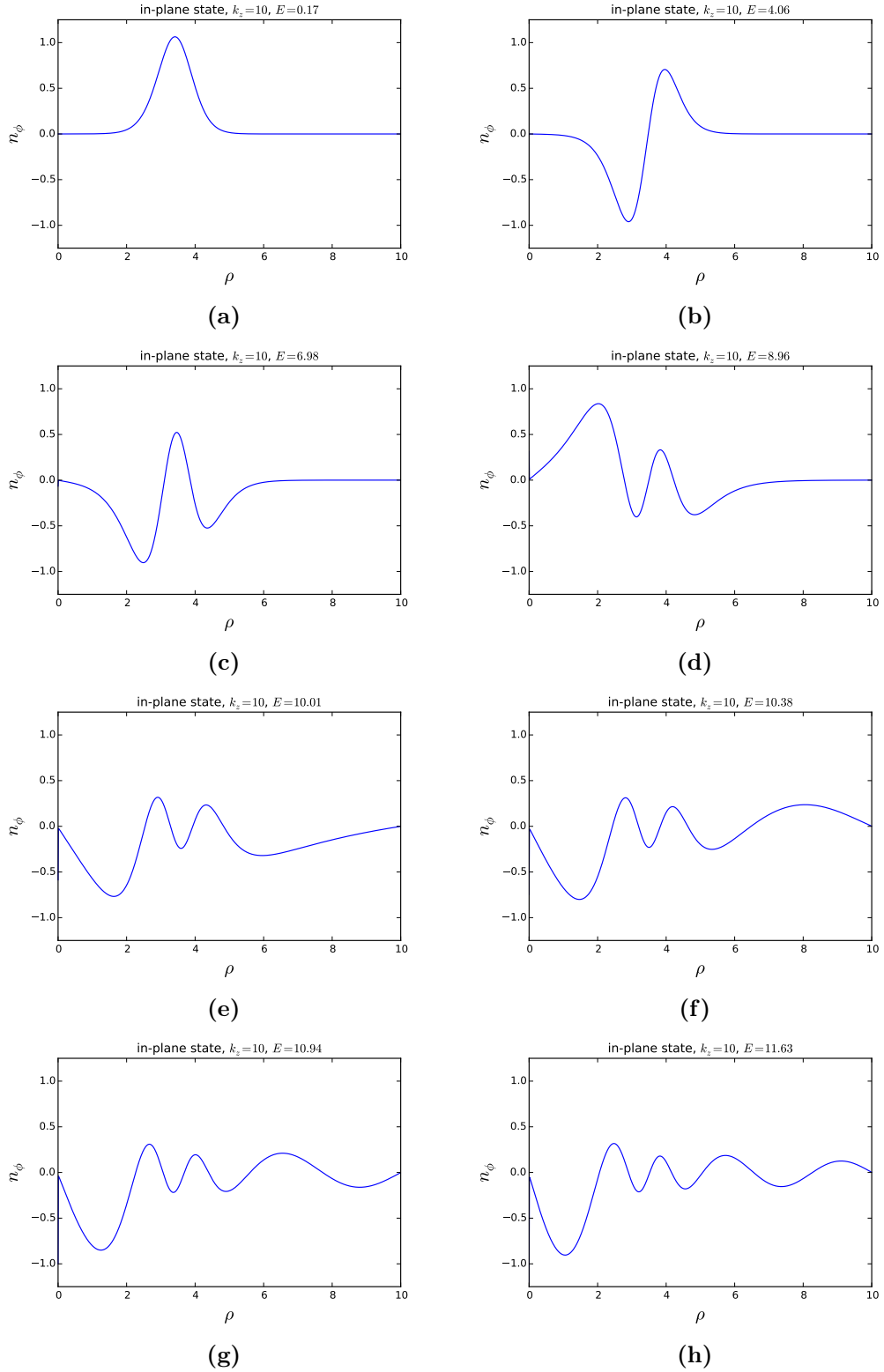

Figure 26: The in-plane wave functions $n^{67}_{\phi,m=0}$ for $k_z = 10$. (a): The localized ground state, with probability density focused around the minima of the potential. (b)-(d): The $1^{\text{st}} - 3^{\text{rd}}$ excited states, all bound. (e)-(h): The $4^{\text{th}} - 7^{\text{th}}$ excited state, all unbound, linear at $0 \lesssim \rho$ and more oscillatory the higher the eigenvalue.

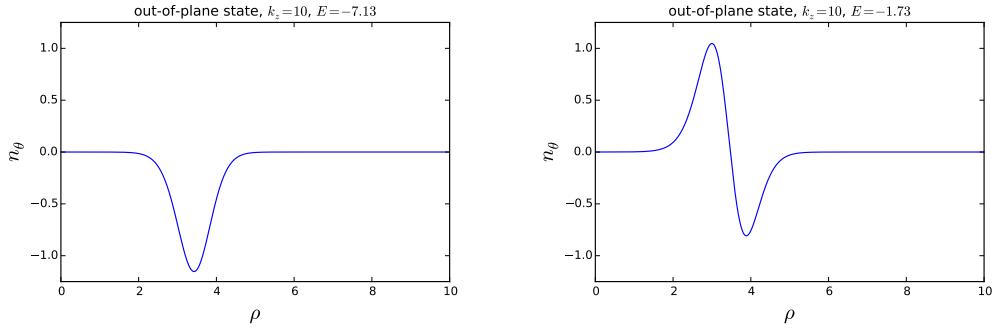

(a)

(b)

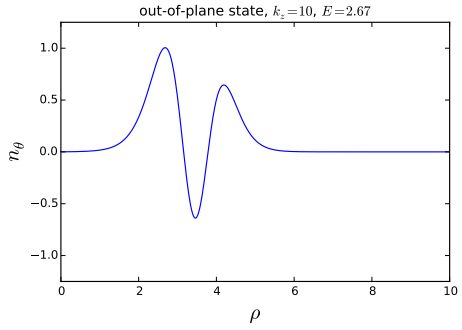

(c)

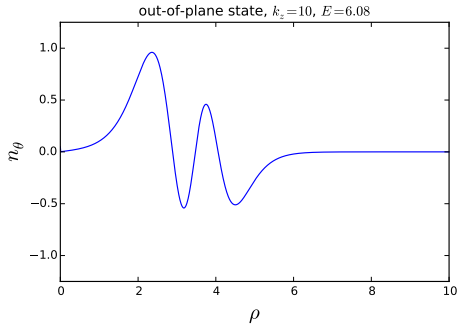

(d)

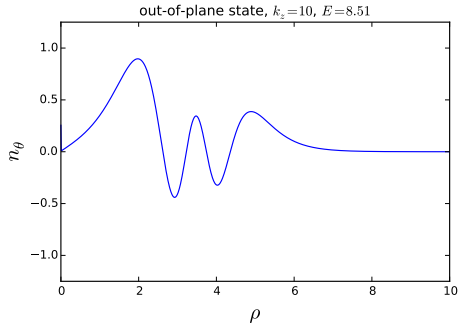

(e)

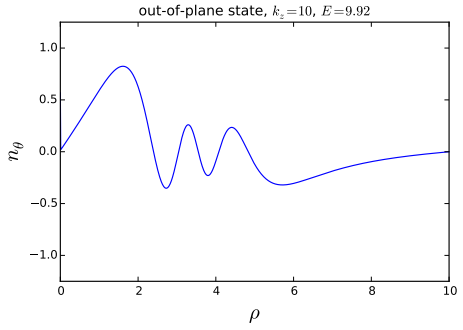

(f)

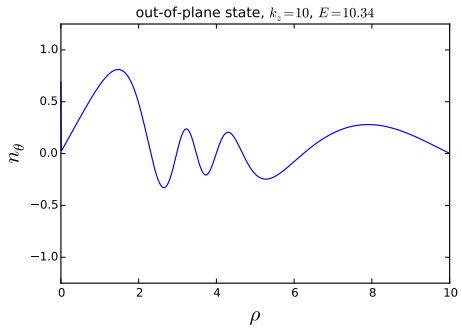

(g)

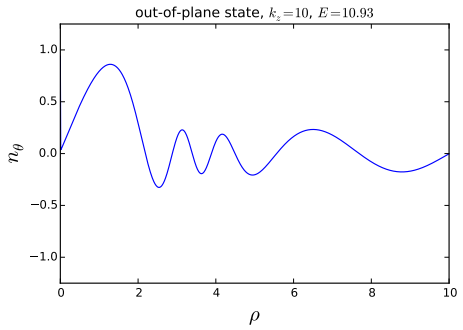

(h)

Figure 27: The out-of-plane wave functions $n_{\theta,l=0}$ for $k_z = 10$. (a): The ground state, with probability density focused around the minima of the skyrmion induced potential. (b): The first excited state, being either evanescent or resonant as the ground state. (c)-(f) The $2^{\text{nd}} - 5^{\text{th}}$ excited states, all being bound. (g)-(h): The 6^{th} and 7^{th} excited state, which are the lowest-lying unbound states.

5.3 Analogy to the easy-plane antiferromagnetic vortex

The antiferromagnetic easy-plane vortex is, similarly to the skyrmion, a topologically protected soliton excitation. They are cylindrically symmetric about the axis orthogonal to the basal plane, and was reported long before the antiferromagnetic skyrmion [79]. In the 1990s, they were widely studied from a theoretical point of view [109, 114, 115, 133, 134], and it was demonstrated that only exchange coupling and easy-plane anisotropy are necessary to stabilize the vortices. Following Ref. [109], the apparent Schrödinger-like equations for the vortices, using μ for n_ϕ and ϑ for n_θ, read

$$q^2\mu = \Big(-\nabla^2 + \frac{\cos^2\Theta}{x^2} - (\partial_x\Theta)^2\Big)\mu - \frac{2\cos\Theta}{x^2}\partial_\phi\vartheta - \cos^2\Theta\mu, \tag{50}$$

and

$$q^2\vartheta = \Big(-\nabla^2 + \frac{\cos 2\Theta}{x^2}\Big)\vartheta + \frac{2\cos\Theta}{x^2}\partial_\phi\mu - \cos 2\Theta\mu. \tag{51}$$

Here, $x = r/\lambda_{\text{vortex}}$ is the dimensionless radial coordinate, with $\lambda_{\text{vortex}} = (\frac{c}{2}\sqrt{\frac{\lambda}{1-\lambda}})$ and λ originating from their Hamiltonian $H = J_s\sum_{\langle \mathbf{n},\mathbf{n}'\rangle}\big(\mathbf{S}_n\cdot\mathbf{S}_{n'} + (\lambda-1)S_n^zS_{n'}^z\big)$ assuming $(1-\lambda)\ll 1$. $q^2 = \omega^2/\omega_0^2$, but for the vortex, the natural eigenfrequency of the system used is $\omega_0 = v/\lambda_{\text{vortex}}$ with the phase velocity $v = (2J_sc/\hbar)\sqrt{1+\lambda}$.

As can be seen from Eqs. (47) and (50), the potential terms $\propto\cos^2\Theta$ from the anisotropy and the exchange coupling are present for both skyrmions and vortices. Also, the out-of-plane Eqs. (48) and (51) contain much of the same structure, with the potential terms $\propto\cos 2\Theta$ from the anisotropy and exchange being the same. The sign flip in the anisotropy terms arise because we have considered easy-axis instead of east-plane anisotropy for the skyrmion.

There are the terms coupling the Schrödinger-like equations that complicates the systems for both skyrmions and vortices. They are proportional to $\cos\Theta$ for both solitons, while skyrmions hold an extra coupling term from the DMI proportional to $\sin\Theta$. For stable delocalized vortices with boundary conditions $\Theta(r\to\infty) = \pi/2$ [48], $\cos\Theta\to 0$ far from the core. The coupling is exponentially decaying [109], which allows for analytic solutions even for nonzero azimuthal quantum numbers. For localized skyrmions, we have $\cos\Theta(r\to\infty) = 1$ and $\sin\Theta(r\to\infty) = 0$. We spot an exponential decay in Θ here too, shown in Figure 28. We have added an

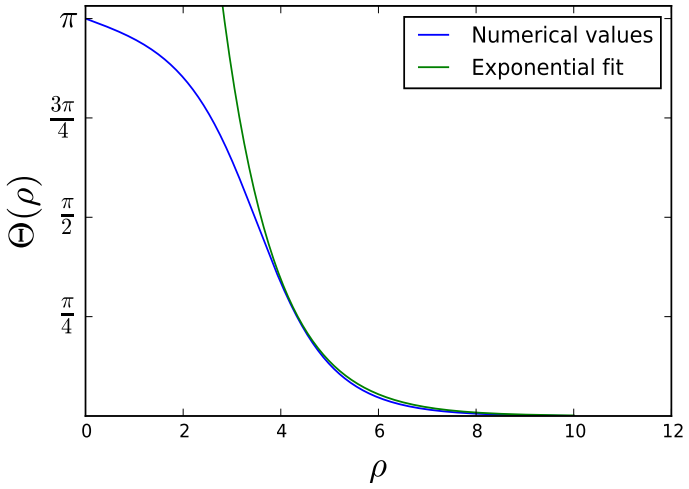

Figure 28: The polar angle $\Theta(\rho)$ between the staggered magnetization $\mathbf{n}_0$ and the z-axis as a function of $\rho = r/\lambda_{\text{sky}}$. The blue line is the exact result obtained by solving Eq. (23), while green line is an ad-hoc exponential function $f(\rho) = ae^{-b\rho}$ added to illustrate the exponential decay of Θ. $a = 42.88$ and $b = 0.92$ are manually adjusted to fit the blue line.

exponential function $f(\rho) = ae^{-b\rho}$ to fit the tail of Θ outside the skyrmion core. The parameters a, b is not based on a least-square method, just manually tweaked to recreate the asymptotic form of Θ. We used $a = 42.88, b = 0.92$. Hence, the coupling between the in-plane and out-of-plane fields for a skyrmion shows a power-law decaying behaviour rather than being exponentially decaying.

Let us now consider the $m = l = 0$ mode for the vortices. We label these lowest-lying angular modes μ_0 and ϑ_0. The delocalized vortex equations decouple, and we can find analytic solutions in the long and short distance limit. Far from the vortex core, we can neglect the derivative of the texture, and the in-plane radial amplitude is a linear combination of zeroth order Bessel functions:

$$\mu_0 = c_1 J_0(z) + c_2 Y_0(z), \tag{52}$$

where $z = x\omega/\omega_0$. Far from the vortex core, with $z \gg \left|\nu^2 - \frac{1}{4}\right|$, we can use the asymptotic behaviour of the Bessel functions:

$$J_\nu(z) \simeq \sqrt{\frac{2}{\pi z}} \cos\left(z - \frac{\nu\pi}{2} - \frac{\pi}{4}\right), \qquad Y_\nu(z) \simeq \sqrt{\frac{2}{\pi z}} \sin\left(z - \frac{\nu\pi}{2} - \frac{\pi}{4}\right), \tag{53}$$

where ν is the order. We have $\nu = 0$, and we combine the Bessel function of first and second kind by writing

$$\mu_0 \propto \frac{1}{\sqrt{r}} \sin(kr + \delta), \qquad k = |\omega|/v, \tag{54}$$

with δ some phase shift and $v = \lambda_{\text{vortex}}\omega_0$ is the magnon velocity. The dispersion relation is defined in this way as $\omega/(\omega_0\lambda_{\text{sky}})$ has units of m^{-1} and appears alongside r, meaning it has the physical interpretation of wavenumber and is a gapless continuous spectrum. For the out-of-plane excitations, the story is a bit different, as $\cos 2\Theta = 1$ far away from the vortex. This gives a gap in the dispersion relation, which allows for the existence of local out-of-plane modes [109].

If we now consider the antiferromagnetic skyrmion instead, the texture derivatives can be neglected in the long-distance limit as $\Theta \simeq 0$, and the asymptotic Schrödinger-like equations read

$$\frac{\omega^2}{\omega_0^2} n_{\phi(\theta),0} = \Big(-\nabla_\rho^2 + \frac{1}{\rho^2} + k_z\Big) n_{\phi(\theta),0}. \tag{55}$$

The wave functions have their argument altered: $z = \frac{r}{\lambda_{\text{sky}}}\sqrt{\omega^2/\omega_0^2 - k_z}$. If $\omega > \omega_{\text{crit}}$, where ω_{crit} is the critical frequency for having bound modes, the argument is real and the solution is that of first order Bessel functions

$$n_{\phi(\theta),0} \propto \frac{1}{\sqrt{r}} \sin(k_{\phi(\theta)} r + \delta_{\phi(\theta)}), \qquad k_{\phi(\theta)} v = \sqrt{\omega_{\phi(\theta)}^2 - k_z \omega_0^2}, \tag{56}$$

where $v = \lambda_{\text{sky}}\omega_0$ is the magnon velocity. We observe that both the in-plane and out-of-plane excitations have a gap for the skyrmion, while only the out-of-plane excitations have a gap for vortices. The wave functions are oscillatory but damped, which is the asymptotic behaviour we found in Chapter 5.2.

If the magnon eigenfrequency does not exceed the threshold, $\omega^2 < k_z\omega_0^2$, the eigenstates turn into modified Bessel functions of first and second kind, $I_1(z), K_1(z)$. The first kind modified Bessel function has an exponential growth in position and are unphysical. Hence, we are left with exponentially decaying eigenstates, i.e. local modes with frequency $\omega = \omega_l, \omega_l^2 < \omega_0^2 k_z$. The solutions are

$$n_{\phi,0}^{local}, n_{\theta,0}^{local} \propto e^{-k_l r}, \qquad k_l v = \sqrt{k_z\omega_0^2 - \omega_l^2}. \tag{57}$$

That is similar to what found for delocalized vortices, but for the $m = l = 0$ mode, the only possible local modes are the out-of-plane excitations. For the antiferromagnetic skyrmion *both* in-plane and out-of-plane excitations can be local modes.

Let us now consider the small distance limit for the $m = l = 0$ modes for the skyrmion. We are close to the skyrmion centre, where $\Theta = \pi$ can be considered a constant, and the spatial texture derivatives can be neglected once again. Also, $\sin 2\Theta = 0$ here. A distinct property of the skyrmion Schrödinger-like equations is that they are invariant in the small- and long-distance limit. For delocalized vortices, this is not the case, as $\cos 2\Theta$ flip signs between ± 1 for $\Theta = 0, \pi/2$. The asymptotic behaviour when $z \to 0$ for Bessel functions is

$$J_\nu(z) \simeq \frac{1}{\Gamma(\nu+1)} \left(\frac{z}{2}\right)^\nu, \tag{58}$$

$$Y_\nu(z) \simeq \begin{cases} \frac{2}{\pi}[\ln(z/2) + \gamma], & \nu = 0 \\ -\frac{\Gamma(\nu)}{\pi} \left(\frac{2}{z}\right)^\nu, & \nu \neq 0. \end{cases} \tag{59}$$

where ν is the order, $\Gamma(\nu)$ is the Gamma function and γ is the Euler-Mascheroni Constant. The skyrmion solutions are first order Bessel functions, but the second kind diverges in the classically forbidden region at the skyrmion core and must be disregarded as it is unphysical. Hence, we obtain

$$n_{\phi,0}, n_{\theta,0} \propto z \tag{60}$$

This approximation is justified if we consider modes with eigenfrequency above the critical threshold. The numerical diagonalization procedure used to find the wave functions in Chapter 5.2 showed the same linear dependency on ρ close to the skyrmion core as the analytic solution derived here for these modes.

Now, let us discuss the implication of rather having a finite sized system. For a finite sized system, we have to impose some boundary conditions at the rim. Both Dirichlet (fixed), Neumann (free) and general (combination of fixed and free) boundary conditions at the edge $r = L$ are possible. They all have in common that we consider the long-distance limit, far from the skyrmion core. In terms of applications, the small frequencies are most interesting. However, if we consider the apparent local mode $\omega_l^2 < k_z \omega_0^2$, the boundary conditions, regardless of type, are always fulfilled

as both the in-plane and out-of-plane wave functions are harshly damped. For the travelling wave states, this is not the case. Fixed boundary conditions imply

$$n_{\phi,0}(r = L), n_{\theta,0}(r = L) = 0, \tag{61}$$

while free boundary conditions yield

$$\partial_r n_{\phi,0}|_{r=L}, \partial_r n_{\theta,0}|_{r=L} = 0. \tag{62}$$

For both cases, the magnon spectrum will be discrete as the solutions are oscillating as a function of r, and fixing r implies that only a discrete (infinite) set of wave numbers k_n are allowed. This is opposite to what discussed above, where we found continuous spectra. In fact, numerical studies suggest that finite sized systems with open boundaries breaking the lattice symmetry are requirements for skyrmions to be a thermodynamically stable phase [67].

Finally, a note about the effective potentials are in place. For skyrmions with nonzero DMI, the potentials in the presence of DMI for both the in- and out-of-plane wave functions are quite complicated as they hold derivatives of the texture in combination with sine and cosine texture-dependent terms. To illustrate the difference to the vortex potentials, we make the analytic ansatz $\Theta^{\text{vortex}} = \frac{\pi}{2} - \frac{\pi}{2} \cdot \frac{1}{1+(x/4)^2}$, which fulfills the boundary conditions $\Theta(0) = 0, \Theta(\infty) = \pi/2$, see Figures 29 and 30. The true potentials are somewhat altered as the profile of Θ is slightly deviating from our ansatz [109]. Nevertheless, the overall form of the potentials is somewhat similar to the skyrmion ones, only with the influence of the anisotropy being stronger for skyrmions. All potentials have a global minima, diverge close to the centres and approach a constant far from the solitons.

5.4 Highly excited magnon regime

The full Schrödinger-like equations (47) and (48) do not permit analytic solutions. From an application point of view, interesting properties such as magnon-mediated spin Hall response have been investigated for highly excited states [135]. The energetic modes will typically require a temperature gradient to reach the necessary level of excitation. For the spin waves, it means that the wavelength is very small compared to the typical length scale of the skyrmion: $\lambda_{\text{sw}} \ll \lambda_{\text{sky}}$. In our search for analytic approximate solutions, we introduce the dimensionless radial coordinate

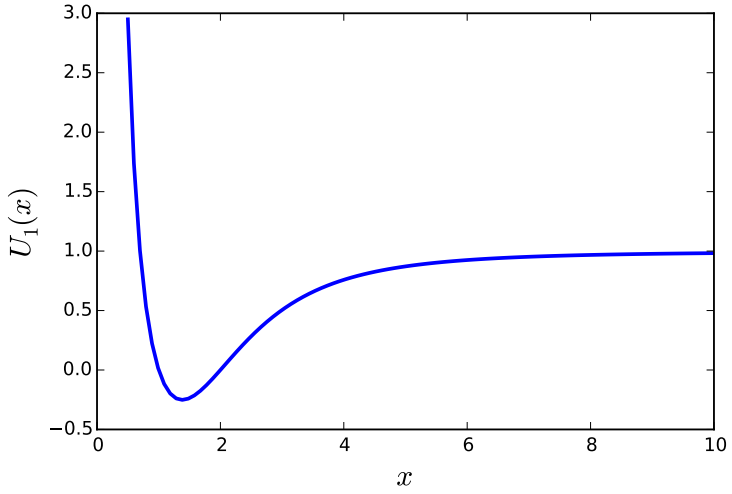

Figure 29: The effective potential $U_1(x) = \cos 2\Theta(1/x^2 - 1)$ for the out-of-plane magnon excitations around the easy-plane antiferromagnetic vortex. $x = r/\lambda_{\text{vortex}}$, with λ_{vortex} being the natural length scale. The potential has the limiting behaviour $U_1(\infty) = 1$ and is attractive, with a global minima and a potential barrier close to the vortex core.

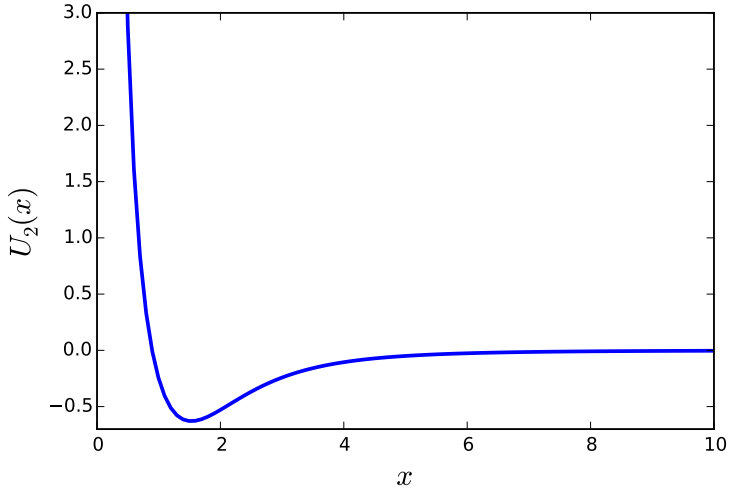

Figure 30: The effective potential $U_2(x) = \cos^2\Theta(1/x^2 - 1) - (\partial_x\Theta)^2$ for the in-plane magnon excitations around the easy-plane antiferromagnetic vortex. $x = r/\lambda_{\text{vortex}}$, with λ_{vortex} being the natural length scale. The potential has the limiting behaviour $U_2(\infty) = 0$, and is attractive, with a global minima and a potential barrier close to the vortex core.

$\tilde{\rho} = r/\lambda_{\mathrm{sw}}$, and write the Schrödinger-like equations as a series expansion in the parameter $\eta = \lambda_{\mathrm{sky}}/\lambda_{\mathrm{sw}}$:

$$\begin{aligned} q_\phi^2 n_\phi = \eta^2 \Big(\Big(-\nabla_{\tilde{\rho}}^2 - (\partial_{\tilde{\rho}}\Theta)^2 + \frac{\cos^2\Theta}{\tilde{\rho}^2} \Big) n_\phi - \frac{2\cos\Theta}{\tilde{\rho}^2} \partial_\phi n_\theta \Big) \\ + \eta \Big(\Big(-\frac{\sin 2\Theta}{2\tilde{\rho}} - \partial_{\tilde{\rho}}\Theta \Big) n_\phi + \frac{\sin\Theta}{\tilde{\rho}} \partial_\phi n_\theta \Big) + k_z \cos^2\Theta n_\phi, \end{aligned} \tag{63}$$

$$q_\theta^2 n_\theta = \eta^2 \Big(\Big(-\nabla_{\tilde{\rho}}^2 + \frac{\cos 2\Theta}{\tilde{\rho}^2} \Big) n_\theta + \frac{2\cos\Theta}{\tilde{\rho}^2} \partial_\phi n_\phi \Big) \tag{64}$$

$$+ \eta \Big(-\frac{\sin 2\Theta}{\tilde{\rho}} n_\theta - \frac{\sin\Theta}{\tilde{\rho}} \partial_\phi n_\phi \Big) + k_z \cos 2\Theta n_\theta. \tag{65}$$

In the short wavelength limit, we only keep the highest order terms in η. Doing so, we rule out the impact of the DMI on the magnons. Also, the anisotropy becomes irrelevant. These coupling mechanisms will only be minor corrections when the spin waves are highly excited. From the Hamiltonian, this makes sense, because the spin waves now carry so much energy that only the most influential interaction mechanisms become important, i.e. the exchange coupling. The new equations, by re-scaling the radial coordinate $\tilde{\rho} \to \rho$ after assuming $\lambda_{\mathrm{sw}} \ll \lambda_{\mathrm{sky}}$ allowing us to only keep the leading order terms, are

$$\frac{\omega_\phi^2}{\omega_0^2} n_\phi = \Big(-\nabla_\rho^2 - (\partial_\rho\Theta)^2 + \frac{\cos^2\Theta}{\rho^2} \Big) n_\phi - \frac{2\cos\Theta}{\rho^2} \partial_\phi n_\theta, \tag{66}$$

$$\frac{\omega_\theta^2}{\omega_0^2} n_\theta = \Big(-\nabla_\rho^2 + \frac{2\cos^2\Theta - 1}{\rho^2} \Big) n_\theta + \frac{2\cos\Theta}{\rho^2} \partial_\phi n_\phi. \tag{67}$$

Despite simplifying the system up to this point, we are still not able to find analytic expression for the eigenfrequencies nor the eigenstates. To do so, we need an analytic expression for the radial dependence of $\Theta(\rho)$. In the simplest form, we could assume a linear function in r as done in Refs. [104, 107], respecting the boundary conditions at $r = 0$ and $r = L$: $\Theta(\rho) = \pi(1 - r/L)$. This is a vast simplification of the profile, yet the solution for magnon excitations of the ferromagnetic skyrmion in Ref. [107] becomes quite intricate. A less trivial ansatz would be to apply the Walker profile for the antiferromagnetic domain wall: $\Theta(r) = 2\arctan e^{(r_0 - r)/\lambda_{\mathrm{sky}}}$, where r_0 determines where $\Theta(r) = \Theta(0)/2$. With this kind of approach, however, the coupling and the complicated expression for Θ do not allow us to obtain analytic solutions of Eqs. (66) and (67) for a general set of angular quantum numbers.

6
Conclusion

In this chapter we will recap the work done in the thesis and summarize the main findings. At the end, we discuss the prospects and challenges for antiferromagnetic magnonics.

6.1 Summary and concluding remarks

In this thesis we have derived a new set of Schrödinger-like equations for in-plane and out-of-plane spin wave excitations of a 2D skyrmion in an insulating two-sublattice antiferromagnet subject to easy-biaxial crystallographic anisotropy, DMI and symmetric exchange coupling. For the inhomogeneous Néel-type skyrmion the new set of Schrödinger-like equations are derived from a variational principle in the micromagnetic limit assuming an orthogonal basis of the spin wave fields to that of the equilibrium texture to first order. The equations are highly coupled to each other, and the symmetry is considerably reduced compared to spin waves around the antiferromagnetic ground state and ferromagnetic inhomogeneous soliton excitations.

The new set of Schrödinger-like equations are solved for the lowest angular azimuthally symmetric eigenmodes for which the excitations decouple. This is identical to solving the equations along a given azimuthal direction. The eigenspectra and the eigenmodes are computed by a 2^{nd} order local truncation error numerical diagonalization scheme, where the texture-induced potential is numerically solved by a shooting method with a 5^{th} order Runge-Kutta integration procedure by minimizing the antiferromagnetic free energy. The effective potentials are strongly dependent on the interaction strength between the anisotropy and the symmetric exchange coupling, and the inhomogeneous DMI.

Both the in-plane and out-of-plane magnon excitations can be evanescent, reso-

nant, bound or travelling wave modes. There are two "Goldstone modes" present, irrespective of the reduced anisotropy parameter. For each of those modes, the magnons are either exponentially damped or growing. The model does not predict whether damping or growth occurs for these modes, and an extension of the model by for instance considering kinetic theory, magnon-magnon coupling or Stoner excitations is necessary to conclude. For the other modes, an increasing reduced anisotropy parameter allows for more bound magnon states. The higher excited delocalized travelling wave states resemble first order cylindrical Bessel functions of the first kind, a behaviour which is analytically confirmed in the short and long-distance limit from the skyrmion core. When comparing to easy-plane antiferromagnetic vortices, we find that both in-plane and out-of-plane excitations can have local modes, while only the out-of-plane vortex modes can be bound and localized.

In the highly excited regime, where the spin wave wavelength is much shorter than the typical length scale of the skyrmion, $\lambda_{\text{sky}} \gg \lambda_{\text{sw}}$, we find that the new set of Schrödinger-like equations reduces to a simplified set where the DMI and the anisotropy are absent. For these energetic modes, only the strongest spin coupling, the symmetric Heisenberg exchange, is present. However, the equations are still coupled, and only display a power-law decaying coupling, as opposed to vortices which have exponentially decaying coupling terms. Full analytic solutions on the entire domain are still not possible without further assumptions on the system.

6.2 Outlook

In further studies of magnon excitations around the antiferromagnetic skyrmion, we suggest applying kinetic theory in terms of the Vlasov or spin-dependent Vlasov-Boltzmann equation to investigate conditions for damping or growth of the "Goldstone" modes. Resonance with Stoner excitations leading to Landau damping and the impact of higher order corrections in the excitations fields should also be addressed. A local rotation of the high-frequency Schrödinger-like equations in Chapter 5.4 similarly to what done earlier for ferromagnets would also be relevant [107]. The intense modes excited by thermal gradients can be of interest in applications [8, 102]. This continuation with emergent electrodynamics could also be compatible to the effective force terms used in kinetic theory. Avoiding the weakness of a linear skyrmion profile by using the antiferromagnetic Walker ansatz [36] could be an intuitive approach, but the calculation will be very technical and analytic solutions

are doubtful.

In addition, a full discrete treatment of the Hamiltonian with magnon excitations is necessary to confirm the micromagnetic limit solutions considered here. Such an approach could be a semi-classical quantum operator representation of the spins, where the eigenmodes are found by the Gram-Schmidt process and self-consistent Gauss-Seidel scheme, which has been applied on vortices [136]. Also, a more rigorous quantum mechanical treatment should be investigated by for instance rewriting the magnonic spin operators by the Holstein-Primakoff transformation to obtain bosonic creation and annihilation operators to diagonalize the original discrete Hamiltonian and thereby solve the Schrödinger equation.

Regarding the experimental challenges, a considerable void in characterizing the spin structure of antiferromagnetic materials has to be probed before antiferromagnets can fully replace today's technology in memory storage and processing [137]. Especially those exotic types with noncollinear staggered magnetization, and their dynamic response to perturbations as spin currents, spin-orbit torques and ac magnetic fields. For the skyrmions, which is exactly one of those exotic spin structures that has been experimentally observed *at* room temperature in the antiferromagnetic/ferromagnetic heterostructure IrMn/CoFeB by nitrogen-vacancy centre-based microscopy and Brillouin light scattering [44], a question to answer is how to create, manipulate and delete them. Numerical simulations show how strong magnetic fields can destabilize the skyrmion, while a skyrmion can be created by Dzyaloshinskii-Moriya interaction combined with out-of-plane uniaxial anisotropy [30], offering techniques for novel memory devices.

Appendices

A

Antiferromagnetic spin interactions

In this appendix we derive the micromagnetic coupling mechanisms from the discrete spin picture of a 2D squared lattice antiferromagnetic material. The starting point for all the contributions to the free energy of the system are two sublattices α, β with magnetization $\mathbf{M}_k$, $k \in \{\alpha, \beta\}$ far below the Curie temperature, such that the modulus of the magnetization is fixed, and only contains orientational degree of freedom [48]. We write $\mathbf{M}_k(\mathbf{x}) = M_s \mathbf{m}_k(\mathbf{x})$, where M_s is the saturation magnetization and $\mathbf{m}_k$ is a unit vector pointing along the magnetization direction of sublattice k. We define the magnetization $\mathbf{m}_{i,j}$ and staggered magnetization $\mathbf{l}_{i,j}$ at lattice site (i, j) as

$$\mathbf{m}_{i,j} = (\mathbf{S}^{\alpha}_{i,j} + \mathbf{S}^{\beta}_{i,j})/2, \qquad \mathbf{l}_{i,j} = (\mathbf{S}^{\alpha}_{i,j} - \mathbf{S}^{\beta}_{i,j})/2, \tag{68}$$

such that

$$\mathbf{S}^{\alpha}_{i,j} = (\mathbf{m}_{i,j} + \mathbf{l}_{i,j}), \qquad \mathbf{S}^{\beta}_{i,j} = (\mathbf{m}_{i,j} - \mathbf{l}_{i,j}). \tag{69}$$

We define the Néel vector $\mathbf{n}_{i,j} = \mathbf{l}_{i,j}/|l|_{i,j}$. In the exchange approximation, $\mathbf{S}^{\alpha}_{i,j} \simeq -\mathbf{S}^{\beta}_{i,j}$.

A.1 Symmetric Heisenberg exchange

In this chapter we derive the symmetric exchange coupling for the antiferromagnetic free energy with the definition of the order parameter and magnetization as given above. The Heisenberg exchange in 2D is

$$\mathcal{H}_{\mathrm{H}} = J_s \sum_{\langle \mathbf{x},\mathbf{x}' \rangle} \mathbf{S}_{\mathbf{x}} \cdot \mathbf{S}_{\mathbf{x}'}, \tag{70}$$

where $\mathbf{S}_{\mathbf{x}}$ denotes the dimensionless spin of unit length at position $\mathbf{x}$. The sum runs over nearest neighbours, where the number of adjacent spins $N_n = 4$ for both types α and β. Substituting in the order parameter and the magnetization gives

$$\begin{aligned}
\mathcal{H}_{\mathrm{H}} = J_s \sum_{i,j}^{N-1,N-1} & [\mathbf{m}_{i,j} - \mathbf{l}_{i,j}] \cdot \Big([\mathbf{m}_{i,j} + \mathbf{l}_{i,j}] + [\mathbf{m}_{i+1,j} + \mathbf{l}_{i+1,j}] + [\mathbf{m}_{i,j+1} + \mathbf{l}_{i,j+1}] \\
& + [\mathbf{m}_{i+1,j+1} + \mathbf{l}_{i+1,j+1}] \Big) \\
\simeq 4J_s \sum_{i,j}^{N,N} & (\mathbf{m}_{i,j}^2 - \mathbf{l}_{i,j}^2) \\
+ \frac{J_s}{2} \sum_{i,j}^{N-1,N-1} & \Big((\mathbf{l}_{i+1,j} - \mathbf{l}_{i,j})^2 + (\mathbf{l}_{i,j+1} - \mathbf{l}_{i,j})^2 + (\mathbf{l}_{i+1,j+1} - \mathbf{l}_{i,j})^2 \\
& - (\mathbf{m}_{i+1,j} - \mathbf{m}_{i,j})^2 - (\mathbf{m}_{i,j+1} - \mathbf{m}_{i,j})^2 - (\mathbf{m}_{i+1,j} - \mathbf{m}_{i,j})^2 \Big) \\
+ J_s \sum_{i,j}^{N-1,N-1} & \Big(\mathbf{m}_{i,j} (\mathbf{l}_{i+1,j} + \mathbf{l}_{i,j+1} + \mathbf{l}_{i+1,j+1} - 3\mathbf{l}_{i,j}) \\
& - \mathbf{l}_{i,j} (\mathbf{m}_{i+1,j} + \mathbf{m}_{i,j+1} + \mathbf{m}_{i+1,j+1} - 3\mathbf{m}_{i,j}) \Big)
\end{aligned} \tag{71}$$

where we have neglected the boundary contributions

$$\epsilon \simeq \sum_{i=1}^{N} 3(\mathbf{m}_{i,N}^2 - \mathbf{l}_{i,N}^2) \pm 3 \sum_{j=1}^{N} (\mathbf{m}_{N,j}^2 - \mathbf{l}_{N,j}^2) \pm \sum_{j=1}^{N} (\mathbf{m}_{1,j}^2 - \mathbf{l}_{1,j}^2) \pm \sum_{i=1}^{N} (\mathbf{m}_{i,1}^2 - \mathbf{l}_{i,1}^2), \tag{72}$$

which are all linear sums, vanishingly small in the large N limit of a physical system. N is the number of lattice sites along each axis of the lattice. For the cubic squared lattice in 2D, we have nearest-neighbour spacing c and the volume of the unit cell $V = \Delta_x \Delta_y = 2c^2$. Here, $\Delta_x = \Delta_y = \Delta$. When considering the micromagnetic limit, we approximate

$$\mathbf{l}_{i+1,j} - \mathbf{l}_{i,j} = \mathbf{l}(x_i + \Delta, y_j) - \mathbf{l}(x_i, y_j) \approx \Delta \partial_x \mathbf{l} \tag{73}$$

$$\mathbf{l}_{i,j+1} - \mathbf{l}_{i,j} = \mathbf{l}(x_i, y_j + \Delta) - \mathbf{l}(x_i, y_j) \approx \Delta \partial_y \mathbf{l} \tag{74}$$

$$\mathbf{l}_{i+1,j+1} - \mathbf{l}_{i,j} = \mathbf{l}(x_i + \Delta, y_j + \Delta) - \mathbf{l}(x_i, y_j) \approx \Delta(\partial_x + \partial_y)\mathbf{l} \tag{75}$$

Similar definitions are used for the magnetization. The form of the approximations allow us to write them using the Jacobian matrix, defined as operating on the vector field $\mathbf{f}$ with elements $\mathcal{J}_{i,j} = \frac{\partial f_i}{\partial x_j}$. Using the Jacobian, in the limit of $\Delta \to 0$, we have

$$\sum_{i,j}^{N-1,N-1} \mathbf{l}_{i+1,j} - \mathbf{l}_{i,j} \approx \frac{1}{V} \int d\mathbf{x}\, \mathcal{J}(\mathbf{l}) \boldsymbol{\Delta}_x, \tag{76}$$

$$\sum_{i,j}^{N-1,N-1} \mathbf{l}_{i.,j+1} - \mathbf{l}_{i,j} \approx \frac{1}{V} \int d\mathbf{x}\, \mathcal{J}(\mathbf{l}) \boldsymbol{\Delta}_y, \tag{77}$$

$$\sum_{i,j}^{N-1,N-1} \mathbf{l}_{i+1,j+1} - \mathbf{l}_{i,j} \approx \frac{1}{V} \int d\mathbf{x}\, (\mathcal{J}(\mathbf{l}) \boldsymbol{\Delta}_x + \mathcal{J}(\mathbf{l}) \boldsymbol{\Delta}_y). \tag{78}$$

Here, $\boldsymbol{\Delta}_i = \Delta \hat{i}$, $i \in \{x, y\}$, is the vector adjoining two neighbouring lattice sites. We use the Jacobians and the integral approximations in the micromagnetic limit to obtain an expression for the Heisenberg exchange. Writing $\mathcal{H}_{\mathrm{H}} = \frac{1}{V} \int d\mathbf{x}\, H(\mathbf{m}, \mathbf{l}, \mathbf{m}', \mathbf{l}')$ with $H(\mathbf{m}, \mathbf{l}, \mathbf{m}', \mathbf{l}')/V$ being the energy density, we obtain

$$\begin{aligned}
\mathcal{H}_{\mathrm{H}} = \frac{J_s}{2c^2} \int d\mathbf{x} \Big(& 4(\mathbf{m}^2 - \mathbf{l}^2) + \frac{1}{2}\Delta^2 \big(2(\partial_x l_x)^2 + 2(\partial_y l_y)^2 + 2(\partial_x l_y)^2 + 2(\partial_y l_x)^2 \\
& + 2\Delta^2 \partial_x l_x \partial_y l_x + 2\Delta^2 \partial_x l_y \partial_y l_y \big) + 2\Delta \mathbf{m} \cdot (\partial_x \mathbf{l} + \partial_y \mathbf{l}) - 2\Delta \mathbf{l} \cdot (\partial_x \mathbf{m} + \partial_y \mathbf{m}) \Big) \\
= \frac{J_s}{c^2} \int d\mathbf{x} \Big(& 2\mathbf{m}^2 + \frac{\Delta^2}{2} \sum_i \big((\partial_i \mathbf{l})^2 - (\partial_i \mathbf{m})^2 \big) + \frac{\Delta^2}{4} \sum_{i \neq j} \partial_i \mathbf{l} \cdot \partial_j \mathbf{l} - \partial_i \mathbf{m} \cdot \partial_j \mathbf{m}) \\
& + \Delta \sum_i \big(\mathbf{m} \cdot \partial_i \mathbf{l} - \mathbf{l} \cdot \partial_i \mathbf{m} \big) \Big),
\end{aligned} \tag{79}$$

where the factor 1/4 in front of the cross-derivative products has been introduced to avoid overcounting. The ground state energy $\mathbf{l}^2$ has been disregarded as it corresponds to a global minima in the energy function, and we consider excitations from the ground state. We get

$$\mathcal{H}_{\mathrm{H}} = \int \frac{d\mathbf{x}}{V} \left(\frac{a}{2}\mathbf{m}^2 + A\Big(\sum_{i=x,y} (\partial_i \mathbf{n})^2 + \frac{1}{2} \sum_{i \neq j} \partial_i \mathbf{n} \cdot \partial_j \mathbf{n} \Big) + L \sum_{i=x,j} (\mathbf{m} \cdot \partial_i \mathbf{n}) \right), \quad (80)$$

with $a = 8J_s, A = 2J_s c^2, L = 2\sqrt{2}J_s c$, and terms higher order in the magnetization ($\partial_i \mathbf{m} \cdot \partial_j \mathbf{m}$, $\partial_i \mathbf{m}$ and $(\partial_i \mathbf{m})^2$) are being disregarded. We have substituted $\mathbf{l} \to \mathbf{n}$ as we consider the exchange approximation.

A.2 Inhomogeneous Dzyaloshinskii-Moriya interaction

The Dzyaloshinskii-Moriya interaction (DMI) between neighbouring spins $\mathbf{S}_{\mathbf{x}}, \mathbf{S}_{\mathbf{x}'}$ in discrete form reads

$$\mathcal{H}_{\mathrm{D}} = \sum_{\langle \mathbf{x}, \mathbf{x}' \rangle} \mathbf{D}_{\mathbf{x},\mathbf{x}'} \cdot (\mathbf{S}_{\mathbf{x}} \times \mathbf{S}_{\mathbf{x}'}), \quad (81)$$

where the DMI vector $\mathbf{D}_{\mathbf{x},\mathbf{x}'}$ is determined by the underlying crystal symmetry. The inhomogeneous DMI, responsible for the Lifschitz invariants stabilizing chiral states, has the DMI vector confined to the basal-plane of the texture. We consider the interfacial DMI with $\mathbf{D}_{\mathbf{x},\mathbf{x}+c\hat{y}} = D\hat{x}$ for adjoining spins along $\hat{y}$ and $\mathbf{D}_{\mathbf{x},\mathbf{x}+c\hat{x}} = -D\hat{y}$ for neighbouring spins in the x-direction. Labeling each of the $N \cdot N$ unit cells by a pair of indices (i, j), we only sum over the bonds with sub-lattice spins β as the centred spin in the square to avoid overcounting. For each cell, there are thus four bonds. The Hamiltonian becomes

$$
\begin{aligned}
\mathcal{H}_{\mathrm{D}} = & \sum_{i,j}^{N-1,N-1} \mathbf{D}_{\mathbf{x},\mathbf{x}'} \cdot \Big([\mathbf{m}_{i,j} - \mathbf{l}_{i,j}] \times \big([\mathbf{m}_{i,j} + \mathbf{l}_{i,j}] + [\mathbf{m}_{i+1,j} + \mathbf{l}_{i+1,j}] + [\mathbf{m}_{i,j+1} + \mathbf{l}_{i,j+1}] \\
& + [\mathbf{m}_{i+1,j+1} + \mathbf{l}_{i+1,j+1}] \big) \Big) \\
= D & \sum_{i,j}^{N_1,N-1} -\hat{y} \Big([\mathbf{m}_{i,j} - \mathbf{l}_{i,j}] \times \Big([\mathbf{m}_{i,j} + \mathbf{l}_{i,j}] + [\mathbf{m}_{i+1,j+1} + \mathbf{l}_{i+1,j+1}] \Big) \Big) \\
& + \hat{x} \Big([\mathbf{m}_{i,j} - \mathbf{l}_{i,j}] \times \Big([\mathbf{m}_{i+1,j} + \mathbf{l}_{i+1,j}] + [\mathbf{m}_{i,j+1} + \mathbf{l}_{i,j+1}] \Big) \Big) \\
\simeq D & \sum_{i,j}^{N_1,N-1} \hat{y} \big(\mathbf{l}_{i,j} \times \mathbf{l}_{i+1,j+1} \big) - \hat{x} \Big(\mathbf{l}_{i,j} \times \big(\mathbf{l}_{i+1,j} + \mathbf{l}_{i,j+1} \big) \Big)
\end{aligned}
\tag{82}
$$

We have disregarded terms containing magnetization components. In the exchange approximation, the symmetric Heisenberg exchange dominates the other coupling mechanisms. That is, $|J_s| \gg |D|$, and as the magnetization is also very small, these terms can be neglected when they are combined with the free energy in Eq. (80). Introducing the Jacobian approximations as in Appendix A.1, we obtain

$$
\begin{aligned}
\mathcal{H}_{\mathrm{D}} = D & \sum_{i,j}^{N-1,N-1} l^z_{i,j} l^x_{i+1,j+1} - l^z_{i+1,j+1} l^x_{i,j} - (l^y_{i,j} l^z_{i+1,j} - l^y_{i+1,j} l^z_{i,j}) - (l^y_{i,j} l^z_{i,j+1} - l^y_{i,j+1} l^z_{i,j}) \\
= D & \sum_{i,j}^{N-1,N-1} l^z_{i,j} (\Delta \partial_x l^x_{i,j} + \Delta \partial_y l^x_{i,j} + l^x_{i,j}) - l^x_{i,j} (\Delta \partial_x l^z_{i,j} + \Delta \partial_y l^z_{i,j} + l^z_{i,j}) \\
& - l^y_{i,j} (\Delta \partial_x l^z_{i,j} + l^z_{i,j}) + l^z_{i,j} (\Delta \partial_x l^y_{i,j} + l^y_{i,j}) - l^y_{i,j} (\Delta \partial_y l^z_{i,j} + l^z_{i,j}) + l^z_{i,j} (\Delta \partial_y l^y_{i,j} + l^y_{i,j}) \\
= D\Delta & \sum_{i,j}^{N-1,N-1} l^z_{i,j} (\partial_x l^x_{i,j} + \partial_y l^x_{i,j} + \partial_x l^y_{i,j} + \partial_y l^y_{i,j}) - (\partial_x l^z_{i,j} + \partial_y l^z_{i,j}) (l^x_{i,j} + l^y_{i,j})
\end{aligned}
\tag{83}
$$

The crystal symmetry of the material at hand determines what type of Lifschitz invariants are present in the free energy [48, 51, 138]. For class D_{2d}, the invariants take the form

$$
D_{2d} : l_z \partial_y l_x - l_x \partial_y l_z + l_z \partial_x l_y - l_y \partial_x l_z. \tag{84}
$$

These forms are not present if the crystallographic structure respects $C_{n\nu}$ symmetry. For this class, the invariants take the form

$$C_{n\nu} : l_z \partial_x l_x - l_x \partial_x l_z + l_z \partial_y l_y - l_y \partial_y l_z. \tag{85}$$

For a crystallographic material with $C_{n\nu}$, we can disregard the Lifschitz invariants that are only present in materials respecting D_{2d} symmetry. In the micromagnetic limit, substituting the discrete sum by the integral as in Appendix A.1, we obtain for materials in the $C_{n\nu}$ class with the basal-plane being the $x - y$ plane:

$$\mathcal{H}_{\mathrm{D}} = \int \frac{d\mathbf{x}}{V} D\big((\hat{z} \cdot \mathbf{n})(\nabla \cdot \mathbf{n}) - (\mathbf{n} \cdot \nabla)(\hat{z} \cdot \mathbf{n})\big). \tag{86}$$

We have redefined the DMI constant, meaning we have made $D\Delta \to D$ in the inhomogeneous DMI free energy in Eq. (86). As $|\mathbf{l}| \approx 1$ in the exchange approximation, we can substitute $\mathbf{l} \to \mathbf{n}$. The inhomogeneity of this free energy arises from the derivatives of the staggered magnetization.

A.3 Homogeneous Dzyaloshinskii-Moriya interaction

The DMI vector can also hold a nonzero component orthogonal to the basal plane of the texture. With the basal plane being the $x - y$ plane, the out-of-plane DMI vector is $\mathbf{d} = (0, 0, d)$.

$$
\begin{aligned}
\mathcal{H}_{\mathrm{D}} = & \sum_{i,j}^{N-1,N-1} d\Big([\mathbf{m}_{i,j} - \mathbf{l}_{i,j}] \times \big([\mathbf{m}_{i,j} + \mathbf{l}_{i,j}] + [\mathbf{m}_{i+1,j} + \mathbf{l}_{i+1,j}] + [\mathbf{m}_{i,j+1} + \mathbf{l}_{i,j+1}] \\
& + [\mathbf{m}_{i+1,j+1} + \mathbf{l}_{i+1,j+1}] \big) \Big)_z \\
= d & \sum_{i,j}^{N-1,N-1} 8 m^x_{i,j} l^y_{i,j} - 8 l^x_{i,j} m^y_{i,j} + m^x_{i,j} (l^y_{i,j+1} - l^y_{i,j} + l^y_{i+1,j} - l^y_{i,j} + l^y_{i+1,j+1} - l^y_{i,j}) \\
& - m^y_{i,j} (l^x_{i,j+1} - l^x_{i,j} + l^x_{i+1,j} - l^x_{i,j} + l^y_{i+1,j+1} - l^x_{i,j}) \\
& - l^x_{i,j} (m^y_{i,j+1} - m^y_{i,j} + m^y_{i+1,j} - m^y_{i,j} + m^y_{i+1,j+1} - m^y_{i,j}) \\
& + l^y_{i,j} (m^x_{i+1,j} - m^x_{i,j} + m^x_{i,j+1} - m^x_{i,j} + m^x_{i+1,j+1} - m^x_{i,j}) \\
& + l^y_{i,j} (l^x_{i+1,j} - l^x_{i,j} + l^x_{i,j+1} - l^x_{i,j} + l^x_{i+1,j+1} - l^x_{i,j}) \\
& - l^x_{i,j} (l^y_{i+1,j} - l^y_{i,j} + l^y_{i,j+1} - l^y_{i,j} + l^y_{i+1,j+1} - l^y_{i,j}),
\end{aligned}
\tag{87}
$$

where we have disregarded quadratic terms in the magnetization as $|\mathbf{m}| \ll |\mathbf{l}|$ and $|d| \ll |J_s|$ in the exchange approximation. In the micromagnetic limit, we introduce the Jacobian matrix as in Appendices A.1 and A.2. The Jacobian formalism introduces gradient terms $l_i \partial_i m_j, l_i \partial_j m_j, m_i \partial_i l_j, m_i \partial_j l_j$. The staggered magnetization is smoothly varying in the exchange approximation as the symmetric Heisenberg coupling dominates, such that spatial derivatives of the Néel field is small compared to the Néel field itself. The same applies for the magnetization. Thus, the terms holding spatial derivatives can all be neglected when combined with the symmetric exchange terms. The remaining part which enters the total free energy of the antiferromagnetic system reads

$$
\mathcal{H}_{\mathrm{D}} = \int \frac{d\mathbf{x}}{V} \big(\mathbf{d} \cdot (\mathbf{m} \times \mathbf{n}) \big),
\tag{88}
$$

where we have redefined the homogeneous DMI vector $8d \to d$ and substituted $\mathbf{l} \to \mathbf{n}$

as we consider the exchange approximation.

B

Derivation of the equations of motion for antiferromagnetic spin waves

In this appendix we give the full derivation of the new equations of motion for the transverse (in-plane and out-of-plane) spin wave excitations around a 2D static antiferromagnetic skyrmion in a material satisfying the $C_{n\nu}$ symmetry group.

We start the quest with the Euclidian action $\mathcal{A}$, the free energy $\mathcal{F}$ and the kinetic energy $\mathcal{K}$ in the antiferromagnetic system. The free energy is

$$\mathcal{F} = \int \frac{d\mathbf{x}}{V} \Big(A(\partial_i \mathbf{n})^2 + a\mathbf{m}^2 - K_z(\mathbf{n}\cdot\hat{z})^2 - 2\mathbf{m}\cdot\mathbf{H} + D\big((\hat{z}\cdot\mathbf{n})(\nabla\cdot\mathbf{n}) - (\mathbf{n}\cdot\nabla)(\hat{z}\cdot\mathbf{n})\big)\Big) \quad (89)$$

where A is the inhomogeneous exchange constant, a is the homogeneous exchange constant, K_z is the easy-axis anisotropy along $\hat{z}$, $\mathbf{H}$ is the external field, D is the inhomogeneous Dzyaloshinskii-Moriya interaction (DMI) constant and V is the volume of the unit cell. The kinetic energy is [50, 94]

$$\mathcal{K} = 2\hbar \int \frac{d\mathbf{x}}{V} \big(\mathbf{m} \cdot (\dot{\mathbf{n}} \times \mathbf{n})\big). \quad (90)$$

The Euclidian action is an arbitrary time integral over the Lagrangian, which again is the kinetic energy minus the free energy of the system, $\mathcal{A} = \int dt\, (\mathcal{K} - \mathcal{F})$. We obtain the equations of motion by zero variation of the action with respect to the set of generalized coordinates $\{\mathbf{q}, \dot{\mathbf{q}}\}$: $\delta_{\mathbf{q}}\mathcal{A} = 0$. The generalized coordinates are the magnetization and the staggered magnetization. Carrying out the functional derivatives gives the equations of motion

$$\dot{\mathbf{n}} = -\frac{1}{2\hbar}\delta_{\mathbf{m}}\mathcal{F} \times \mathbf{n}, \quad (91)$$

$$\dot{\mathbf{m}} = -\frac{1}{2\hbar}\delta_{\mathbf{n}}\mathcal{F} \times \mathbf{n} - \frac{1}{2\hbar}\delta_{\mathbf{m}}\mathcal{F} \times \mathbf{m} \tag{92}$$

For linear spin wave excitations around the static antiferromagnetic skyrmion, we put all the time-dependence of the staggered magnetization into the linear spin wave deviations and allow for a non-trivial spatial variation of both the spin wave fields and the texture. That is,

$$\mathbf{n}(\mathbf{x}, t) = \mathbf{n}_0(\mathbf{x}) + \delta\mathbf{n}_\perp(\mathbf{x}, t), \tag{93}$$

under the assumption $|\delta\mathbf{n}(\mathbf{x}, t)| \ll |\mathbf{n}_0|$. We only consider an expansion up to first order in the excitations for the equations of motion. The linear excitations are orthogonal to the static equilibrium texture. We construct the effective forces to explicitly fulfill the orthogonality constraints on $\mathbf{m}$ and $\mathbf{n}$, similarly to what done in Refs. [139, 140]. For the first term on the right side in the Eq. (92) we have

$$\begin{aligned} -\delta_{\mathbf{n}}\mathcal{F} \times \mathbf{n} = 2\Big(& A(\mathbf{n}_0 + \delta\mathbf{n}_\perp) \times (\nabla^2(\mathbf{n}_0 + \delta\mathbf{n}_\perp) \times (\mathbf{n}_0 + \delta\mathbf{n}_\perp)) \\ & + K_z((\mathbf{n}_0 + \delta\mathbf{n}_\perp) \cdot \hat{z})(\mathbf{n}_0 + \delta\mathbf{n}_\perp) \times (\hat{z} \times (\mathbf{n}_0 + \delta\mathbf{n}_\perp)) \\ & - ((\mathbf{n}_0 + \delta\mathbf{n}_\perp) \cdot \mathbf{H})\mathbf{m} \\ & - D\big(\hat{z}(\nabla \cdot (\mathbf{n}_0 + \delta\mathbf{n}_\perp) - \nabla(\hat{z} \cdot (\mathbf{n}_0 + \delta\mathbf{n}_\perp))\big)\Big) \times (\mathbf{n}_0 + \delta\mathbf{n}_\perp) \end{aligned} \tag{94}$$

For the first term in Eq. (94), we get

$$\begin{aligned} A\mathbf{n} \times (\nabla^2\mathbf{n} \times \mathbf{n}) \times \mathbf{n} &= A(\mathbf{n}_0 + \delta\mathbf{n}_\perp) \times (\nabla^2(\mathbf{n}_0 + \delta\mathbf{n}_\perp) \times (\mathbf{n}_0 + \delta\mathbf{n}_\perp)) \times (\mathbf{n}_0 + \delta\mathbf{n}_\perp) \\ &= -A\mathbf{n}_0 \times \mathbf{n}_0(\delta\mathbf{n}_\perp \cdot \nabla^2\mathbf{n}_0 + A(\nabla^2\delta\mathbf{n}_\perp \times \mathbf{n}_0 - \mathbf{n}_0 \times \mathbf{n}_0(\mathbf{n}_0 \cdot \delta\mathbf{n}_\perp)) \\ &\quad - A\delta\mathbf{n}_\perp \times \mathbf{n}_0(\mathbf{n}_0 \cdot \nabla^2\mathbf{n}_0 + A(\nabla^2\mathbf{n}_0 \times \delta\mathbf{n}_\perp - \mathbf{n}_0 \times \delta\mathbf{n}_\perp(\mathbf{n}_0 \cdot \nabla^2\mathbf{n}_0)) \\ &= A(\nabla^2\delta\mathbf{n}_\perp \times \mathbf{n}_0 + \nabla^2\mathbf{n}_0 \times \delta\mathbf{n}_\perp), \end{aligned} \tag{95}$$

where we have expanded the vector triple products, utilized that $\mathbf{n}_0 \perp \delta\mathbf{n}_\perp$, disregarded higher order excitation terms and terms not containing the linear deviations at all. The reason why we disregard the zeroth order terms is if the excitations are zero, which is physically possible, the terms which are zeroth order in the excitations combine to zero to first order. They are ground state contributions only. For the anisotropy term, we get

$$
\begin{aligned}
K_z((\mathbf{n}\cdot\hat{z})\mathbf{n}\times(\hat{z}\times\mathbf{n}))\times\mathbf{n} &= K_z\Big(((\mathbf{n}_0+\delta\mathbf{n}_\perp)\cdot\hat{z})(\mathbf{n}_0+\delta\mathbf{n}_\perp)\times(\hat{z}\times(\mathbf{n}_0+\delta\mathbf{n}_\perp))\Big)\\
&\qquad\times(\mathbf{n}_0+\delta\mathbf{n}_\perp)\\
&= K_z(\mathbf{n}_0\cdot\hat{z})(\hat{z}\times\delta\mathbf{n}_\perp-\mathbf{n}_0\times\delta\mathbf{n}_\perp(\hat{z}\cdot\mathbf{n}_0))\\
&\quad - K_z(\mathbf{n}_0\cdot\hat{z})(\delta\mathbf{n}_\perp\times\mathbf{n}_0(\mathbf{n}_0\cdot\hat{z}))+K_z(\delta\mathbf{n}_\perp\cdot\hat{z})(\hat{z}\times\mathbf{n}_0)\\
&= K_z(\mathbf{n}_0\cdot\hat{z})(\hat{z}\times\delta\mathbf{n}_\perp)+K_z(\delta\mathbf{n}_\perp\cdot\hat{z})\hat{z}\times\mathbf{n}_0
\end{aligned}
\tag{96}
$$

For the third term involving the external magnetic field we get

$$
(\mathbf{n}\cdot\mathbf{H})\mathbf{m}\times\mathbf{n} = (\mathbf{n}_0\cdot\mathbf{H})\mathbf{m}\times\mathbf{n}_0 \tag{97}
$$

For the last term arising from the DMI, we obtain

$$
\begin{aligned}
D\big(\hat{z}(\nabla\cdot\mathbf{n})-\nabla(\hat{z}\cdot\mathbf{n})\big) &= D\big(\hat{z}(\nabla\cdot(\mathbf{n}_0+\delta\mathbf{n}_\perp)-\nabla(\hat{z}\cdot(\mathbf{n}_0+\delta\mathbf{n}_\perp)\big)\times(\mathbf{n}_0+\delta\mathbf{n}_\perp)\\
&= D(\nabla\cdot\mathbf{n}_0)\hat{z}\times\delta\mathbf{n}_\perp+D\hat{z}\times\mathbf{n}_0(\nabla\cdot\delta\mathbf{n}_\perp)-D\nabla(\hat{z}\cdot\mathbf{n}_0)\times\delta\mathbf{n}_\perp\\
&\quad - D\nabla(\hat{z}\cdot\delta\mathbf{n}_\perp)\times\mathbf{n}_0
\end{aligned}
\tag{98}
$$

Putting everything together, the first effective force acting on the magnetization is

$$
\begin{aligned}
-\frac{1}{2\hbar}\delta_{\mathbf{n}}\mathcal{F}\times\mathbf{n} = \frac{1}{\hbar}\Big(&A(\nabla^2\delta\mathbf{n}_\perp\times\mathbf{n}_0+\nabla^2\mathbf{n}_0\times\delta\mathbf{n}_\perp)+K_z\big((\mathbf{n}_0\cdot\hat{z})\hat{z}\times\delta\mathbf{n}_\perp\\
&+(\delta\mathbf{n}_\perp\cdot\hat{z})\hat{z}\times\mathbf{n}_0\big)-(\mathbf{n}_0\cdot\mathbf{H})\mathbf{m}\times\mathbf{n}_0-D\big((\nabla\cdot\mathbf{n}_0)\hat{z}\times\delta\mathbf{n}_\perp\\
&+\hat{z}\times\mathbf{n}_0(\nabla\cdot\delta\mathbf{n}_\perp)-\nabla(\hat{z}\cdot\mathbf{n}_0)\times\delta\mathbf{n}_\perp-\nabla(\hat{z}\cdot\delta\mathbf{n}_\perp)\times\mathbf{n}_0\big)\Big)
\end{aligned}
\tag{99}
$$

The second force term in Eq. (92) is

$$
\begin{aligned}
-\frac{1}{2\hbar}\delta_{\mathbf{m}}\mathcal{F}\times\mathbf{m} &= \frac{1}{\hbar}(-a\mathbf{m}+(\mathbf{n}_0+\delta\mathbf{n}_\perp)\times(\mathbf{H}\times(\mathbf{n}_0+\delta\mathbf{n}_\perp))\times\mathbf{m}\\
&= \frac{1}{\hbar}(\mathbf{H}\times\mathbf{m}-(\mathbf{H}\cdot\mathbf{n}_0)\mathbf{n}_0\times\mathbf{m})
\end{aligned}
\tag{100}
$$

The last force term in the equations of motion is the driving force of the staggered magnetization in Eq. (91), which reads

$$
\begin{aligned}
-\frac{1}{2\hbar}\delta_{\mathbf{m}}\mathcal{F}\times\mathbf{n} &= \frac{1}{\hbar}(-a\mathbf{m}+(\mathbf{n}_0+\delta\mathbf{n}_\perp)\times(\mathbf{H}\times(\mathbf{n}_0+\delta\mathbf{n}_\perp))\times(\mathbf{n}_0+\delta\mathbf{n}_\perp)\\
&= \frac{1}{\hbar}\Big(-a\mathbf{m}\times\mathbf{n}_0+\mathbf{H}\times\mathbf{n}_0+\mathbf{H}\times\delta\mathbf{n}_\perp-\mathbf{n}_0\times\delta\mathbf{n}_\perp(\mathbf{H}\cdot\mathbf{n}_0)\\
&\quad-\delta\mathbf{n}_\perp\times\mathbf{n}_0(\mathbf{H}\cdot\mathbf{n}_0)\Big)\\
&= \frac{1}{\hbar}\big(-a\mathbf{m}\times\mathbf{n}_0+\mathbf{H}\times\delta\mathbf{n}_\perp\big)
\end{aligned}
\tag{101}
$$

The form of the effective force acting on the staggered magnetization allows us to write the magnetization as a slave variable of the staggered order parameter by Eq. (91):

$$
\mathbf{m}=\frac{\hbar}{a}\delta\dot{\mathbf{n}}_\perp\times\mathbf{n}_0-\frac{1}{a}\delta\mathbf{n}_\perp(\mathbf{H}\cdot\mathbf{n}_0)
\tag{102}
$$

We take the time derivative of Eq. (102) and substitute $\dot{\mathbf{m}}$ with the force terms Eqs. (99) and (100) above according to Eq. (92) and obtain

$$
\begin{aligned}
\frac{\hbar^2}{a}\delta\ddot{\mathbf{n}}_\perp\times\mathbf{n}_0 &= \frac{\hbar}{a}\delta\dot{\mathbf{n}}_\perp(\mathbf{H}\cdot\mathbf{n}_0)+\frac{\hbar}{a}\delta\mathbf{n}_\perp(\dot{\mathbf{H}}\cdot\mathbf{n}_0)\\
&\quad+A(\nabla^2\delta\mathbf{n}_\perp\times\mathbf{n}_0+\nabla^2\mathbf{n}_0\times\delta\mathbf{n}_\perp)\\
&\quad+K_z((\mathbf{n}_0\cdot\hat{z})\hat{z}\times\delta\mathbf{n}_\perp+(\delta\mathbf{n}_\perp\cdot\hat{z})\hat{z}\times\mathbf{n}_0)\\
&\quad-(\mathbf{n}_0\cdot\mathbf{H})\mathbf{m}\times\mathbf{n}_0\\
&\quad-D\big((\nabla\cdot\mathbf{n}_0)\hat{z}\times\delta\mathbf{n}_\perp+\hat{z}\times\mathbf{n}_0(\nabla\cdot\delta\mathbf{n}_\perp)-\nabla(\hat{z}\cdot\mathbf{n}_0)\times\delta\mathbf{n}_\perp\\
&\quad-\nabla(\hat{z}\cdot\delta\mathbf{n}_\perp)\times\mathbf{n}_0\big)+(\mathbf{H}\times\mathbf{m}-(\mathbf{H}\cdot\mathbf{n}_0)\mathbf{n}_0\times\mathbf{m})\\
&= \frac{\hbar}{a}\delta\dot{\mathbf{n}}_\perp(\mathbf{H}\cdot\mathbf{n}_0)+\frac{\hbar}{a}\delta\mathbf{n}_\perp(\dot{\mathbf{H}}\cdot\mathbf{n}_0)+A(\nabla^2\delta\mathbf{n}_\perp\times\mathbf{n}_0+\nabla^2\mathbf{n}_0\times\delta\mathbf{n}_\perp)\\
&\quad+K_z((\mathbf{n}_0\cdot\hat{z})\hat{z}\times\delta\mathbf{n}_\perp+(\delta\mathbf{n}_\perp\cdot\hat{z})\hat{z}\times\mathbf{n}_0\\
&\quad-D\Big((\nabla\cdot\mathbf{n}_0)\hat{z}\times\delta\mathbf{n}_\perp+\hat{z}\times\mathbf{n}_0(\nabla\cdot\delta\mathbf{n}_\perp)-\nabla(\hat{z}\cdot\mathbf{n}_0)\times\delta\mathbf{n}_\perp\\
&\quad-\nabla(\hat{z}\cdot\delta\mathbf{n}_\perp)\times\mathbf{n}_0\Big)+\mathbf{H}\times\Big(\frac{\hbar}{a}\delta\dot{\mathbf{n}}_\perp\times\mathbf{n}_0-\frac{1}{a}\delta\mathbf{n}_\perp(\mathbf{H}\cdot\mathbf{n}_0)\Big)
\end{aligned}
\tag{103}
$$

Denote that time derivatives of the linear excitations are orthogonal to the static equilibrium texture: $\delta\dot{\mathbf{n}}_\perp\cdot\mathbf{n}_0=\mathrm{d}_t(\delta\mathbf{n}_\perp\cdot\mathbf{n}_0)-\delta\mathbf{n}_\perp\cdot\partial_t\mathbf{n}_0=0\Rightarrow\delta\ddot{\mathbf{n}}_\perp\perp\mathbf{n}_0$. Hence, all the terms proportional to $\mathbf{n}_0$ are to be removed in this leading order approach when we isolate $\delta\ddot{\mathbf{n}}_\perp$ by taking the vector product with $\mathbf{n}_0$:

$$\begin{aligned}\frac{\hbar^2}{a}\delta\ddot{\mathbf{n}}_\perp &= A\nabla^2\delta\mathbf{n}_\perp - A\delta\mathbf{n}_\perp(\nabla^2\mathbf{n}_0\cdot\mathbf{n}_0)\\ &\quad - K_z(\mathbf{n}_0\cdot\hat{z})^2\delta\mathbf{n}_\perp + K_z(\delta\mathbf{n}_\perp\cdot\hat{z})\hat{z}\\ &\quad + D(\nabla\cdot\mathbf{n}_0)(\mathbf{n}_0\cdot\hat{z})\delta\mathbf{n}_\perp - D(\nabla\cdot\delta\mathbf{n}_\perp)\hat{z} - D((\nabla(\hat{z}\cdot\mathbf{n}_0)\cdot\mathbf{n}_0)\delta\mathbf{n}_\perp + D\nabla(\hat{z}\cdot\delta\mathbf{n}_\perp)\\ &\quad + \frac{2\hbar}{a}\mathbf{n}_0\times\delta\dot{\mathbf{n}}_\perp(\mathbf{H}\cdot\mathbf{n}_0) + \frac{\hbar}{a}\mathbf{n}_0\times\delta\mathbf{n}_\perp(\dot{\mathbf{H}}\cdot\mathbf{n}_0) + \frac{1}{a}(\mathbf{H}\cdot\mathbf{n}_0)^2\delta\mathbf{n}_\perp.\end{aligned} \tag{104}$$

This is the equation of motion governing small-amplitude excitations of the staggered magnetization for a general position-dependent texture.

For the antiferromagnetic skyrmion, which is symmetric about the out-of-plane axis $\hat{z}$, we make the following parameterization of the static equilibrium staggered magnetization:

$$\mathbf{n}_0(\mathbf{x}) = (\sin\Theta\cos\zeta, \sin\Theta\sin\zeta, \cos\Theta), \tag{105}$$

with $\Theta = \Theta(\mathbf{x})$ and $\phi = \phi(\mathbf{x})$. For certain crystallographic classes, we have that the azimuthal angle equals that of the position vector, i.e. $\zeta = \phi$. For the symmetry group $C_{n\nu}$ that is the case [69]. Following Ref. [49], we adapt a local spherical coordinate frame descried by the skyrmion angles, with the following unit vectors(components being in the (x,y,z)-direction):

$$\begin{aligned}\hat{r} &= (\sin\Theta\cos\phi, \sin\Theta\sin\phi, \cos\Theta)\\ \hat{\theta} &= (\cos\Theta\cos\phi, \cos\Theta\sin\phi, -\sin\Theta)\\ \hat{\phi} &= (-\sin\phi, \cos\phi, 0)\end{aligned} \tag{106}$$

We Taylor expand the staggered magnetization around its equilibrium in small deviations h in these three directions:

$$\mathbf{n}(\mathbf{x},t) = \left(1 - \frac{h^2}{2}(n_\theta^2(\mathbf{x},t) + n_\phi^2(\mathbf{x},t))\right)\hat{r} + h(n_\theta(\mathbf{x},t)\hat{\theta} + n_\phi(\mathbf{x},t)\hat{\phi}) \tag{107}$$

Hence, to first order, the linear excitation of the staggered magnetization is

$$\delta\mathbf{n}_\perp = hn_\theta(\mathbf{x},t)\hat{\theta} + hn_\phi(\mathbf{x},t)\hat{\phi}. \tag{108}$$

To find Schrödinger-like equations for the transverse excitation fields, we substitute our ansatz Eqs. (105), (106) and (107) into Eq. (104). We extract the temporal dependence in the transverse fields accordingly: $n_{\theta(\phi)}(\mathbf{x},t) = n_{\theta(\phi)}(\mathbf{x})e^{-i\omega_{\theta(\phi)}t}$. We will individually compute the contributions from the terms on the right-hand side to ease the writing and limit the size of the equation. After considering each term, we combine them component-wise to give the equations for the in-plane field n_ϕ and the out-of-plane field n_θ. We call it in-plane as $\hat{\phi}$ lies in the basal plane, so the out-of-plane excitations are all encoded into n_θ. We drop the expansion parameter as all terms are linear in h.

For the first term on the right of Eq. (104), we have:

$$
\begin{aligned}
A\nabla^2\delta\mathbf{n}_\perp &= A\nabla^2(n_\theta(\mathbf{x},t)\hat{\theta} + n_\phi(\mathbf{x},t)\hat{\phi}) \\
&= \hat{x}A\Big(r^{-2}\partial_\phi^2 n_\theta\cos\Theta\cos\phi - r^{-2}\partial_\phi^2 n_\phi\sin\theta + \cos\Theta\cos\phi\partial_r^2 n_\theta - \sin\theta\partial_r^2 n_\phi \\
&\quad - \cos\phi n_\theta\sin\Theta\partial_r^2\Theta - 2r^{-1}\cos\phi(r\partial_r\Theta\sin\Theta - \frac{1}{2}\cos\Theta)\partial_r n_\theta \\
&\quad - n_\theta(\partial_r\Theta)^2\cos\Theta\cos\phi - n_\theta\partial_r\Theta\sin\Theta\cos(\phi)r^{-1} - \partial_r n_\phi\sin\phi r^{-1} \\
&\quad - 2\partial_\phi n_\theta\cos\Theta\sin\phi r^{-2} - n_\theta\cos\Theta\cos\phi r^{-2} - 2\partial_\phi n_\phi\cos\phi r^{-2} \\
&\quad + n_\phi\sin\phi r^{-2}\Big) \\
&+ \hat{y}A\Big(r^{-2}\partial_\phi^2 n_\theta\sin\phi\cos\Theta + r^{-2}\partial_\phi^2 n_\phi\cos\phi + \sin\phi\cos\Theta\partial_r^2 n_\theta \\
&\quad + \cos\phi\partial_r^2 n_\phi - \sin\phi n_\theta\sin\Theta\partial_r^2\Theta - 2\sin\phi r^{-1}(r\partial_r\Theta\sin\Theta - \frac{1}{2}\cos\Theta)\partial_r n_\theta \\
&\quad - \sin\phi\cos\Theta n_\theta(\partial_r\Theta)^2 - n_\theta\sin\phi\partial_r\Theta\sin\Theta r^{-1} + \partial_r n_\phi\cos\phi r^{-1} \\
&\quad + 2\partial_\phi n_\theta\cos\phi\cos\Theta r^{-2} - n_\theta\sin\phi\cos\Theta r^{-2} - 2\partial_\phi n_\phi\sin\phi r^{-2} \\
&\quad - n_\phi\cos\phi r^{-2}\Big) \\
&- \hat{z}A\Big(\sin\Theta(\partial_r^2 n_\theta + r^{-1}\partial_r n_\theta + r^{-2}\partial_\phi^2 n_\theta) + 2\cos\Theta\partial_r\Theta\partial_r n_\theta \\
&\quad + n_\theta(-\sin\Theta(\partial_r\Theta)^2 + \cos\Theta\partial_r^2\Theta + r^{-1}\cos\Theta\partial_r\Theta)\Big)
\end{aligned}
\tag{109}
$$

For the second term, we get

$$
\begin{aligned}
A\delta\mathbf{n}_\perp(\nabla^2\mathbf{n}_0\cdot\mathbf{n}_0) = &-\hat{x}A\big((\partial_r\Theta)^2+r^{-2}\sin^2\Theta\big)(n_\theta\cos\Theta\cos\phi-n_\phi\sin\phi)\\
&-\hat{y}A\big((\partial_r\Theta)^2+r^{-2}\sin^2\Theta\big)(n_\theta\cos\Theta\sin\phi+n_\phi\cos\phi)\\
&+\hat{z}A\big(\partial_r\Theta)^2+r^{-2}\sin^2\Theta\big)n_\theta\sin\Theta
\end{aligned}
\tag{110}
$$

For the third term, we get

$$
\begin{aligned}
K_z(\mathbf{n}_0\cdot\hat{z})^2\delta\mathbf{n}_\perp = &\hat{x}K_z\cos^2\Theta(n_\theta\cos\Theta\cos\phi-n_\phi\sin\phi)\\
&+\hat{y}K_z\cos^2\Theta(n_\theta\cos\Theta\sin\phi+n_\phi\cos\phi)\\
&-\hat{z}K_z\cos^2\Theta n_\theta\sin\Theta
\end{aligned}
\tag{111}
$$

For the fourth term we have

$$
K_z(\delta\mathbf{n}_\perp\cdot\hat{z})\hat{z} = -\hat{z}K_z n_\theta\sin\Theta \tag{112}
$$

For the fifth term we get

$$
\begin{aligned}
D(\nabla\cdot\mathbf{n}_0)(\hat{z}\cdot\mathbf{n}_0)\delta\mathbf{n}_\perp = &\hat{x}D\cos\Theta(r^{-1}\sin\Theta+\cos\Theta\partial_r\Theta)(n_\theta\cos\Theta\cos\phi-n_\phi\sin\phi)\\
&+\hat{y}D\cos\Theta(r^{-1}\sin\Theta+\cos\Theta\partial_r\Theta)(n_\theta\cos\Theta\sin\phi+n_\phi\cos\phi)\\
&-\hat{z}D\cos\Theta(r^{-1}\sin\Theta+\cos\Theta\partial_r\Theta)n_\theta\sin\Theta
\end{aligned}
\tag{113}
$$

For the sixth term, we get

$$
\begin{aligned}
D(\nabla\cdot\delta\mathbf{n}_\perp)\hat{z} = &\hat{z}D\big(\cos\Theta\cos\phi(\cos\phi\partial_r n_\theta - r^{-1}\sin\phi\partial_\phi n_\theta)+n_\theta\cos\phi(-\cos\phi\sin\Theta\partial_r\Theta)\\
&+n_\theta\cos\Theta r^{-1}\sin^2\phi-\sin\phi(\cos\phi\partial_r n_\phi - r^{-1}\sin\phi\partial_\phi n_\phi)+n_\phi r^{-1}\sin\phi\cos\phi\\
&+\cos\Theta\sin\phi(\sin\phi\partial_r n_\theta + r^{-1}\cos\phi\partial_\phi n_\theta)+n_\theta\sin\phi(-\sin\phi\sin\Theta\partial_r\Theta)\\
&+n_\theta\cos\Theta\cos^2\phi r^{-1}+\cos\phi(\sin\phi\partial_r n_\phi + r^{-1}\cos\phi\partial_\phi n_\phi)-n_\phi r^{-1}\cos\phi\sin\phi\big)\\
= &\hat{z}D\big(\cos\Theta\partial_r n_\theta - n_\theta\sin\Theta\partial_r\Theta+n_\theta r^{-1}\cos\Theta+r^{-1}\partial_\phi n_\phi\big)
\end{aligned}
\tag{114}
$$

For the seventh term, we have

$$
\begin{aligned}
D((\nabla(\hat{z}\cdot\mathbf{n}_0)\cdot\mathbf{n}_0)\delta\mathbf{n}_\perp &= D((\nabla\cos\Theta\cdot\mathbf{n}_0))\delta\mathbf{n}_\perp\\
&= -\hat{x}D\sin^2\Theta(\partial_r\Theta)[n_\theta\cos\Theta\cos\phi-n_\phi\sin\phi)\\
&\quad-\hat{y}D\sin^2\Theta(\partial_r\Theta)(n_\theta\cos\Theta\sin\phi+n_\phi\cos\phi)\\
&\quad+\hat{z}D\sin^2\Theta(\partial_r\Theta)n_\theta\sin\Theta
\end{aligned}
\tag{115}
$$

For the eight term, we have

$$\begin{aligned} D\nabla(\hat{z}\cdot\delta\mathbf{n}_\perp) &= -D\nabla(\sin\Theta n_\theta) \\ &= -\hat{x}D(\sin\Theta\cos\phi\partial_r n_\theta - \sin\Theta\sin\phi r^{-1}\partial_\phi n_\theta + n_\theta\cos\phi\cos\Theta\partial_r\Theta) \\ &\quad - \hat{y}D(\sin\Theta\sin\phi\partial_r n_\theta + \sin\Theta\cos\phi r^{-1}\partial_\phi n_\theta + n_\theta\sin\phi\cos\Theta\partial_r\Theta) \end{aligned} \tag{116}$$

For the ninth we need to use that the external field has to be in the z-direction, with the possibility of having a temporal variation as discussed in Refs. [48, 69, 94, 140]: $\mathbf{H}(\mathbf{x},t) = H(t)\hat{z}$. We obtain

$$\begin{aligned} \frac{2}{a}\mathbf{n}_0\times\delta\dot{\mathbf{n}}_\perp(\mathbf{H}\cdot\mathbf{n}_0) &= -\hat{x}i\frac{2}{a}(H\cos\Theta)(-n_\theta\sin^2\Theta\sin\phi - n_\theta\cos^2\Theta\sin\phi - n_\phi\cos\Theta\cos\phi) \\ &\quad - \hat{y}i\frac{2}{a}(H\cos\Theta)(n_\theta\cos^2\Theta\cos\phi - n_\phi\cos\Theta\sin\phi + n_\theta\sin^2\Theta\cos\phi) \\ &\quad - \hat{z}i\frac{2}{a}(H\cos\Theta)(n_\theta\sin\Theta\cos\Theta\sin\phi\cos\phi + n_\phi\sin\Theta\cos^2\phi \\ &\qquad\qquad - n_\theta\sin\Theta\cos\Theta\sin\phi\cos\phi + n_\phi\sin^2\phi\sin\Theta) \\ &= -\hat{x}i\frac{2}{a}(H\cos\Theta)(-\omega_\theta n_\theta\sin\phi - \omega_\phi n_\phi\cos\Theta\cos\phi) \\ &\quad - \hat{y}i\frac{2}{a}(H\cos\Theta)(\omega_\theta n_\theta\cos\phi - \omega_\phi n_\phi\cos\Theta\sin\phi) \\ &\quad - \hat{z}i\frac{2}{a}(H\cos\Theta)(\omega_\phi n_\phi\sin\Theta) \end{aligned} \tag{117}$$

For the tenth term, we can use the result from Eq. (117):

$$\begin{aligned} \frac{1}{a}(\dot{\mathbf{H}}\cdot\mathbf{n}_0)\mathbf{n}_0\times\delta\mathbf{n}_\perp &= \hat{x}\frac{1}{a}(\dot{H}\cos\Theta)(-n_\theta\sin\phi - n_\phi\cos\Theta\cos\phi) \\ &\quad + \hat{y}\frac{1}{a}(\dot{H}\cos\Theta)(n_\theta\cos\phi - n_\phi\cos\Theta\sin\phi) \\ &\quad + \hat{z}\frac{1}{a}(\dot{H}\cos\Theta)(n_\phi\sin\Theta) \end{aligned} \tag{118}$$

For the eleventh term, we have

$$\begin{aligned} \frac{1}{a}(\mathbf{H}\cdot\mathbf{n}_0)^2\delta\mathbf{n}_\perp &= \hat{x}\frac{1}{a}\cos^2\Theta(n_\theta\cos\Theta\cos\phi - n_\phi\sin\phi) \\ &\quad + \hat{y}\frac{1}{a}\cos^2\Theta(n_\theta\cos\Theta\sin\phi + n_\phi\cos\phi) \\ &\quad - \hat{z}\frac{1}{a}\cos^2\Theta n_\theta\sin\Theta \end{aligned} \tag{119}$$

For the term on the left hand side, we get

$$\begin{aligned}\frac{\hbar}{a}\delta\ddot{\mathbf{n}}_\perp = &-\hat{x}\frac{\hbar}{a}(\omega_\theta^2 n_\theta \cos\Theta\cos\phi - \omega_\phi^2 n_\phi \sin\phi)\\ &-\hat{y}\frac{\hbar}{a}(\omega_\theta^2 n_\theta \cos\Theta\sin\phi + \omega_\phi^2 n_\phi \cos\phi)\\ &+\hat{z}\frac{\hbar}{a}(\omega_\theta^2 n_\theta \sin\Theta)\end{aligned} \tag{120}$$

Now, we have three equations, one for the x-, y- and z-component, respectively. We can combine them to simplify the expressions. The first equation we obtain by taking the x-component, multiplying it with $\sin\phi$ and subtract the y-equation with all terms multiplied with $\cos\phi$. We get

$$\begin{aligned}\frac{\omega_\phi^2\hbar^2}{a}n_\phi = &\left(A\Big(-\nabla^2 - (\partial_r\Theta)^2 + \frac{\cos^2\Theta}{r^2}\Big) + K_z\cos^2\Theta - D\Big(\frac{\sin 2\Theta}{2r} + \partial_r\Theta\Big) - \frac{H^2}{a}\cos^2\Theta\right)n_\phi\\ &-\left(\Big(\frac{2A\cos\Theta}{r^2} - \frac{D\sin\Theta}{r}\Big)\partial_\phi - \frac{i2\hbar H\omega_\theta\cos\Theta}{a} + \frac{\hbar\dot{H}\cos\Theta}{a}\right)n_\theta.\end{aligned} \tag{121}$$

Next, we need an equation for the out-of-plane field n_θ. We add the x-equation with all terms multiplied with $\cos\phi$ and the y-equation with all terms multiplied with $\sin\phi$, before subtracting this sum multiplied with $\cos\Theta$ from the z-equation multiplied with $\sin\Theta$. We get

$$\begin{aligned}\frac{\omega_\theta^2\hbar^2}{a}n_\theta = &\left(A\Big(-\nabla^2 + \frac{\cos 2\Theta}{r^2}\Big) + K_z\cos 2\Theta - \frac{D\sin 2\Theta}{r} - \frac{H^2}{a}\cos^2\Theta\right)n_\theta\\ &+\left(\Big(\frac{2A\cos\Theta}{r^2} - \frac{D\sin\Theta}{r}\Big)\partial_\phi - \frac{i2\hbar H\omega_\phi\cos\Theta}{a} + \frac{\hbar\dot{H}\cos\Theta}{a}\right)n_\phi.\end{aligned} \tag{122}$$

These are the new, unreported coupled Schrödinger-like equations for magnon excitations around a static antiferromagnetic skyrmion stabilized by DMI, easy-axis anisotropy and an external magnetic field orthogonal to the basal-plane in the exchange approximation. The fields are strongly coupled, which is different compared to the 1D domain wall scenario where the fields are decoupled [49, 141]. When comparing to easy-plane antiferromagnetic 2D vortices, these equations are more complicated as they are more tightly coupled [47, 115, 133].

Bibliography

[1] A. K. Sethi, *The Business of Electronics: A Concise History*. London, UK: Palgrave Macmillan, 2013.

[2] J. J. Thomson, "Cathode rays," in *The Electrician*, Bouverie House, 1897.

[3] R. A. Millikan, "On the elementary electrical charge and the Avogadro constant," *Phys. Rev.*, vol. 2, Aug. 1913.

[4] H. Kasai, "Spintronics and moltronics," *Journal of Physics: Condensed Matter*, vol. 26, 10, Mar. 2014.

[5] B. G. Park *et al.*, "A spin-valve-like magnetoresistance of an antiferromagnet-based tunnel junction," *Nature Materials*, vol. 10, 5, Mar. 2011.

[6] T. Jungwirth, X. Marti, P. Wadley, and J. Wunderlich, "Antiferromagnetic spintronics," *Nature Nanotechnology*, vol. 11, 3, Mar. 2016.

[7] C. Kittel, "Theory of antiferromagnetic resonance," *Phys. Rev.*, vol. 82, 4, May 1951.

[8] S. Seki *et al.*, "Thermal generation of spin current in an antiferromagnet," *Phys. Rev. Lett.*, vol. 115, 26, Dec. 2015.

[9] N. Nagaosa and Y. Tokura, "Topological properties and dynamics of magnetic skyrmions," *Nature Nanotechnology*, vol. 8, 12, Dec. 2013.

[10] W. Heisenberg, "Mehrkörperproblem und resonanz in der quantenmechanik," *Zeitschrift für Physik*, vol. 38, 6, Jun. 1926.

[11] F. Bloch, "Zur theorie des ferromagnetismus," *Zeitschrift fur Physik*, vol. 61, Mar. 1930.

[12] L. Néel, "Magnetism and local molecular field," *Science*, vol. 174, 4013, Dec. 1971.

[13] I. Dzyaloshinsky, "A thermodynamic theory of "weak" ferromagnetism of antiferromagnetics," *Journal of Physics and Chemistry of Solids*, vol. 4, 4, 1958.

[14] T. Moriya, "New mechanism of anisotropic superexchange interaction," *Phys. Rev. Lett.*, vol. 4, 5, Mar. 1960.

[15] E. Lifshitz and L. Pitaevskii, *Course of Theoretical Physics Vol 9 Statistical Physics Part 2*. Exeter, UK: Permagon Press, 1980.

[16] M. N. Baibich *et al.*, "Giant magnetoresistance of (001)Fe/(001)Cr magnetic superlattices," *Phys. Rev. Lett.*, vol. 61, 21, Nov. 1988.

[17] G. Binasch, P. Grünberg, F. Saurenbach, and W. Zinn, "Enhanced magnetoresistance in layered magnetic structures with antiferromagnetic interlayer exchange," *Phys. Rev. B*, vol. 39, 7, Mar. 1989.

[18] L. Berger, "Emission of spin waves by a magnetic multilayer traversed by a current," *Phys. Rev. B*, vol. 54, 13, Oct. 1996.

[19] J. Slonczewski, "Current-driven excitation of magnetic multilayers," *Journal of Magnetism and Magnetic Materials*, vol. 159, 1, Jun. 1996.

[20] D. Apalkov, B. Dieny, and J. M. Slaughter, "Magnetoresistive random access memory," *Proceedings of the IEEE*, vol. 104, 10, Oct. 2016.

[21] N. D. Rizzo *et al.*, "A fully functional 64 Mb DDR3 ST-MRAM built on 90 nm CMOS technology," *Magnetics, IEEE Transactions on*, vol. 49, 7, Jul. 2013.

[22] A. H. Macdonald and M. Tsoi, "Antiferromagnetic metal spintronics," *Philosophical Transactions of the Royal Society A*, vol. 369, 1948, Aug. 2011.

[23] A. S. Nunez, R. A. Duine, P. Haney, and A. H. MacDonald, "Theory of spin torques and giant magnetoresistance in antiferromagnetic metals," *Phys. Rev. B*, vol. 73, 21, Jun. 2006.

[24] P. Wadley *et al.*, "Electrical switching of an antiferromagnet," *Science*, vol. 351, 6273, Jan. 2016.

[25] O. Boulle *et al.*, "Room-temperature chiral magnetic skyrmions in ultrathin magnetic nanostructures," *Nature Nanotechnology*, vol. 11, 5, Jan. 2016.

[26] P. M. Buhl, F. Freimuth, S. Blugel, and Y. Mokrousov, "Topological spin Hall effect in antiferromagnetic skyrmions," *Physica Status Solidi. Rapid Research Letters*, vol. 11, 4, Apr. 2017.

[27] P. F. Bessarab *et al.*, "Stability and lifetime of antiferromagnetic skyrmions," *ArXiv e-prints*, Sep. 13, 2017.

[28] A. Fert, V. Cros, and J. Sampaio, "Skyrmions on the track," *Nature Nanotechnology*, vol. 8, 3, Mar. 2013.

[29] L. Kong and J. Zang, "Dynamics of an insulating skyrmion under a temperature gradient," *Phys. Rev. Lett.*, vol. 111, 6, Aug. 2013.

[30] Z. Liu and H. Ian, "Numerical studies on antiferromagnetic skyrmions in nanodisks by means of a new quantum simulation approach," *Chemical Physics Letters*, vol. 649, Apr. 2016.

[31] O. Gomonay, T. Jungwirth, and J. Sinova, "High antiferromagnetic domain wall velocity induced by Néel spin-orbit torques," *Phys. Rev. Lett.*, vol. 117, 1, Jun. 2016.

[32] O. Gomonay, V. Baltz, A. Brataas, and Y. Tserkovnyak, "Part of a collection of reviews on antiferromagnetic spintronics. Antiferromagnetic dynamics, spin-texures, and nanostructures," *ArXiv e-prints*, May 29, 2017.

[33] J. Bass and W. P. Pratt Jr, "Spin-diffusion lengths in metals and alloys, and spin-flipping at metal/metal interfaces: An experimentalist's critical review," *Journal of Physics: Condensed Matter*, vol. 19, 18, Apr. 2007.

[34] S. O. Demokritov, B. Hillebrands, and A. N. Slavin, "Brillouin light scattering studies of confined spin waves: Linear and nonlinear confinement," *Physics Reports*, vol. 348, 6, Jul. 2001.

[35] J. Lan, W. Yu, and X. Jiang, "Antiferromagnetic domain wall as spin wave polarizer and retarder," *Nature Communications*, vol. 8, 1, Aug. 2017.

[36] W. Yu, J. Lan, and J. Xiao, "Antiferromagnetic domain wall motion driven by polarized spin waves," *ArXiv e-prints*, Nov. 24, 2017.

[37] D. Atkinson *et al.*, "Magnetic domain-wall dynamics in a submicrometre ferromagnetic structure," *Nature Materials*, vol. 2, 2, Jan. 2003.

[38] A. V. Chumak, A. A. Serga, and B. Hillebrands, "Magnon transistor for all-magnon data processing," *Nature Communications*, vol. 5, Aug. 2014.

[39] K. Vogt *et al.*, "Realization of a spin-wave multiplexer," *Nature Communications*, vol. 5, Apr. 2014.

[40] K. Wagner *et al.*, "Magnetic domain walls as reconfigurable spin-wave nanochannels," *Nature Nanotechnology*, vol. 11, 5, Feb. 2016.

[41] K.-S. Lee and S.-K. Kim, "Conceptual design of spin wave logic gates based on a Mach-Zehnder-type spin wave interferometer for universal logic functions," *Journal of Applied Physics*, vol. 104, 5, Sep. 2008.

[42] S. Louis, I. Lisenkov, S. Nikitov, V. Tyberkevych, and A. Slavin, "Bias-free spin-wave phase shifter for magnonic logic," *AIP Advances*, vol. 6, 6, Jun. 2016.

[43] F. J. Buijnsters, Y. Ferreiros, A. Fasolino, and M. I. Katsnelson, "Chirality-dependent transmission of spin waves through domain walls," *Phys. Rev. Lett.*, vol. 116, 14, Apr. 2016.

[44] G. Yu *et al.*, "Room-temperature skyrmions in an antiferromagnet-based heterostructure," *Nano Letters*, vol. 18, 2, Feb. 2018.

[45] M. C. et. al., *Magnetism Fundamentals*. New York, USA: Springer, 2005.

[46] F. D. M. Haldane, "Nonlinear field theory of large-spin Heisenberg antiferromagnets: Semiclassically quantized solitons of the one-dimensional easy-axis Néel state," *Phys. Rev. Lett.*, vol. 50, 15, Apr. 1983.

[47] A. Bogdanov and A. Shestakov, "Vortex states in antiferromagnetic crystals," *Physics of the Solid State*, vol. 40, 8, Aug. 1998.

[48] A. N. Bogdanov, U. K. Rössler, M. Wolf, and K.-H. Müller, "Magnetic structures and reorientation transitions in noncentrosymmetric uniaxial antiferromagnets," *Phys. Rev. B*, vol. 66, 21, Dec. 2002.

[49] E. G. Tveten, A. Qaiumzadeh, and A. Brataas, "Antiferromagnetic domain wall motion induced by spin waves," *Phys. Rev. Lett.*, vol. 112, 14, Apr. 2014.

[50] E. G. Tveten, T. Müller, J. Linder, and A. Brataas, "Intrinsic magnetization of antiferromagnetic textures," *Phys. Rev. B*, vol. 93, 10, Mar. 2016.

[51] A. Bogdanov, "On the stability of localized states in nonlinear field models with Lifshitz invariants," *JETP Letters*, vol. 68, 4, Aug. 1998.

[52] A. Crépieux and C. Lacroix, "Dzyaloshinsky-Moriya interactions induced by symmetry breaking at a surface," *Journal of Magnetism and Magnetic Materials*, vol. 182, 3, Mar. 1998.

[53] G. H. Derrick, "Comments on nonlinear wave equations as models for elementary particles," *Journal of Mathematical Physics*, vol. 5, 9, Sep. 1964.

[54] A. Bogdanov, "New localized solutions of the nonlinear field-equations," *JETP Letters*, vol. 62, 3, Aug. 1995.

[55] S. Mühlbauer *et al.*, "Skyrmion lattice in a chiral magnet," *Science*, vol. 323, 5916, Feb. 2009.

[56] X. Z. Yu *et al.*, "Real-space observation of a two-dimensional skyrmion crystal," *Nature*, vol. 465, 7300, Jun. 2010.

[57] F. Zhuo and Z. Z. Sun, "Field-driven domain wall motion in ferromagnetic nanowires with bulk Dzyaloshinskii-Moriya interaction," *Scientific Reports*, vol. 6, 1, Apr. 2016.

[58] S. Heinze *et al.*, "Spontaneous atomic-scale magnetic skyrmion lattice in two dimensions," *Nature Physics*, vol. 7, 9, Jul. 2011.

[59] A. Thiaville, S. Rohart, É. Jué, V. Cros, and A. Fert, "Dynamics of Dzyaloshinskii domain walls in ultrathin magnetic films," *EPL*, vol. 100, 5, Dec. 2012.

[60] M. Belmeguenai *et al.*, "Interfacial Dzyaloshinskii-Moriya interaction in perpendicularly magnetized $Pt/Co/AlO_x$ ultrathin films measured by brillouin light spectroscopy," *Phys. Rev. B*, vol. 91, 18, May 2015.

[61] K. Di *et al.*, "Direct observation of the Dzyaloshinskii-Moriya interaction in a Pt/Co/Ni film," *Phys. Rev. Lett.*, vol. 114, 4, Jan. 2015.

[62] S. Woo *et al.*, "Observation of room-temperature magnetic skyrmions and their current-driven dynamics in ultrathin metallic ferromagnets," *Nature Materials*, vol. 15, 5, May 2016.

[63] C. S. Edmund, "Ferromagnetism: Magnetization curves," *Reports on Progress in Physics*, vol. 13, 1, Jan. 1950.

[64] J. Stöhr and H. C. Siegmann, *Magnetism From Fundamentals to Nanoscale Dynamics*. New York, USA: Springer, 2006.

[65] J. Cardy, *Scaling and Renormalization in Statistical Physics*. Cambrige, UK: Cambridge University Press, 1996.

[66] R. Skomski, *Simple Models of Magnetism*. New York, USA: Oxford University Press, 2008.

[67] R. Keesman, M. Raaijmakers, A. E. Baerends, G. T. Barkema, and R. A. Duine, "Skyrmions in square-lattice antiferromagnets," *Phys. Rev. B*, vol. 94, 5, Aug. 2016.

[68] S. Das Sarma, J. Fabian, X. Hu, and I. Zutic, "Spin electronics and spin computation," *Solid State Communications*, vol. 119, 4, Jul. 2001.

[69] H. Velkov *et al.*, "Phenomenology of current-induced skyrmion motion in antiferromagnets," *New Journal of Physics*, vol. 18, 7, Jul. 2016.

[70] J. C. Fisher, "Antiferromagnetic ground state," *Journal of Physics and Chemistry of Solids*, vol. 10, 1, Apr. 1959.

[71] T. Oguchi, "Antiferromagnetic ground state," *Journal of Physics and Chemistry of Solids*, vol. 24, 8, Aug. 1963.

[72] N. A. Spaldin, *Magnetic materials : fundamentals and applications*. Cambridge, UK: Cambridge Univesity Press, 2011.

[73] E. Colineau *et al.*, "Antiferromagnetic ground state in NpCoGe," *Phys. Rev. B*, vol. 89, 11, Mar. 2014.

[74] P. V. S. Reddy, V. Kanchana, G. Vaitheeswaran, A. V. Ruban, and N. E. Christensen, "Evidence for the antiferromagnetic ground state of Zr_2TiAl: A first-principles study," *Journal of Physics: Condensed Matter*, vol. 29, 26, May 2017.

[75] R. A. Duine, *Spintronics*, (lecture notes in the course "Spintronics"). University of Utrecht, Utrecht, Netherlands, Feb. 2010. [Online]. Available: `https://www.staff.science.uu.nl/~duine102/RembertDuine_Spintronics.pdf`.

[76] M. Ewerlin *et al.*, "Magnetic dipole and higher pole interaction on a square lattice," *Phys. Rev. Lett.*, vol. 110, 17, Apr. 2013.

[77] O. Gomonay, S. Kondovych, and V. Loktev, "Shape-induced anisotropy in antiferromagnetic nanoparticles," *Journal of Magnetism and Magnetic Materials*, vol. 354, 2014.

[78] D. I. Paul, "Interaction of antiferromagnetic spin waves with a Bloch wall," *Phys. Rev.*, vol. 126, 1, Apr. 1962.

[79] J. Wu *et al.*, "Direct observation of imprinted antiferromagnetic vortex state in CoO/Fe/Ag(001) disks," *Nature Physics*, vol. 7, 4, Jan. 2011.

[80] K. Everschor, "Current-induced dynamics of chiral magnetic structures," PhD thesis, University of Cologne, Jun. 2012.

[81] T. Skyrme, "A unified field theory of mesons and baryons," *Nuclear Physics*, vol. 31, Supplement C, 1962.

[82] S. L. Sondhi, A. Karlhede, S. A. Kivelson, and E. H. Rezayi, "Skyrmions and the crossover from the integer to fractional quantum Hall effect at small Zeeman energies," *Phys. Rev. B*, vol. 47, 24, May 1993.

[83] U. A. Khawaja and H. Stoof, "Skyrmion in a ferromagnetic Bose-Einstein condensate," *Nature*, vol. 411, 6840, Jun. 2001.

[84] A. Bogdanov and A. Hubert, "Thermodynamically stable magnetic vortex states in magnetic crystals," *Journal of Magnetism and Magnetic Materials*, vol. 138, 3, Dec. 1994.

[85] A. Abanov and V. L. Pokrovsky, "Skyrmion in a real magnetic film," *Phys. Rev. B*, vol. 58, 14, Oct. 1998.

[86] Y. Yang, *Solitons in field theory and nonlinear analysis*. New York, USA: Springer, 2001.

[87] A. Bogdanov and A. Hubert, "The stability of vortex-like structures in uniaxial ferromagnets," *Journal of Magnetism and Magnetic Materials*, vol. 195, 1, Apr. 1999.

[88] X. Zhang, Y. Zhou, and M. Ezawa, "Antiferromagnetic skyrmion: Stability, creation and manipulation," *Scientific Reports*, vol. 6, 1, Apr. 2016.

[89] X. Zhang *et al.*, "All-magnetic control of skyrmions in nanowires by a spin wave," *Nanotechnology*, vol. 26, 22, Jun. 2015.

[90] B. Hillebrands and K. Ounadjela, *Spin Dynamics in Confined Magnetic Structures 1*. New York, USA: Springer, 2002.

[91] T. L. Gilbert and J. M. Kelly, "Anomalous rotational damping in ferromagnetic sheets," *New York: American Institute of Electrical Engineers*, Oct. 1955.

[92] W. Döring, "On the intertia of walls between weiss domains," *Z. Naturrforsch*, vol. 3a, 1948.

[93] V. G. Bar'yakhtar, "Phenomenological description of relaxation processes in magnetic materials," *JETP Letters*, vol. 60, 4, Oct. 1984.

[94] B. A. Ivanov and A. K. Kolezhuk, "Solitons with internal degrees of freedom in 1D Heisenberg antiferromagnets," *Phys. Rev. Lett.*, vol. 74, 10, Apr. 1995.

[95] E. Fradkin and M. Stone, "Topological terms in one- and two-dimensional quantum Heisenberg antiferromagnets," *Phys. Rev. B*, vol. 38, 10, Oct. 1988.

[96] A. Altland and B. D. Simons, *Condensed Matter Field Theory*. Cambridge, UK: Cambridge University Press, Mar. 2010.

[97] H. Schmidt, "Magnetization reversal by coherent rotation in single-domain magnets with arbitrary anisotropy," *Journal of Applied Physics*, vol. 93, 4, Jan. 2003.

[98] T. Devolder and C. Chappert, "Precessional switching of thin nanomagnets: Analytical study," *The European Physical Journal B - Condensed Matter and Complex Systems*, vol. 36, 1, Nov. 2003.

[99] M. Behrmann and F. Lechermann, "Large-amplitude spin oscillations triggered by nonequilibrium strongly correlated t2g electrons," *Phys. Rev. B*, vol. 91, 7, Feb. 2015.

[100] R. Khymyn, I. Lisenkov, V. Tiberkevich, B. A. Ivanov, and A. Slavin, "Antiferromagnetic THz-frequency Josephson-like oscillator driven by spin current," *Scientific Reports*, vol. 7, Mar. 2017.

[101] R. Cheng, M. W. Daniels, J.-G. Zhu, and D. Xiao, "Antiferromagnetic spin wave field-effect transistor," *Scientific Reports*, vol. 6, Apr. 2016.

[102] Y. Ando *et al.*, "Thermally excited spin wave modes in synthetic antiferromagnetic stripes," *Journal of Magnetism and Magnetic Materials*, vol. 310, 2, Mar. 2007.

[103] J. Barker and O. A. Tretiakov, "Static and dynamical properties of antiferromagnetic skyrmions in the presence of applied current and temperature," *Phys. Rev. Lett.*, vol. 116, 14, Apr. 2016.

[104] E. G. Tveten, A. Qaiumzadeh, O. A. Tretiakov, and A. Brataas, "Staggered dynamics in antiferromagnets by collective coordinates," *Phys. Rev. Lett.*, vol. 110, 12, Mar. 2013.

[105] G. Gitgeatpong *et al.*, "Nonreciprocal magnons and symmetry-breaking in the noncentrosymmetric antiferromagnet," *Phys. Rev. Lett.*, vol. 119, 4, Jul. 2017.

[106] A. Qaiumzadeh, L. A. Kristiansen, and A. Brataas, "Controlling chiral domain walls in antiferromagnets using spin-wave helicity," *Phys. Rev. B*, vol. 97, 2, Jan. 2018.

[107] K. A. van Hoogdalem, Y. Tserkovnyak, and D. Loss, "Magnetic texture-induced thermal Hall effects," *Phys. Rev. B*, vol. 87, 2, Aug. 2012.

[108] B. A. Ivanov, "Local modes and scattering of spin waves by a soliton in an isotropic 2D ferromagnet," *JETP Letters*, vol. 61, 11, Jun. 1995.

[109] B. A. Ivanov, A. K. Kolezhuk, and G. M. Wysin, "Normal modes and soliton resonance for vortices in 2D classical antiferromagnets," *Phys. Rev. Lett.*, vol. 76, 3, Jan. 1996.

[110] E. G. Galkina, A. Y. Galkin, B. A. Ivanov, and F. Nori, "Magnetic vortex as a ground state for micron-scale antiferromagnetic samples," *Phys. Rev. B*, vol. 81, 18, May 2010.

[111] B. Costa, M. Gouvea, and A. Pires, "Vortex-magnon interaction in the 2D XY ferromagnetic model," *Physics Letters A*, vol. 165, 2, Feb. 1992.

[112] B. A. Ivanov, H. J. Schnitzer, F. Mertens, and G. Wysin, "Magnon modes and magnon-vortex scattering in two-dimensional easy-plane ferromagnets," *Phys. Rev. B*, vol. 58, 13, Oct. 1998.

[113] G. M. Wysin and A. R. Völkel, "Normal modes of vortices in easy-plane ferromagnets," *Phys. Rev. B*, vol. 52, 10, Sep. 1995.

[114] A. R. Pereira, F. O. Coelho, and A. S. T. Pires, "Normal modes of vortices in easy-plane antiferromagnets: Exact results and Born approximation," *Phys. Rev. B*, vol. 54, 9, Sep. 1996.

[115] A. Pereira and A. Pires, "Magnon waveforms in the presence of a vortex-pair in easy-plane antiferromagnets," *Solid State Communications*, vol. 111, 2, Jun. 1999.

[116] Y. Le Maho, J.-V. Kim, and G. Tatara, "Spin-wave contributions to current-induced domain wall dynamics," *Phys. Rev. B*, vol. 79, 17, May 2009.

[117] A. Piel, *Plasma Physics: An Introduction to Laboratory, Space, and Fusion Plasmas*. Berlin, Germany: Springer, 2010.

[118] S. Sarkar, S. Paul, and R. Denra, "Bump-on-tail instability in space plasmas," *Physics of Plasmas*, vol. 22, 10, Oct. 2015.

[119] L. D. Landau, "On the vibrations of the electronic plasma," *J. Phys.(USSR)*, vol. 10, 1, 1946.

[120] T. Moriya, *Spin fluctuations in itinerant electron magnetism*. New York, USA: Springer, 1985.

[121] Y. Xia, J. Xu, B.-A. Li, and W. Q. Shen, "Equations of motion of test particles for solving the spin-dependent Boltzmann-Vlasov equation," *Physics Letters B*, vol. 759, Aug. 2016.

[122] L. J. Cornelissen, K. J. H. Peters, G. E. W. Bauer, R. A. Duine, and B. J. van Wees, "Magnon spin transport driven by the magnon chemical potential in a magnetic insulator," *Phys. Rev. B*, vol. 94, 1, Jul. 2016.

[123] S. M. Rezende, "Magnon coherent states and condensates," in *Magnonics: From Fundamentals to Applications*, vol. 125, Berlin, Germany: Springer, 2013, ch. 4.

[124] V. L. Safonov, *Nonequilibrium Magnonics: Theroy, Experiment and Applications*. Weinheim, Germany: Wiley-VCH, 2013.

[125] F. Fang, R. Olf, S. Wu, H. Kadau, and D. M. Stamper-Kurn, "Condensing magnons in a degenerate ferromagnetic spinor Bose gas," *Phys. Rev. Lett.*, vol. 116, 9, Mar. 2016.

[126] P. W. Terry, D. A. Baver, and S. Gupta, "Role of stable eigenmodes in saturated local plasma turbulence," *Physics of Plasmas*, vol. 13, 2, Feb. 2006.

[127] A. J. Heeger, "Spin-wave instability and premature saturation in antiferromagnetic resonance," *Phys. Rev.*, vol. 131, 2, Jul. 1963.

[128] E. L. Fjærbu, N. Rohling, and A. Brataas, "Electrically driven Bose-Einstein condensation of magnons in antiferromagnets," *Phys. Rev. B*, vol. 95, 14, Apr. 2017.

[129] L. M. Sandratskii and P. Buczek, "Lifetimes and chirality of spin waves in antiferromagnetic and ferromagnetic ferh from the perspective of time-dependent density functional theory," *Phys. Rev. B*, vol. 85, 2, Jan. 2012.

[130] K. Cao, H. Lambert, P. G. Radaelli, and F. Giustino, "Ab initio calculation of spin fluctuation spectra using time-dependent density functional perturbation theory, plane waves, and pseudopotentials," *Phys. Rev. B*, vol. 97, 2, Jan. 2018.

[131] A. Gurevich and G. A. Melkov, *Magnetization Oscillation and Waves*. Boca Raton, USA: CRC Press, 1996.

[132] S. Schäfer, V. Kegel, A. A. Serga, B. Hillebrands, and M. P. Kostylev, "Variable damping and coherence in a high-density magnon gas," *Phys. Rev. B*, vol. 83, 18, May 2011.

[133] G. M. Wysin and A. Völkel, "Comparison of vortex normal modes in easy-plane ferromagnets and antiferromagnets," *Phys. Rev. B*, vol. 54, 18, Nov. 1996.

[134] B. A. Ivanov, V. M. Muravev, and D. D. Sheka, "Soliton-magnon scattering in a two-dimensional isotropic magnetic material," *Journal of Experimental and Theoretical Physics*, vol. 89, 3, Sep. 1999.

[135] V. A. Zyuzin and A. A. Kovalev, "Magnon spin Nernst effect in antiferromagnets," *Phys. Rev. Lett.*, vol. 117, 21, Nov. 2016.

[136] G. Wysin, "Relaxation schemes for normal modes of magnetic vortices: Application to the scattering matrix," *Phys. Rev. B*, vol. 63, 9, Mar. 2001.

[137] M. B. Jungfleisch, W. Zhang, and A. Hoffmann, "Perspectives of antiferromagnetic spintronics," *Physics Letters A*, vol. 382, 13, Feb. 2018.

[138] A. N. Bogdanov and A. D. Yablonskii, "Contribution to the theory of inhomogeneous states of magnets in the region of magnetic-field-indiced phase transitions. Mixed state of antiferromagnets," *Journal of Experimental and Theoretical Physics*, vol. 69, 1, Jul. 1989.

[139] R. E. Troncoso, C. Ulloa, F. Pesce, and A. S. Nunez, "Antiferromagnetic magnonic crystals," *Phys. Rev. B*, vol. 92, 22, Dec. 2015.

[140] K. M. D. Hals, Y. Tserkovnyak, and A. Brataas, "Phenomenology of current-induced dynamics in antiferromagnets," *Phys. Rev. Lett.*, vol. 106, 10, Mar. 2011.

[141] S. K. Kim, Y. Tserkovnyak, and O. Tchernyshyov, "Propulsion of a domain wall in an antiferromagnet by magnons," *Phys. Rev. B*, vol. 90, 10, Sep. 2014.